

Aus dem Lehrstuhl für Physiologische Genomik,
Biomedizinisches Centrum (BMC)
Institut der Universität München
Vorstand: Prof. Dr. Magdalena Götz



DISSECTION AND PROTEOME ANALYSIS

TO CHARACTERIZE THE ADULT NEURAL STEM CELL NICHE

Dissertation
zum Erwerb des Doktorgrades der Medizin
an der Medizinischen Fakultät der
Ludwig-Maximilians-Universität zu München

vorgelegt von
Christian Johannes Frieß
aus
Ebersberg
Jahr
2023

Mit Genehmigung der Medizinischen Fakultät
der Universität München

Berichterstatter:	Prof. Dr. Magdalena Götz
Mitberichterstatter:	Prof. Dr. Rainer Glaß Prof. Dr. Ralf Huss Prof. Dr. Jochen Herms
Mitbetreuung durch den promovierten Mitarbeiter:	Dr. Jacob Kjell
Dekan:	Prof. Dr. med. Thomas Gudermann
Tag der mündlichen Prüfung:	27.04.2023

Table of Contents

TABLE OF CONTENTS	3
SUMMARY	4
ZUSAMMENFASSUNG	5
LIST OF ABBREVIATIONS	6
1. INTRODUCTION	8
1.1 THE SEZ NEUROGENIC NICHE	10
1.1.1 <i>Cells of the SEZ Neurogenic Niche</i>	10
1.1.2 <i>Microenvironment of the SEZ Neurogenic Niche</i>	11
1.1.2.1 Extracellular Matrix of the SEZ Niche	13
1.1.2.2 Vasculature of the SEZ Niche	15
1.1.2.3 Choroid Plexus, Cerebrospinal Fluid, and the SEZ Niche	16
1.2 INVESTIGATING THE MICROENVIRONMENT OF THE SEZ NICHE	17
1.2.1 <i>Aim of the Project</i>	17
1.2.2 <i>Choosing a Proteomic Approach</i>	17
1.2.3 <i>Dissecting the SEZ Neurogenic Niche</i>	18
1.2.4 <i>Achieving Sufficient Proteomic Depth with Mass Spectrometry</i>	19
1.2.5 <i>Comparison groups</i>	20
2. RESULTS	22
2.1 AIM OF THE STUDY I – DEVELOPING AND VALIDATING THE CRYO-SECTION DISSECTION	22
2.2 AIM OF THE STUDY II – CONSTITUTING THE PROTEOME OF THE SEZ NEUROGENIC NICHE	38
3. PUBLICATION BIBLIOGRAPHY	80
LIST OF PUBLICATIONS	90
DECLARATION OF AUTHOR CONTRIBUTION	91
AFFIDAVIT	92
ACKNOWLEDGEMENTS	93

Summary

Stem cell niches in the adult mammalian brain are decisively shaped by their microenvironment. In these niches, extracellular signals modulate stem cell quiescence, proliferation, migration, and differentiation. Conversely, the microenvironment in the remainder of the brain merely permits gliogenesis, restricts neuronal plasticity, and limits the neurogenic potential of neural precursors. Elucidating the mechanisms rendering neurogenic niches permissive for neurogenesis might foster the improvement of cell replacement therapies for neurological disorders involving neural cell loss. To better understand the molecular composition, the architecture, and the physical properties responsible for the neurogenic nature of the microenvironment in neural stem cell niches, this study pursued a characterization of the subependymal zone of the lateral ventricle (SEZ), which is the largest stem cell niche of the murine brain. To investigate the microenvironment of the SEZ, a bottom-up proteomic approach using mass spectrometry was employed. The analysis of the extracellular microenvironment of this region requires a precise dissection method with minimal tissue perturbation, applicable to unfixed tissue. For this purpose, a novel dissection method, termed Cryo-section Dissection (CSD), was developed. In the first step of the CSD protocol the cortex and the corpus callosum covering the lateral ventricles are removed from the unfixed murine brain. Then, after freezing the tissue on dry ice, the brain is sectioned coronally. Finally, the SEZ is manually isolated from each section using a pre-cooled scalpel. The SEZ as adult neural stem cell niche was compared to the non-neurogenic somatosensory cortex, the olfactory bulb as site of neuronal integration, and the structurally similar, but mostly non-neurogenic medial wall of the lateral ventricle, termed medial ependymal zone (MEZ). A library-matched single shot mass spectrometry analysis employing a label-free quantification algorithm was applied to generate the proteome data of the SEZ, the somatosensory cortex, the olfactory bulb, and the MEZ. This proteome data was used to investigate niche specific protein clusters and filtered for individual candidate proteins. Promising candidates were subjected to immunohistochemical staining. This analysis enabled the detection of the candidate proteins C1qI3, Kininogen 1, and S100a6 potentially involved in neurogenesis. Additionally, the influence of niche stiffness on neural stem cell physiology was investigated, and the extracellular neurogenesis regulator Transglutaminase 2 could be identified.

Zusammenfassung

Stammzellnischen im adulten Säugetiergehirn werden entscheidend durch die extrazelluläre Umgebung geformt. In diesen Nischen modulieren extrazelluläre Signale den Erhalt der Reserve, die Proliferation, die Migration und die Differenzierung von Stammzellen. Dagegen lässt die extrazelluläre Umgebung im übrigen Gehirn vor allem die Entstehung von Gliazellen zu, schränkt die neuronale Plastizität ein und limitiert das neurogene Potential von neuronalen Vorläuferzellen. Das Erforschen des neurogenen Potentials der Nischen könnte die Entwicklung von Behandlungsmethoden für neurologische Erkrankungen, die mit einem Verlust von Nervenzellen einhergehen, fördern. Um das Verständnis der molekularen Zusammensetzung, der Architektur und der physikalischen Eigenschaften zu verbessern, die dem neurogenen Einfluss der Nischen zugrunde liegen, wurde in dieser Studie eine Charakterisierung der extrazellulären Umgebung der subependymalen Zone der Seitenventrikel (SEZ) angestrebt. Die SEZ stellt die größte Stammzellnische des Mausgehirns dar. Zum Zwecke der Aufklärung der molekularen Zusammensetzung der SEZ wurde diese mittels Massenspektrometrie untersucht. Die Nische muss dazu präzise aus dem Gehirn der Maus isoliert werden, ohne das Gewebe zu fixieren. Um das zu erreichen, wurde eine neue Dissektionsmethode entwickelt, genannt Cryo-section Dissection (CSD). Im ersten Schritt des CSD-Protokolls wird der Kortex und das Corpus Callosum, welche die Seitenventrikel bedecken, vom nicht fixierten Mausgehirn entfernt. Danach wird das Gehirn auf Trockeneis gefroren, um dann koronare Schnitte desselben anzufertigen. Schließlich kann die SEZ mit einem vorgekühlten Skalpell freihändig aus jedem Schnitt isoliert werden. Die SEZ als adulte neurale Stammzellnische wurde mit dem nicht-neurogenen somatosensorischen Kortex, dem Bulbus Olfactorius als Ort der neuronalen Integration sowie der strukturell ähnlichen, aber vorwiegend nicht neurogenen medialen Wand der Seitenventrikel, genannt mediale ependymale Zone (MEZ), verglichen. Eine massenspektrometrische Analyse, die einen Label-freien Quantifizierungs-Algorithmus und einen die Detektionsrate erhöhenden Abgleich mit einer zuvor erstellten Datenbank nutzt, wurde zur Generierung eines proteomischen Datensatzes der SEZ, des somatosensorischen Kortex, des Bulbus Olfactorius sowie der MEZ verwendet. Dieser Datensatz wurde auf nischenspezifische Protein-Cluster und individuelle Kandidaten-Proteine durchsucht. Vielversprechende Kandidaten wurden mittels Immunhistochemie weiter untersucht. Im Zuge der Analyse wurden die Kandidatenproteine C1ql3, Kininogen 1 und S100a6 mit möglichem Einfluss auf die Neurogenese untersucht. Zusätzlich wurde der Einfluss der Steifheit des Gewebes auf die Stammzellproliferation erforscht und das extrazelluläre Protein Transglutaminase 2 entdeckt, das die Neurogenese reguliert.

List of Abbreviations

CSD	Cryo-section Dissection
CSF	cerebrospinal fluid
ECM	extracellular matrix
EGF	epidermal growth factor
FGF2	fibroblast growth factor 2
HPLC	high-performance liquid chromatography
Hspg2	heparan sulfate proteoglycan 2
IGF2	insulin-like growth factor 2
LCM	laser capture microdissection
LFQ	label-free quantification
LMSS	library-matched single shot
LV	lateral ventricle
MEZ	medial ependymal zone
MS	mass spectrometry
NSC	neural stem cell
OB	olfactory bulb
RMS	rostral migratory stream
SDF1	stromal cell-derived factor 1
SEZ	subependymal zone
SGZ	subgranular zone
Thbs4	thrombospondin 4
TnC	tenascin C

INTRODUCTION

1. Introduction

Brain diseases are a leading cause for disability and death in our society. Stroke, traumatic brain injury, and neurodegenerative disease are among the most frequent neurological disorders. Globally, stroke is accountable for a large part of disability and death, especially in the group of over 50-year-old individuals (Vos et al. 2020; Saini et al. 2021). Ischemic stroke is mostly the consequence of thromboembolism or atherosclerosis. The administration of thrombolytic drugs or mechanical thrombectomy can mitigate neural cell loss. However, cell death in the infarct core can neither be prevented nor reverted. Similarly, traumatic brain injury is a significant reason for long-term disability (Capizzi et al. 2020). Acute treatment is basically restricted to the management of intracranial hemorrhage and the reduction of intracranial pressure. Especially following moderate to severe trauma, complete functional recovery is unlikely to be reached due to permanent tissue damage. Another major group of incapacitating brain disorders are neurodegenerative diseases. The prevalence and incidence of neurodegenerative diseases such as Alzheimer's disease or Parkinson's disease notably increase over lifetime (Erkkinen et al. 2018). Therefore, a further increase in disease burden and healthcare expenses caused by this group of diseases can be expected in an aging society. Progressive neural cell loss is a joint pathophysiological feature of neurodegenerative diseases. To this day, therapeutic approaches fail to revert or even halt this gradual decline. Taken together, in all three disease entities, the brain cannot regenerate lost neural tissue. Unfortunately, an endogenous replacement for neurons dying in brain diseases is lacking. Certainly, the integrity of neural circuitry as well as the complex interplay of neurons with glial cells are indispensable for the preservation of a physiological brain function (Lalo et al. 2021; Paterno et al. 2017). Therefore, restoring the lost brain tissue might enable the recovery of lost brain function and could thereby reduce the disease burden caused by stroke, traumatic brain injury, and neurodegenerative disease (Gioia et al. 2020; Huang and Zhang 2019; Rolfe, Sun 2015; Barker et al. 2018). Hence, to address the disease burden imposed by neurological disorders, it is important to find ways of replacing neurons in the human brain.

Several tissues react to injury with a replacement of lost cells. The adult mammalian brain mostly lacks this capacity. The response of the brain to tissue lesion consists of a clearance of cell debris, reactive gliosis, and the production of a glial scar. The impact of glial scarring on disease and healing progression appears to be double-edged. Reactive astrocytes have been demonstrated to curtail neural cell loss after injury (Faulkner et al. 2004). However, scar formation, particularly the involved upregulation of chondroitin-sulfate proteoglycans, ultimately impedes axonal outgrowth (Adams and Gallo 2018; Pekny and Pekna 2014). Despite the predominant scar formation, some rudimentary mechanisms aiming at the restitution of lost tissue can be observed in the mouse brain. Although adult mammalian neurons are largely postmitotic (Frisén 2016), postnatal neurogenesis exists in the adult murine brain. However, it is mostly restricted to the subependymal zone (SEZ) of the lateral walls of the lateral ventricle (LV) (Bordiuk et al. 2014; Llorente et al. 2022) and the subgranular zone (SGZ) of the hippocampus (Kuhn et al. 2018; Cope and Gould 2019). Endogenous neural stem cell (NSC) proliferation is upregulated upon ischemia (Macas et al. 2006; Koh and Park 2017; Xu et al. 2020). Also, neuroblasts show a limited migratory behaviour

towards the lesion site (Arvidsson et al. 2002; Kreuzberg et al. 2010; David-Bercholz et al. 2021). Unfortunately, these mechanisms remain insufficient for the achievement of a structural or functional recovery (Lindvall and Kokaia 2015).

The deficiency of neural recovery is not solely caused by a lack of endogenous proliferative and migratory capacity. Neurogenesis is actively restricted in the adult mammalian brain, not only by the glial cells, but also by signals from the extracellular microenvironment. Physiologically, the microenvironment of adult brain parenchyma only permits gliogenesis (Götz et al. 2016). Moreover, neuronal progenitor (Winkler et al. 1998) and even committed precursor (Seidenfaden et al. 2006) cells differentiate into glial cells when transplanted into adult murine brain tissue. Conversely, transplanting neuronal precursors into stem cell niches leads to neuronal differentiation of the grafted cells (Herrera et al. 1999; Lois and Alvarez-Buylla 1994). So, only the microenvironment of adult neurogenic niches permits neurogenesis (Conover and Todd 2017; Obernier and Alvarez-Buylla 2019). Conversely, the rest of the brain prevents neuronal proliferation and differentiation. In adult brain parenchyma, the extracellular matrix (ECM) confines neuronal plasticity by building a specialized structure around neurons termed “perineuronal nets” (Deepa et al. 2006). Chondroitin sulfate proteoglycans, an ECM component of the perineuronal nets, but also of glial scar tissue, impedes axon regeneration (Fawcett 2015; Sharma et al. 2012). NSC niches in the murine brain lack perineuronal nets because of the absence of terminally differentiated neurons. Apart from the presence or absence of perineuronal nets, the respective molecular composition of the extracellular microenvironment in NSC niches in contrast to adult brain parenchyma is largely unknown. Moreover, the overall mechanisms responsible for the dissimilar properties of NSC niches contrary to the remaining brain tissue in general are barely explored.

Understanding the mechanisms responsible for the restriction of neural tissue regeneration in the adult mammalian brain can promote the development of cell replacement therapies that overcome the hurdles of endogenous repair. Being able to engineer the microenvironment of brain tissue after neural cell loss in such a way that it acquires the neurogenic potential of stem cell niches and sheds the repair restrictive features might enable further improvement of therapeutic approaches addressing neural cell loss. To this end, first understanding the cause of the differences in neurogenic potential between the microenvironment of brain tissue and of neurogenic niches is crucial. For this purpose, this study pursues to elucidate what distinguishes the microenvironment in neurogenic stem cell niches from the microenvironment in the gliogenic remainder of the brain.

1.1 The SEZ Neurogenic Niche

Entailing the SEZ of the LVs and the SGZ of the hippocampus, the adult mouse brain exhibits two major NSC niches suitable for the analysis of a stem cell microenvironment. The SEZ is the largest neurogenic niche in the mouse brain (Bordiuk et al. 2014). Also, being located adjacent to the ependymal layer, the SEZ can be readily accessed through the LV, which facilitates tissue dissection. Neuroblasts formed in the SEZ migrate to the olfactory bulb (OB) to terminally differentiate. Hence, the place of stem cell maintenance and proliferation can be investigated separately from the region of differentiation and integration. Therefore, in this study the SEZ was chosen over the SGZ for the analysis of a stem cell microenvironment. Two major components constitute the SEZ neurogenic niche: cells and the extracellular microenvironment.

1.1.1 Cells of the SEZ Neurogenic Niche

The cells present in the SEZ as well as whether and how they are involved in neurogenesis have already been subjected to comprehensive analysis (Lim and Alvarez-Buylla 2016; Götz et al. 2016; Obernier and Alvarez-Buylla 2019). In brief, the cell-fraction of the SEZ niche is composed of NSCs (Type B cells), transit-amplifying cells (Type C cells), migrating neuroblasts (Type A Cells) (Lim and Alvarez-Buylla 2016), endothelial cells (Fujioka et al. 2019), microglial cells (Sato 2015), and ependymal cells (Shah et al. 2018). Type B cells reside adjacent to the ependymal layer, contacting the cerebrospinal fluid (CSF) with an apical process and the blood vessels with basal end feet. Upon activation, the nestin⁺ quiescent NSCs give rise to transit-amplifying progenitors, that in turn, after few rounds of division, produce doublecortin⁺ neuroblasts. In the rostral migratory stream (RMS), neuroblasts migrate from the ventricle to the OB, where they terminally differentiate into granule neurons or periglomerular neurons and integrate into pre-existing circuits (Figure 1). In summary, NSCs in the SEZ evolve from resident Type B cells to migratory Type A cells, which perform a remarkable journey from the LV to the OB. The respective local microenvironment facilitates each step of this process.

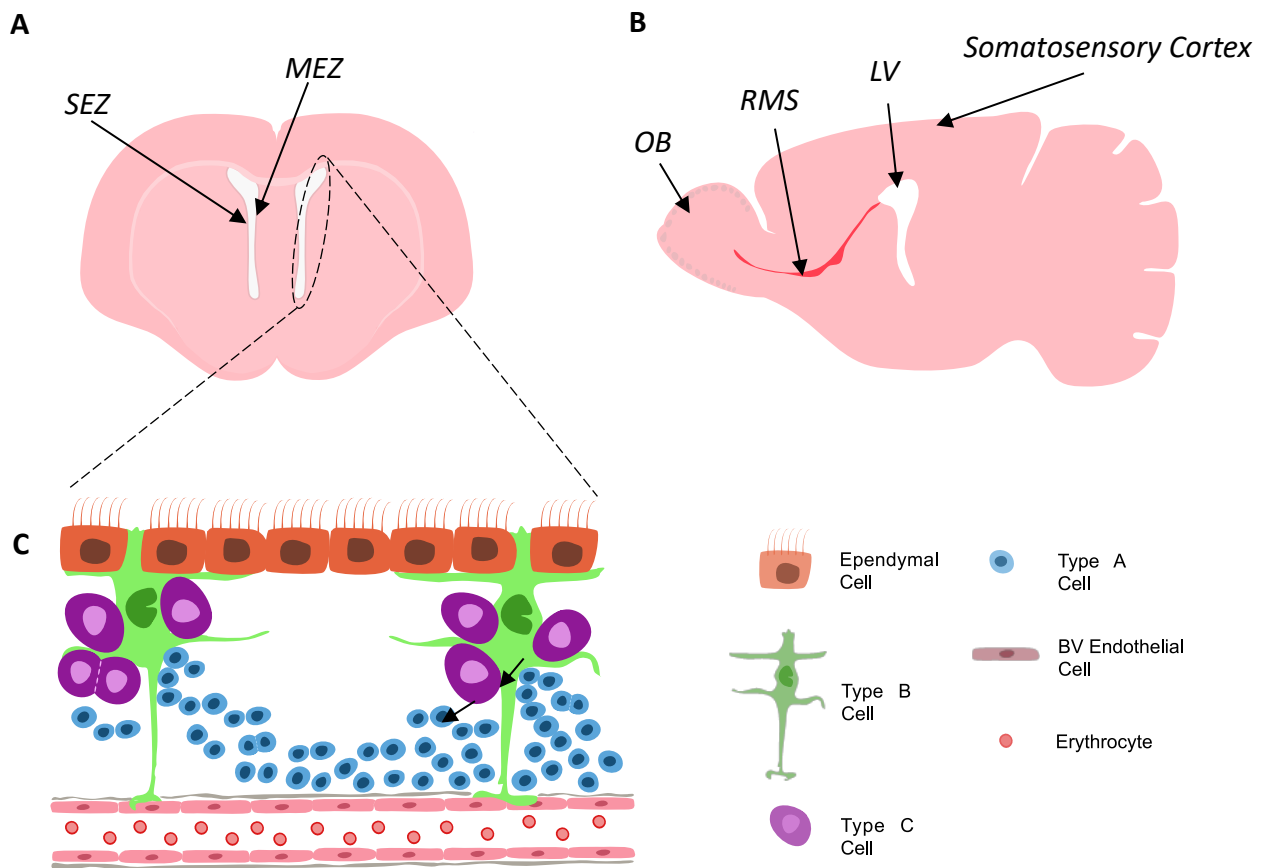


Figure 1: Architecture and cellular composition of the murine SEZ neurogenic niche. **A** Coronal section depicting the LV as well as the SEZ and MEZ **B** Sagittal section showing the RMS originating from the LV and extending to the OB **C** SEZ cells: ependymal cells (orange colored), type B cells (green colored), type C cells (purple colored), type A cells (blue colored), blood vessel (BV, red colored).

1.1.2 Microenvironment of the SEZ Neurogenic Niche

In complex organisms like humans or mice, cells are embedded in an extracellular microenvironment. The extracellular microenvironment comprises the entirety of molecules arranged in a three-dimensional structure around cells. It is composed of ECM as well as soluble molecules like growth factors or cytokines originating from local cells, but also distant sources, such as the blood stream. Extracellular matrices can be divided based on solubility into an insoluble, covalently linked core-matrix and soluble, non-covalently linked matrix-associated proteins. Topographically, the ECM consists of a pericellular and an interstitial matrix (Theocharis et al. 2016). Basement membranes constitute a key part of the pericellular matrix. They provide a scaffold to cells to reside on, orchestrate their three-dimensional arrangement, and contribute to the mechanical properties of the ECM (Khalilgharibi and Mao 2021).

Apart from providing a scaffold to cells, the ECM plays a pivotal role in modifying cellular physiology, such as cell growth, migration, and differentiation (Walker et al. 2018). The ECM can communicate with cells

by remodeling the matrix and thereby changing its mechanical properties, by releasing signaling molecules from the matrix using proteolytic cleavage, and by interacting with cells via cell surface receptors (Clause and Barker 2013). Cell-matrix communication using cell surface receptors is in part established by integrins, capable of binding a variety of ECM molecules, such as collagen or laminin (Barczyk et al. 2010; Domogatskaya et al. 2012). Thereby, the transmission of chemical or mechanical signals from the ECM to the cell nucleus is possible. Consequently, mechanical forces like tissue elasticity and stiffness, which is in part regulated by the degree of cross-linking of collagen fibers (Levental et al. 2009), can be measured by cells and integrated with other signals to guide their behavior (Chaudhuri et al. 2020), among others, in stem cell microenvironments (Petzold and Gentleman 2021; Vining and Mooney 2017). Thus, changes in the microenvironment can alter the gene expression profile of a cell.

Among the most significant molecular matrix components are collagens, laminins, fibronectin, integrins, matricellular proteins, and proteoglycans (Theocharis et al. 2016). Collagens are the protein group featuring the highest abundance in the ECM (Soroushanova et al. 2019). Fibrillar collagens such as collagen-I provide tissue with tensile strength (Tang 2020). Network-forming collagens like collagen-IV can be found in basement membranes (Khalilgharibi and Mao 2021). Laminins are trimeric proteins, consisting of an alpha, a beta, and a gamma subunit (Domogatskaya et al. 2012) and also constitute an integral part of basement membranes. Integrins are dimeric transmembrane proteins, composed of alpha and beta subunits. They mediate cell-matrix-interactions by serving as receptors capable of activating signal transduction cascades (Barczyk et al. 2010). Matricellular proteins such as tenascin C (TnC) or thrombospondin 4 (Thbs4) support cell-matrix and cell-cell interactions, thereby modifying cellular functions (Bornstein 2009; Bornstein and Sage 2002; Theocharis et al. 2016; Midwood et al. 2016). Mechanistically, matricellular proteins either contact cellular receptors directly (Garg et al. 2011) or mediate receptor activation by growth factors (Nozaki et al. 2006). Proteoglycans consist of a core protein with covalently attached glycosaminoglycan side chains (Iozzo and Schaefer 2015). They participate in cell signaling (Schaefer et al. 2017) and influence cell proliferation, migration, and differentiation (Theocharis et al. 2010; Schwartz and Domowicz 2018) by the interaction with extracellular molecules, growth factors, and chemokines. Accordingly, in addition to its physical properties, also individual molecular components of the extracellular microenvironment modulate cellular physiology.

Concluding, the extracellular microenvironment not only bonds cells together. It is crucially involved in the function of the biological structure cells constitute. This function is carried by the molecular components and the physical properties of the extracellular microenvironment. In stem cell niches, a specialized extracellular microenvironment modulates stem cell quiescence, proliferation, and differentiation (Crane et al. 2017; Donnelly et al. 2018; Vining and Mooney 2017). In the SEZ niche, signals originating from the vasculature, the choroid plexus, and the CSF complement local ECM components (Figure 2), which in principle could concertedly influence NSC physiology. However, this has never been examined comprehensively and in an unbiased manner at the proteome level.

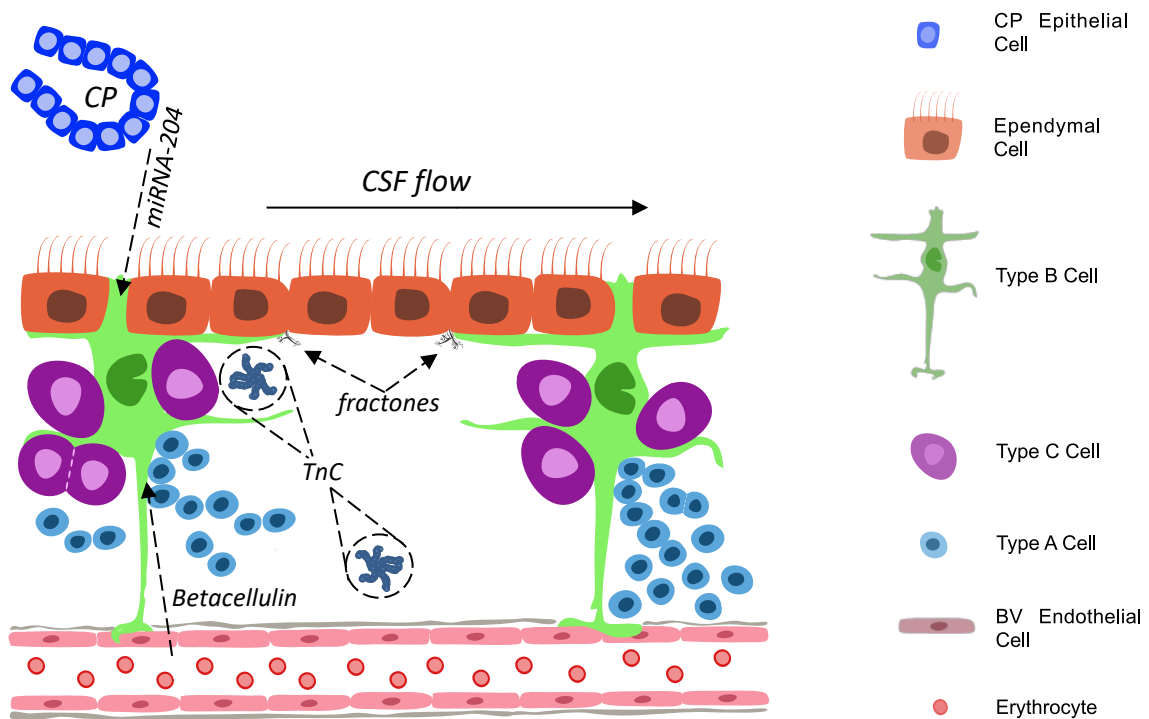


Figure 2: Microenvironment of the SEZ Niche. Overview of different elements constituting the niche and influencing stem cells: *CSF flow* as mechanical signal, choroid plexus-derived factors such as *miRNA-204*, *Betacellulin* as representative of vasculature derived soluble factors, NSCs contacting endothelial cells of the vasculature, *TnC* as example of ECM molecules uniquely present in neurogenic niches, *fractones* as specialized ECM structures exclusively present around ventricles contacting SEZ stem cells.

1.1.2.1 Extracellular Matrix of the SEZ Niche

The ECM of the SEZ, the RMS, and the OB features exceptional ultrastructural and molecular characteristics. The subependymal layer adjacent to the LV exhibits unique ECM structures, termed fractones (Mercier et al. 2002). In light microscopy, the bulbs appear as small laminin-positive punctate spots, in electron microscopy they reveal a fractal ultrastructure. Fractones exhibit a basement-membrane-like composition with collagen-IV, laminin, heparan-sulfate proteoglycans, and nidogen (Mercier 2016). Their trunk was suggested to originate perivascular while the bulb protrudes towards the ventricular lumen to directly contact NSCs (Mercier et al. 2002). However, wholemount SEZ immunostainings detecting a fractone arrangement largely independent of the vasculature challenged the proposition of a vascular origin of fractones or the mere existence of a fractone-blood vessel basement membrane continuity established via fractone stems (Sato et al. 2019). Laminin $\alpha 5$, a key component of fractone bulbs, was suggested to be produced by ependymal cells (Nascimento et al. 2018), but also by GFAP+ astrocytic NSCs (Sato et al. 2019). Neural stem and progenitor cells proliferate close to fractones (Kerever et al. 2007). In vitro, perturbing the generation of fractones appears to reduce the proliferative capacity of NSCs (Sato et al. 2019).

Evidence permits the hypothesis that heparan sulfate proteoglycans present in fractones bind fibroblast growth factor 2 (FGF2) (Kerever et al. 2007) and thereby promote its proliferative effect (Douet et al. 2013). Also, bone morphogenetic protein-4 (Mercier and Douet 2014) and bone morphogenetic protein-7 (Douet et al. 2012) were shown to bind to the heparan sulfate proteoglycane components of fractones, which moderate their inhibitory effect on neurogenesis. It is therefore plausible that, in form of fractones, the neurogenic subependymal layer comprises a specialized ECM structure regulating NSC proliferation.

Several molecular microenvironment components of the SEZ have already been found to modulate neurogenesis. A well-studied ECM niche regulator is the matricellular protein TnC, an extracellular glycoprotein mostly expressed in NSC niches (Faissner et al. 2017; Tucić et al. 2021), but hardly in the remainder of adult murine brain tissue (Šekeljčić and Andjus 2012). In vitro, neural stem and progenitor cells derived from the SEZ of TnC knockout mice exhibit a reduced responsiveness to epidermal growth factor (EGF) stimulation, which might be a result of the observed reduced EGF-receptor expression (Schaberg et al. 2022). TnC has already been proposed to be involved into the EGF-receptor acquisition of NSCs (Garcion et al. 2004). Additionally, the TnC knockout appeared to reduce the cell cycle length of neural stem and progenitor cells and seemed to influence the migratory behavior of neuroblasts (Schaberg et al. 2022). Taken together, TnC can be hypothesized to be involved in modulating NSC activation, proliferation, and neuroblast migration.

Also, heparan sulfate glycosaminoglycans are reported to be an integral component of the SEZ microenvironment (Kerever and Arikawa-Hirasawa 2021), as side chains of heparan sulfate proteoglycans such as heparan sulfate proteoglycan 2 (Hspg2) were shown to moderate receptor binding of FGF2 (Brickman et al. 1995; Aviezer et al. 1994). In vivo, the knockout of Hspg2 leads to a reduced number of NSCs, transit amplifying progenitor cells, and neuroblasts in the SEZ (Kerever et al. 2014). Also, in contrast to an exclusive FGF2 injection, co-injection of FGF2 and the HPSG side chain digesting enzyme heparinitase-1 into the LV diminished the proliferative effect of FGF2 on the SEZ (Douet et al. 2013). Taken together, Hspg2 appears to be relevant for neurogenesis, possibly by mediating FGF2 signalling in the SEZ niche.

In the basement membrane of cerebral blood vessels, the laminin family of ECM proteins is present. In the SEZ, laminin also exists in fractones. Fractone bulbs contain laminin α 5 and laminin α 2 chains, which are produced by ependymal cells. Deleting the LAMA5 gene in ependymal cells provoked an increase of laminin α 2 expression and SEZ cell proliferation (Nascimento et al. 2018). In vitro, an artificial hydrogel-based microenvironment enriched with a peptide containing a laminin motive and polylysine exerted an augmenting effect on neurogenesis (Farrukh et al. 2017). Laminin was also found to increase the number of primary neurospheres (Hall et al. 2008), suggesting a beneficial effect of laminin on proliferation or survival of neural stem or progenitor cells. Taken together, laminin influences SEZ stem cell physiology.

Thus, ECM molecules present in the SEZ have already been found to be involved in neurogenesis, as exemplified with TnC, heparan-sulfate proteoglycans, and laminin.

Thbs4 is an ECM component particularly expressed in neurogenic regions. In the adult RMS Thbs4 might be involved in the guidance of neuroblasts to the RMS, as Thbs4 deficient mice exhibit a disorganized RMS and a reduced number of neuroblasts arriving at the OB (Girard et al. 2014). Furthermore, evidence suggests that the ECM proteins tenascin-R and Reelin switch the tangential migration mode of neuroblasts in the RMS to a radial mode in the OB (Hack et al. 2002; David et al. 2013). Hence, in the RMS ECM components influencing the migratory behaviour of neuroblasts could be identified.

Taken together, one architectural specialization and some molecular components of the SEZ influencing neurogenesis of the SEZ have already been detected. However, ample knowledge about the physical properties of the matrix and its influence on neurogenesis is lacking. Additionally, it appears unlikely that the sparse list of molecular factors rendering the niche neurogenic is already complete, which calls out to a comprehensive proteome analysis.

1.1.2.2 Vasculature of the SEZ Niche

Beside the ECM, the SEZ vasculature regulates adult neurogenesis. Migrating neuroblasts use blood vessels as guidance to the OB (Bovetti et al. 2007; Snapyan et al. 2009; Fujioka et al. 2019), and proliferating SEZ cells have been found to lie preferentially adjacent to the vascular niche (Tavazoie et al. 2008). One facility of vascular influence is cell-to-cell interaction. Transit-amplifying cells contact blood vessels directly at sites devoid of astrocyte end feet and pericytes (Tavazoie et al. 2008). Immediate contact with endothelial cells keeps the NSCs in a quiescent state via ephrinB2 and Jagged1 (Ottone et al. 2014). Endothelial laminin appears to bond SEZ NSCs through $\alpha6\beta1$ -integrin, (Shen et al. 2008; Rosa et al. 2016), as binding of neurosphere cells to an endothelial cell monolayer was inhibited by blocking the interaction of $\alpha6\beta1$ -integrin and laminin. Furthermore, in vivo infusion of an $\alpha6$ -integrin blocking antibody significantly increased the distance between progenitor cells and the vasculature. The progenitor cell binding to endothelial laminin via $\alpha6\beta1$ -integrin was suggested to regulate stemness, as inhibiting the contact of endothelial cells and stem cells decreased the number of Sox2+ cells in a SEZ and endothelial cell coculture (Rosa et al. 2016). Another means of vascular influence on SEZ neurogenesis are signalling molecules. The chemokine stromal cell-derived factor 1 (SDF1) promotes the migration and binding of activated NSCs and progenitor cells to the vasculature by interacting with the chemokine receptor CXCR4 (Kokovay et al. 2010; Zhu et al. 2019). Interestingly, in vitro SDF1 was also found to promote the expression of $\alpha6$ -integrin in activated NSCs and progenitor cells (Kokovay et al. 2010). So, SDF1 appears to regulate the homing of neural stem and progenitor cells to the vasculature. Endothelial cells express Betacellulin, an epidermal growth factor receptor binding cytokine. Intraventricular infusion of Betacellulin leads to an increased NSC proliferation in the adult murine brain, and blocking Betacellulin in vivo leads to a reduced number of SEZ stem and progenitor cells (Gómez-Gaviro et al. 2012). Hence, Betacellulin not only appears to be beneficial, but also necessary for physiological NSC proliferation in the SEZ. Pigment-epithelium-derived-factor, expressed by vascular endothelial cells, participates in SEZ NSC regulation. It promotes self-renewal

in adult SEZ stem cells (Ramírez-Castillejo et al. 2006) by regulating the Notch signalling pathway (Andreu-Agulló et al. 2009). Brain-derived neurotrophic factor secreted by endothelial cells was shown to promote neuroblast migration (Snayyan et al. 2009; Petridis and El Maarouf 2011). Furthermore, the SEZ vascular niche exhibits a blood-brain-barrier of increased permeability compared to non-neurogenic brain tissue (Tavazoie et al. 2008), facilitating the hypothesis of a potential influence of small blood-borne factors on the regulation of neurogenesis.

Thus, secreted molecules and cell-to-cell contact establish the vascular influence on neurogenesis. However, if and how the more permeable blood-brain-barrier engages in neurogenesis is unknown.

1.1.2.3 Choroid Plexus, Cerebrospinal Fluid, and the SEZ Niche

The choroid plexus and the CSF were hypothesised to constitute an important part of the SEZ stem cell niche (Falcão et al. 2012). Type B cells of the SEZ directly contact the CSF with their apical process (Obernier and Alvarez-Buylla 2019). Thereby, NSCs are exposed to molecules secreted into the CSF. To a large part, the CSF is produced by the choroid plexus. The adult choroid plexus expresses several signalling molecules, among them insulin-like growth factor 2 (IGF2), Slit-proteins, bone morphogenetic proteins, members of the FGF-family, EGF (Marques et al. 2011), and miRNA-204 (Lepko et al. 2019). CSF-derived IGF2 was found to bind to the ventricular surface and to promote the proliferation of progenitor cells in the developing brain (Lehtinen et al. 2011). IGF2 is also highly expressed in the adult choroid plexus (Marques et al. 2011) and present in the secretome of the choroid plexus of the adult LV (Silva-Vargas et al. 2016). Adult IGF2-knockout mice exhibited markedly reduced IGF2-mRNA levels in the choroid plexus. Interestingly, this knockout lead to a reduction in SEZ NSCs (Ziegler et al. 2019). Slit2, a protein with a chemo repulsive effect on migrating neurons in development (Hu 1999), is expressed in the choroid plexus. Transplanting a wild-type choroid plexus ectopically to the anterior LV of an adult mouse brain led to an almost complete inhibition of neuroblast migration towards the OB, while transplanting the choroid plexus of a Slit1/2 knockout mouse into the same location barely interfered with rostral neuroblast migration (Sawamoto et al. 2006). Hence, in the adult murine brain, the establishment of a dorsoventral Slit1 and Slit2 gradient by choroid plexus secretion can be hypothesised to be necessary for a physiological neuroblast migration to the OB. An increase in neurogenesis can be achieved by the injection of FGF2 or EGF into the LV of the adult murine brain (Kuhn et al. 1997). FGF2 was also found to be present in the secretome of the choroid plexus (Silva-Vargas et al. 2016). The choroid plexus produces and releases miRNA-204 into the CSF, which stabilizes the quiescence of NSC in the SEZ (Lepko et al. 2019). Additionally, the CSF flow itself regulates adult murine neurogenesis. Abolishing the CSF flow by an ependymal cilia defect impedes the coordinated migration of neuroblast (Sawamoto et al. 2006). Furthermore, CSF flow sensed by the epithelial sodium channel ENaC embedded in the apical process of Type B cells, promotes NSC proliferation by inducing intracellular calcium signalling (Petrik et al. 2018).

In summary, the CSF not only contains growth factors secreted by the choroid plexus, but also modulates neurogenesis. Though, which CSF molecules bind to or are enriched by the ECM of the SEZ is currently unknown.

1.2 Investigating the Microenvironment of the SEZ Niche

1.2.1 Aim of the Project

In summary, the SEZ niche is neurogenic, its ECM differs from non-neurogenic brain tissue, and signals from the choroid plexus as well as the vasculature modulate neurogenesis. Some mechanisms of how the SEZ microenvironment influences NSCs have been elucidated. However, so far, the register of components of the ECM is not complete, and how the extracellular proteins are assembled is to a large part unidentified. There is little knowledge about the influence of blood-borne factors in the SEZ. Given the rich choroid plexus secretome and the abundance of growth factors in the CSF, the few established influences on the niche may not be complete. Stem cells are mechanosensitive to CSF flow, however, the physical properties of the SEZ niche itself and whether they influence neurogenesis are unknown. To improve the understanding of what renders the SEZ niche neurogenic, this study sought to generate an inventory of niche constituents as complete as possible with state-of-the-art technology. The data generated was employed for the comparison to other brain regions, to foster the search for candidate niche neurogenesis regulators, to elucidate protein clusters, and to investigate physical properties rendering the niche neurogenic.

1.2.2 Choosing a Proteomic Approach

To generate an inventory of niche constituents, an unbiased, bottom-up omics approach is well suited. Although research has been dedicated to the SEZ transcriptome (Beckervordersandforth et al. 2010; Cogeda et al. 2014; Lim et al. 2006; Kalamakis et al. 2019; Llorens-Bobadilla et al. 2015; Cebrian-Silla et al. 2021; Mizrak et al. 2019), a comprehensive, unbiased proteome attempting to characterize this niche was lacking. However, the informative value of a transcriptomic analysis of a microenvironment is limited. Transcriptomic gene expression values have been found to be insufficient to throughout reliable predict protein abundance levels, for instance for the ECM (Schiller et al. 2015; Angelidis et al. 2019). One plausible reason for this is the low turnover of ECM proteins that allows the maintenance of high protein levels with low transcriptomic activity. Also, not only the level of transcriptional, but also translational activity can regulate protein production. Hence, the protein product of a gene can exhibit a low concentration while simultaneously featuring high mRNA levels. Therefore, a sufficient correlation between the proteome and transcriptome of the ECM in the SEZ cannot be assumed. Additionally, distant protein sources

like the choroid plexus or the blood stream can modify the SEZ niche. Information about this remote influence might not emerge in a SEZ transcriptome. Therefore, the generation and analysis of a SEZ proteome promises to uncover additional information about the niche physiology undetectable with transcriptomics. Consequently, this study targets the creation of a proteomic characterization of the SEZ stem cell niche. For the generation of the proteome data, mass spectrometry (MS) was employed.

1.2.3 Dissecting the SEZ Neurogenic Niche

Collecting tissue specimen of the SEZ for a MS analysis requires a method with high precision. The method must capture the 20-50µm thin paraventricular ribbon containing stem cells while excluding the tissue of the adjacent striatum. Furthermore, for analysing the extracellular microenvironment, the dissection must feature minimal tissue perturbation. Otherwise, soluble proteins such as growth factors or cytokines could easily be washed away. Additionally, insoluble core-matrisome proteins might become too strongly cross-linked for MS, for instance due to paraformaldehyde fixation. Hence, dissecting fresh frozen tissue is superior to fixed or stained tissue for the purpose of proteomic research of the extracellular microenvironment. A common SEZ wholemount dissection removes the SEZ with scissors in one piece (Mirzadeh et al. 2010). This standard dissection is fast with little tissue perturbation. However, striatal contamination of the samples cannot be securely excluded (Friess et al. 2021). Conversely, the laser capture microdissection (LCM) features the outstanding advantage of surpassing dissection precision. However, visualising the region of interest under the dissection microscope requires a tissue modification, such as a background staining. During a staining procedure, small or soluble proteins of interest, e.g., growth factors or cytokines, may be washed away. Furthermore, slides spend different time periods at room temperature during the laser removal. Also, the laser itself might denature proteins of interest. Concluding, despite featuring individual strengths, neither the wholemount dissection nor the LCM is ideally suited to collect SEZ tissue for MS. Thus, to combine the strengths of both the standard dissection and the LCM, a novel method termed Cryo-section Dissection (CSD) was developed (Friess et al. 2021). According to the CSD protocol, first the cortex and the corpus callosum covering the LVs are removed from the unfixed brain. After the removal of the choroid plexus, the unfixed brain is frozen on dry ice. Then, coronal sections of the brain are prepared. Finally, the SEZ and the medial wall of the LV, termed medial ependymal zone (MEZ) (Figure 1), are manually isolated from each section using a pre-cooled scalpel. The CSD provides sufficient precision to exclude striatal contamination from SEZ samples, while simultaneously featuring a short dissection time and minor tissue perturbation.

1.2.4 Achieving Sufficient Proteomic Depth with Mass Spectrometry

Due to the low abundance of potentially interesting cytokines or growth factors in the extracellular microenvironment, the proteomic characterization of the SEZ niche should achieve considerable depth. A MS analysis of the mouse brain detected over 11,500 proteins in a single run by matching the MS run against a deep proteome library of the brain, generated by a fractionated analysis of brain tissue and cells (Sharma et al. 2015). To reach comparable proteome coverage allowing a thorough ECM characterization and detection of novel ECM proteins defining the neurogenic niche, the CSD was combined with a library-matched single shot (LMSS) MS analysis. For the generation of the library, samples from four mice were pooled. Pooled samples were separated into eight fractions according to a nano-fractionation method (Kulak et al. 2017). In brief, the nano-fractionation method employs a rotor-valve that distributes peptides eluting from a high-performance liquid chromatography (HPLC) column. The valve pours the column content into a pre-defined number of fractions, and continually switches between these fractions after a constant time interval. In contrast to merely employing a HPLC-based peptide fractionation, the nano-fractionator allows loss-less fractionation of tissue amounts in the μg range, while still enabling the quantification of almost 10,000 proteins. Hence, for the analysis of a particularly small region such as the SEZ, this nano-fractionator seemed well suited to generate the deep proteome library. The four single-shot samples used to generate the proteome data set of the SEZ, MEZ, OB, and somatosensory cortex were matched based on retention time between each other and to the library, thereby collectively increasing the detection rate of individually indistinct peptide identifications. In a comprehensive MS study analysing tissue and bronchoalveolar lavage fluid of the murine lung in a bleomycin induced lung injury model (Schiller et al. 2015) the quantification of over 8,000 proteins was achieved. For quantifying detected proteins a label-free quantification (LFQ) algorithm was used. Thereby, a thorough matrisome characterization as well as the detection of novel ECM proteins upregulated upon lung injury was possible without requiring isotope labelling. For this study of the SEZ microenvironment, this label-free quantification algorithm was employed, allowing to quantify peptide intensities without isotope labelling (Cox et al. 2014). To correctly quantify a peptide, its abundance in every fraction must be summed up. To account for differences introduced by processing fractions separately, each fraction requires a normalization factor. This factor, however, is unknown in advance. The LFQ-algorithm solves this problem by postponing the normalization procedure. The algorithm sums up peptide intensities over all fractions with individual normalization coefficients as variables. Then, coefficients are determined by means of a nonlinear optimization model that minimises overall changes of all peptides in all fractions, exploiting the assumption that most proteins do not differ between two fractions.

The generated MS dataset was filtered for ECM proteins using the annotation available under <http://matrisome.org> and the uniprot database.

1.2.5 Comparison groups

The somatosensory cortex, the MEZ, and the OB were included in the MS analysis as comparison groups (Figure 1). The exploration of factors determining the neurogenic potential of the stem cell niche is facilitated by the direct comparison to a non-neurogenic microenvironment. This is the reason for the inclusion of the somatosensory cortex in the analysis, given that this region canonically exhibits no neurogenesis at all in an uninjured adult mammalian brain. The MEZ consists of ependymal cells together with a subependymal layer of astrocytes covering the septum. SEZ and MEZ exhibit a high structural and cellular similarity. Both regions lie adjacent to the ventricles and are thereby exposed to the CSF, host ependymal cells as well as astrocytes and exhibit fractones. However, in contrast to the SEZ, the MEZ harbours almost no NSCs or neuroblasts. Hence, the comparison to the MEZ promises to foster the detection of what renders the SEZ microenvironment neurogenic. The OB was included into the MS experiment to compare the microenvironment of the site of stem cell repository and proliferation to the site of neuronal differentiation and integration.

This study pursued the proteomic characterization of the SEZ stem cell niche of the murine brain. A novel dissection method termed CSD (Friess et al. 2021) specifically developed for this purpose in combination with LMSS MS was used to achieve a precise and deep proteome of the SEZ stem cell niche. The data was analysed to generate a bioinformatical characterization of the niche, thereby enabling the detection of the neurogenesis regulator Transglutaminase 2 and potential candidate niche regulators such as S100a6, Kininogen 1, and C1qI3 as well as the identification of the influence of niche stiffness on NSCs (Kjell et al. 2020). This proteomic in-depth characterization of the SEZ stem cell niche advanced the current understanding of SEZ stem cell niche physiology. Furthermore, the provided data constitutes a powerful resource comprising the potential to foster future research of the neurogenic stem cell microenvironment and might support the development of therapeutic approaches addressing neural cell loss.

RESULTS

2. Results

2.1 Aim of the study I – Developing and Validating the Cryo-section Dissection

The aim of this project was to develop a method capable of dissecting the unfixed and unaltered subependymal zone precisely without contamination by adjacent tissue, especially suitable for mass spectrometry analysis of the extracellular microenvironment.

“Cryo-section Dissection of the Adult Subependymal Zone for Accurate and Deep Quantitative Proteome Analysis.”

Christian Friess, Magdalena Götz, and Jacob Kjell

For this publication as first author, I developed and validated the Cryo-section Dissection method for the sub- and medial ependymal zone of the lateral ventricles, performed the data analysis and experiments except the standard dissection protocol of the subependymal zone, which was done by Tatiana Simon-Ebert and the proteolytic tissue sample preparation for mass spectrometry, which was done by Jacob Kjell. I wrote and revised the manuscript as well as the video script together with Jacob Kjell and Magdalena Götz.

The paper is published in the Journal of Visualized Experiments (176), October 7, 2021, e63047, doi: [10.3791/63047](https://doi.org/10.3791/63047)

As open access paper and author of this JoVe article, I have the right to include it in a thesis or dissertation, provided it is not published commercially.

Cryo-section Dissection of the Adult Subependymal Zone for Accurate and Deep Quantitative Proteome Analysis

Christian Friess¹, Magdalena Götz^{1,2,3}, Jacob Kjell^{1,2,4}

¹ Division of Physiological Genomics, Biomedical Center, Ludwig Maximilian University of Munich ² Institute for Stem Cell Research, Helmholtz Zentrum München ³ SYNERGY, Excellence Cluster Systems Neurology, University of Munich ⁴ Department of Clinical Neuroscience, Karolinska Institutet

Corresponding Author

Jacob Kjell
jacob.kjell@ki.se

Citation

Friess, C., Götz, M., Kjell, J. Cryo-section Dissection of the Adult Subependymal Zone for Accurate and Deep Quantitative Proteome Analysis. *J. Vis. Exp.* (176), e63047, doi:10.3791/63047 (2021).

Date Published

October 7, 2021

DOI

10.3791/63047

URL

jove.com/video/63047

Abstract

The subependymal neurogenic niche consists of a paraventricular ribbon of the lateral ventricular wall of the lateral ventricle. The subependymal zone (SEZ) is a thin and distinct region exposed to the ventricles and cerebrospinal fluid. The isolation of this niche allows the analysis of a neurogenic stem cell microenvironment. However, extraction of small tissues for proteome analysis is challenging, especially for the maintenance of considerable measurement depth and the achievement of reliable robustness. A new method termed cryo-section-dissection (CSD), combining high precision with minimal tissue perturbation, was developed to address these challenges. The method is compatible with state-of-the-art mass spectrometry (MS) methods that allow the detection of low-abundant niche regulators. This study compared the CSD and its proteome data to the method and data obtained by laser-capture-microdissection (LCM) and a standard wholemount dissection. The CSD method resulted in twice the quantification depth in less than half the preparation time compared to the LCM and simultaneously clearly outperformed the dissection precision of the wholemount dissection. Hence, CSD is a superior method for collecting the SEZ for proteome analysis.

Introduction

As neurogenesis is restricted in the adult brain, various central nervous system repair strategies would greatly benefit from an increased understanding of the underpinnings of adult neural replacement. Rodents have helped us understand the basic mechanisms of postnatal neurogenesis, although it should be noted that adult neurogenesis is greatly species-dependent. In mice, there are three adult neural stem cell

(NSC) niches. The hypothalamus is an adult NSC niche with neurogenic potential^{1,2}, while continuous adult neurogenesis is mainly restricted to the hippocampus³ and the SEZ of the lateral walls of the lateral ventricles^{4,5,6}. The SEZ is the largest germinal region containing NSCs (type B cells) that develop into neuroblasts (type A cells) via transit-amplifying progenitor cells (type C cells). The SEZ contains 20-35%

of type B cells, 1-15% of type C cells, 1-30% of type A cells, and 25-50% of ependymal cells⁷. The SEZ features a complex microarchitecture, with endothelial cells, microglial cells, and ependymal cells residing in and influencing the stem cell niche^{8,9,10}. Although neurons are scarce in the SEZ, axons emanating from distant sources such as the striatum, the ventral tegmental area, or the hypothalamus reach and influence type B cells⁴. A unique feature of this stem cell niche is the separation between the site of proliferation and the site of differentiation. After proliferation, the neuronal progenitors migrate several millimeters from the SEZ to the olfactory bulb, where they terminally differentiate into neurons and integrate into pre-existing neural circuits. Investigations into cell-intrinsic programs associated with neurogenesis have already provided knowledge important for experimental therapeutic cell reprogramming and transplantation strategies^{15,16,17,18,19,20}. However, cell-extrinsic signals also regulate neurogenesis, and tissue environments can determine the neurogenic fate of stem cells^{11,12,14,21,22,23}. Consequently, the investigation of the microenvironment of the neurogenic niches and its interaction with the stem cells is of crucial importance.

The extracellular matrix (ECM) and other secreted proteins are a large part of the microenvironment. For accurate identification and quantification, a proteomic approach is better suited than a transcriptomic approach to determine ECM composition due to the low correlation between transcriptome and protein levels for ECM^{24,25}. Moreover, there is substantial evidence that niche regulators in the SEZ are not exclusively produced by cells populating the niche itself. More distant locations, such as the choroid plexus, secrete modulatory signals transmitted to the stem cells via the cerebrospinal fluid^{22,23}. Investigating the niche proteome can help to identify niche regulators present in the niche

independent of their production site, given that a substantial proportion of the extracellular microenvironment is assembled by proteins.

To collect the murine ventricular zone for unbiased proteomic analysis, a method with high precision is required, capturing the ca. 50 μm thin paraventricular ribbon containing stem cells while excluding the tissue of the adjacent striatum. Furthermore, tissue perturbation during the dissection must be minimized for analyzing the extracellular microenvironment because soluble proteins, including growth factors or cytokines, could be washed away easily. Although it is possible to analyze the mass spectra of fixed tissue, the required agent, such as paraformaldehyde, will reduce the protein identification depth and may introduce posttranslational modifications. A common wholemount SEZ dissection, e.g., for the collection of cells for fluorescence-activated cell sorting analysis, removes the whole SEZ with scissors²⁶. This standard dissection is fast with minimal tissue perturbation. However, striatal contamination of the samples cannot be avoided. Conversely, LCM has the outstanding advantage of superior dissection precision. However, LCM may introduce tissue perturbations, for instance, due to background staining or laser-caused protein denaturation. To combine the strengths of the wholemount dissection and LCM, a novel method that is compatible with MS, termed cryo-section-dissection (CSD), was developed (**Figure 1A-D**). The CSD allows the extraction of the SEZ and the dissection of the SEZ of the medial walls of the lateral ventricles (MEZ), which is an ideal, mostly non-neurogenic control region for the SEZ (see the protocol). The niche proteome obtained by the combination of CSD and state-of-the-art MS methods proved to be useful for the characterization and identification of novel regulators in this

adult NSC niche²⁵. Hence, this method will be useful for the determination of SEZ tissue protein composition.

Protocol

All experimental procedures in this study were performed in accordance with German and European Union guidelines and were approved by the institutional animal care committee and the government of upper Bavaria (Regierung von Oberbayern). Only male C57Bl6 mice between the ages of 8-10 weeks were used for the experiments.

1. Preparation of the mouse brain (~ 15 min per mouse)

1. Prepare the dissection medium by adding 5 mL of 1 M HEPES (final concentration 10 mM) to 500 mL of 1x Hank's Balanced Salt Solution (HBSS).

NOTE: The storage time of the dissection medium (+4 °C) should not exceed 2 weeks.

2. Sacrifice the mice by cervical dislocation and carefully dissect the brain.

NOTE: When investigating the ECM, the tissue should preferably be unmodified. Cervical dislocation keeps dissection time as short as possible, thereby preventing post-mortal enzymatic autodigestion as much as possible. If removal of blood is critical to the research question, simply perfuse the mouse transcardially with phosphate-buffered saline (PBS) before removing the brain.

3. Extract the brain by manual dissection and place it in a culture dish containing ice-cold dissection medium (**Figure 1B - 1**).

NOTE: Keep the brains in dissection medium on ice throughout the dissection.

4. Remove the olfactory bulb (OB) with a scalpel (**Figure 1B - 2**) by a straight coronal cut between the OB and the anterior pole of the cortex.

5. Remove the anterior pole of the cortex with the scalpel using a coronal cut to make the lateral ventricles visible in the coronal plane (**Figure 1B - 3**).

NOTE: Make sure the coronal cut is made ~5 mm rostrally from the optic chiasm; otherwise, the rostral part of the SEZ/MEZ will be lost.

6. Using scissors, open both lateral ventricles from the top, starting with a sagittal section from the cortical surface to the ventricular lumen, and elongate this cut in a c-shaped manner following the ventricular flexion (**Figure 1B - 4**).

7. Connect the caudal ends of the left and right sagittal incision by means of an additional coronal cut with the scissors.

NOTE: The three cuts now form a trapezoid and will facilitate the removal of the cortex and corpus callosum in the next step.

8. Remove the cortex and corpus callosum covering the lateral ventricles using forceps (**Figure 1B - 5**). Then, remove the cortex and corpus callosum that cover the medial ventricular walls. Here, make additional cuts if the tissue is attached to the medial ventricular walls, or simply lift the cortex and corpus callosum with scissors to dislodge the tissue.

9. Carefully spread the ventricular walls with forceps (**Figure 1B - 6**). Remove the choroid plexus with forceps.

NOTE: Complete removal of the choroid plexus is important to avoid interference with the following dissection steps and avoid potential contamination of the SEZ/MEZ samples.

- Put the brain on a glass slide and place the glass slide on top of dry ice to freeze the brain. Maintain the ventricular walls in the open configuration.

NOTE: Ensure enough distance between the lateral and medial walls of the ventricle to facilitate precise and exclusive dissection of SEZ and MEZ. If the tissue contracts back into a closed configuration, use the forceps to fix the walls in the desired position during freezing. Avoid any damage to the SEZ/MEZ. Try applying minimal force, mainly at the top edge of the opened ventricles.

2. Sectioning of the prepared brain (~ 15 min per mouse)

- Cut 50-100 μm thick coronal sections of the brain until the end of the lateral ventricle using a cryostat and mount the sections onto glass slides. Ensure that the brain is attached to the cryostat attachment plate at the hindbrain with OCT medium and that no OCT comes in contact with the forebrain, especially at the ventricles.

NOTE: OCT medium will interfere with MS measurements. However, if the tissue will be used for an antibody assay, it is unnecessary to exclude OCT medium. The use of coated glass slides is not recommended. Coated slides apply too much adhesive force on the tissue, thereby impeding the translocation of the tissue specimen from the slides into the microcentrifuge tube in the following steps.

3. Free-hand dissection of brain slices (~ 30 min per mouse)

- Place the glass slides with the brain sections on dry ice under a dissection microscope (**Figure 1C - 1**).

- Prepare the microcentrifuge tubes on dry ice, and ensure that the tubes stay on dry ice for at least 1 min to be sufficiently cold before specimen transfer.

NOTE: Use microcentrifuge tubes of high quality, as some low-quality tubes may shed plastic in the subsequent tissue digestion steps associated with MS measurements.

- Lift the slices from the dry ice for 15-30 s to achieve a brief, incomplete thawing to render the compact myelin of the striatum observable as dense white dots.

NOTE: Locating the border between the SEZ and the striatum becomes feasible (**Figure 1C - 2**, see **Figure 2A** for the exclusion of myelin and a comparison with the wholemount method). If thawing takes too long, the process can be accelerated by pressing a glove-covered finger onto the opposite side of the glass slide. However, this maneuver should be practiced as excessive thawing occurs easily.

- Separate the SEZ with a precooled scalpel from the adjacent striatum (**Figure 1C,D**).
- Transfer the SEZ either as a whole piece or sectioned into 2-4 parts into a microcentrifuge tube by using the blunt edge of the cooled scalpel. If the tissue is to be used for another type of analysis other than MS, transfer the tissue specimen into the appropriate container instead (e.g., a 96-well plate).

NOTE: Cutting the completely frozen tissue may lead to tissue rapidly breaking away and falling off the slide. Cutting completely thawed tissue leads to the disintegration of the tissue. Ensure that the tissue is neither completely frozen nor completely thawed.

Representative Results

When following the above steps, the tissue samples in the microcentrifuge tubes are ready for and compatible with MS sample preparation. After sample preparation, we obtained ~5-7 μg of peptides per sample of either SEZ or MEZ per mouse. However, the final amounts of the peptides may depend on the MS preparation method. In the proteome comparisons below, protein identification and quantification depth (500-1,000 proteins per sample) were increased by computationally matching the peptide spectra to peptide spectra libraries created for each tissue region^{25,27}. Notably, the loss-less nano fractionation method used here for the creation of the peptide spectra libraries is currently not commercially available. The raw MS data were analyzed using the MaxQuant software²⁸, achieving mass accuracies in the parts per billion range²⁹. The Max Quant environment allows matching between MS runs. Protein abundance was quantified using a label-free quantification algorithm³⁰. Immunohistochemical staining was done on fresh frozen tissues and performed as previously reported²⁵ (see the **Table of Materials**).

Cryo-section-dissection

The complete SEZ and MEZ of adult mice ($n = 4$) were obtained using CSD (see **Figure 1** and protocol). The somatosensory cortex (Cx) was dissected with surgical scissors. Additional 4 mice were dissected in the same manner; however, the dissected tissue was pooled into one sample per region to create the proteome library (10,923 identified proteins) for increased protein identification and quantification in the individual samples²⁵. In the four individual samples, (mean \pm SD) $6,673 \pm 317.4$ proteins were quantified in the SEZ and $6,747 \pm 37.7$ in the MEZ. All the MS proteomics data were deposited in the

ProteomeXchange Consortium via the PRIDE³¹ partner repository, and the accession number for the proteomes reported here is ProteomeXchange: PXD016632 (<http://proteomecentral.proteomexchange.org>).

Comparison to wholemound dissection

Wholemound dissection was performed according to a standard protocol²⁶. Wholemound dissection revealed a similar number of proteins (approximately 6,000 for SEZ and 6,000 for Cx, $n = 4$ per group) compared to CSD²⁵. One of the intended improvements of using CSD for the SEZ, instead of a wholemound dissection protocol, is the reduction of potential striatal contamination. In SEZ samples contaminated with tissue from another region, detected candidate proteins cannot be allocated to a region as significant enrichment can result from the region of interest and the contaminator. Immunohistochemically, the myelin-associated glycoprotein (MAG) positive myelin-rich internal capsules of the striatum were identified in the wholemound samples but seldom in the CSD samples (**Figure 2A**). The striatal contamination in the wholemound samples could be confirmed by identifying the enrichment of myelin proteins in the SEZ compared to the somatosensory cortex (Cx) Grey Matter (GM) samples (**Figure 2B**). Note that large parts of the Cx GM, especially the upper Cx layers, are unmyelinated³².

As large fiber bundles pass through the striatum, contamination by this region resulted in the enrichment of myelin proteins compared to the Cx. The myelin proteins used as markers for striatal contamination in the SEZ samples were the myelin basic protein (MBP), the myelin-associated glycoprotein (MAG), the proteolipid-protein 1 (Plp1), and the 2',3'-cyclic-nucleotide 3'-phosphodiesterase (Cnp). All myelin-marker proteins were significantly enriched in the SEZ compared to the Cx. Conversely, comparisons

for the four myelin marker proteins in the CSD dataset yielded no significant differences when comparing SEZ to Cx (**Figure 2B**). Proteomic data of the striatum³³ supports the hypothesis that the enrichment of myelin proteins in the SEZ samples of the wholemount dissection was caused by the contamination with striatal tissue. Hence, the CSD largely prevented contamination by striatal tissue (rich in compact myelin) compared to a wholemount dissection.

Unbiased proteome analysis of non-dissociated tissue can reveal interesting extracellular proteins. With improved dissection using the CSD, extracellular-associated proteins were significantly enriched in the samples compared to the wholemount samples (**Figure 2C**, annotation enrichment test). The CSD and wholemount dissection display a comparable enrichment of the gene ontology (GO) terms "extracellular vesicular exosome" and "extracellular region part." However, the GO term "Matrisome-associated" is slightly more enriched in the CSD than in the wholemount dissection. Accordingly, the ECM cross-binding enzyme and recently discovered neurogenesis regulator transglutaminase-2 (Tgm2) were found enriched in the SEZ compared to Cx using the CSD²⁵. In contrast, no difference was found between SEZ and Cx samples obtained by the wholemount dissection (**Figure 2D**). Proteomic data of the striatum³³ support the hypothesis that the detection of the neurogenesis regulator Tgm2 by wholemount dissection was impeded by the contamination with striatal tissue. Hence, overall, the cryo-section-dissection is a successful but also necessary improvement to the standard dissection for niche-specific proteome analysis.

Comparison to Laser-capture-microscopy

The front half of the SEZ and the MEZ of 3 adult mice were obtained for LCM (**Figure 3A**). Overall, the LCM method

exhibits some disadvantages, specifically regarding tissue perturbation and efficiency. To visualize the region of interest under the dissection microscope, background staining is necessary, potentially washing away small or soluble proteins of interest, e.g., growth factors, cytokines, or ECM regulators such as enzymes. Furthermore, slides spend varying times at room temperature during laser removal. Moreover, the laser itself might denature proteins of interest.

CSD has a considerable advantage over LCM regarding the time and effort necessary to perform the dissection: step 1 of the protocol must be performed similarly for both CSD and LCM; without this step, ventricular walls remain adherent, making the separation of MEZ and SEZ samples difficult. Given that the CSD sections (100 μm) are 6-7 times thicker than the maximum thickness³⁴ of the LCM sections (15 μm), step 2 (sectioning of the brain) and step 3 (removing the MEZ and SEZ from each coronal section) will take at least 6-7 times longer for LCM. The necessary background staining and setting up the laser microscope will consume additional time. Here, it took three times longer to harvest 50% of the SEZ and MEZ of 3 animals by LCM compared to 100% of the SEZ and MEZ of 4 animals by CSD, constituting an eightfold speed advantage of CSD. In summary, LCM not only requires a notable amount of additional effort, but the tissue is also subjected to a substantially longer period of manipulation and temperature changes that can compromise the dynamics and reliability of data generated by subsequent analysis.

The MS results of CSD were compared to the results from the laser capture microdissection (LCM). Both datasets were matched to the proteomic library generated by pooling CSD samples. On average, LCM yielded $3,441 \pm 270.0$ and $3,613 \pm 238.7$ individual proteins in the SEZ and medial ventricular zone, respectively (**Figure 3B**). Given

the remarkable difference in protein identification, principal component analysis (PCA) displayed distinct separation according to the dissection method (component 1: 62.7%, not shown). Component 2 displayed the greatest separation for SEZ and MEZ among the LCM samples (8.5%, **Figure 3C**). Component 3 also seems to separate LCM and CSD; however, this difference might result from method-based differences rather than the number of identified proteins (6.4%). Nevertheless, the overall regional separation remained strikingly distinct for the cryo-dissection data and vastly better than for LCM. This discrepancy in data dynamics may result from different times spent by the specimens at room temperature during the laser dissection or a higher susceptibility of small tissue amounts to variability in the subsequent proteomics protocols and mass spectrometry measurements.

To search for differences in the proteome profile of the ECM, a 2D annotation enrichment test between CSD and LCM was performed for the SEZ and MEZ (**Figure 3D**). Calculating the relative enrichment of GO terms between LCM and CSD samples allows the comparison of relative proteome dynamics of the ECM protein clusters between the two methods despite the unequal amount of tissue and the differences in the dissection protocol. The plots reveal a good correlation between LCM and CSD. The annotations "extracellular region part" and "extracellular membrane-bound organelle" are similarly enriched in both methods and regions. Hence, the increased time demand of LCM does not appear to be compensated by a relatively

higher sensitivity for ECM-associated proteins. Instead, CSD provides more robust identification/quantification when comparing the sample data for the neurogenesis and SEZ-associated ECM proteins Tgm2, Thrombospondin-4 (Thbs4), S100a6, and Tenacin-C (Tnc) (**Figure 3E**). In the case of TnC, although quantified in all samples, only CSD displayed enrichment for SEZ compared to MEZ. Nevertheless, the SEZ-associated basal membrane proteins Nidogen-1 (Nid1), Laminin subunit beta-2 (Lamb2), and basement membrane-specific heparan sulfate proteoglycan core protein (Hspg2)³⁵ displayed an even more robust enrichment in the SEZ (compared to MEZ) in the LCM samples than in the CSD samples (not shown). Hence, CSD can provide tissue samples that provide an accurate and deep quantitative proteome for SEZ characterization in a reasonable timeframe, without worrying about compromised tissue integrity or protein loss.

Statistics

Statistical testing, 2D annotation enrichment tests, and PCA were done in the Perseus environment. Proteins were included in the analysis if a valid value was detected for each method in at least one sample. Protein abundance and number comparisons were visualized using data analysis software (see the **Table of Materials**). A permutation-based control of the false discovery rate (FDR) (FDR was set to 0.05, 250 randomizations) was employed for protein comparisons. For the 2D-annotation enrichment tests³⁶, the displayed GO terms are significantly enriched (FDR was set to 0.02 using the Benjamini-Hochberg FDR-control method).

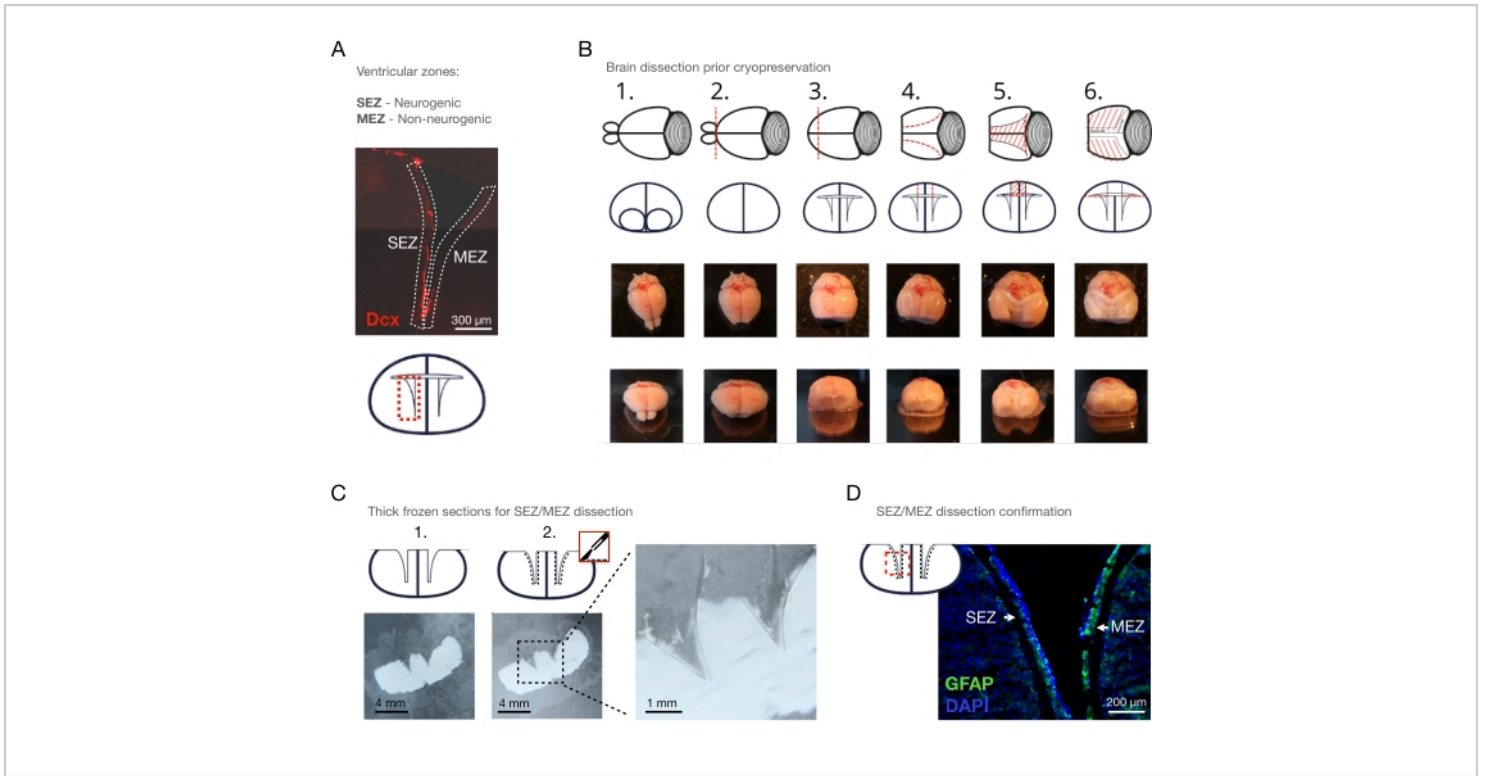


Figure 1: The Cryo-Section-Dissection method. (A) Overview of the region of interest: the lateral ventricle with the neurogenic SEZ and the non-neurogenic MEZ. Neuroblasts immunostained with Dcx. (B) Stepwise removal of the OB, the anterior pole, the cortex, and corpus callosum above the ventricles and the choroid plexus: 1. placement in dissection medium, 2. removal of OB, 3. removal of the anterior pole of the cortex, 4. sagittal incisions of the ventricular top, 5. removal of the ventricular top, 6. spreading of the ventricular walls. (C) 100 µm coronal slices of the fresh-frozen mouse brain, (1.) before and (2.) after the removal of the ventricular walls with an ice-cold scalpel. Scale bars = 4 mm (D) Staining of a coronal section of a lateral ventricle (GFAP: **green**; DAPI: **blue**), showing the SEZ and MEZ dissected with the CSD. Scale bars = 300 µm (A), 200 µm (D). Abbreviations: CSD = cryo-section dissection; SEZ = subependymal zone; MEZ = medial ependymal zone; Dcx = Doublecortin; OB = olfactory bulb; GFAP = glial fibrillary acidic protein; DAPI = 4',6-diamidino-2-phenylindole. [Please click here to view a larger version of this figure.](#)

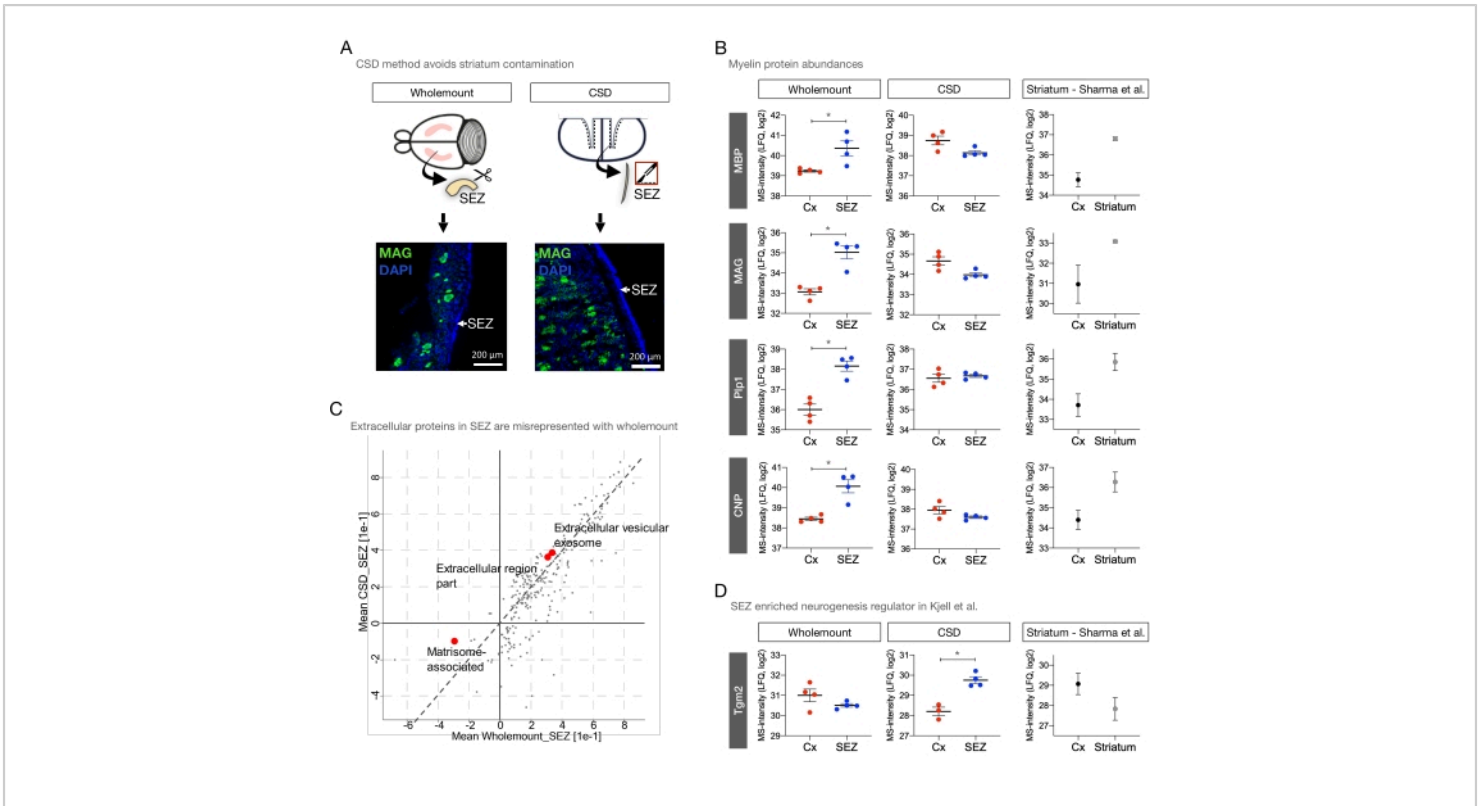


Figure 2: Superior dissection-precision with the cryo-section-dissection compared to wholmount dissection. (A) Immunohistochemical image of an SEZ sample obtained by wholmount dissection (left). The inclusion of myelin-rich striatal tissue is visualized by staining against MAG (green). Staining of a SEZ dissected with the CSD (right). In CSD, almost all the striatal myelin (staining against MAG, green) is excluded from the sample ribbon. Nuclei were visualized using DAPI (blue). (B) Comparison of myelin marker enrichment in SEZ vs. Cx from wholmount (MBP: $p = 0.0074$; MAG: $p = 0.0016$; Plp1: $p = 0.0011$; CNP: $p = 0.0029$) and CSD (MBP: $p = 0.0667$; MAG: $p = 0.0236$; Plp1: $p = 0.3420$; CNP: $p = 0.1842$). (C) 2D-annotation enrichment test comparing the wholmount-SEZ with the CSD-SEZ samples. The GO terms extracellular space and Matrisome-associated are more enriched in the CSD data than in the wholmount data. (D) The protein abundance of the NSC regulator Tgm2²⁵ plotted for the wholmount dissection and the CSD. Tgm2 is significantly enriched in the SEZ compared to the Cx in CSD (CSD: $p = 0.0029$; Wholmount: $p = 0.1775$). For B and D: As reference, proteome data from Sharma et al.³³ with measurements of striatum and cortex plotted for the corresponding proteins displayed in the wholmount and CSD samples. Scale bars = 200 μ m (A). Abbreviations: CSD = cryo-section dissection; SEZ = subependymal zone; MAG = myelin-associated glycoprotein; Cx = somatosensory cortex; MBP = myelin basic protein; Plp1 = proteolipid-protein 1; CNP = 2',3'-cyclic-nucleotide 3'-phosphodiesterase; GO = gene ontology; NSC = neural stem cell; Tgm2 = transglutaminase 2; DAPI = 4',6-diamidino-2-phenylindole; LFQ = label-free quantitation. [Please click here to view a larger version of this figure.](#)

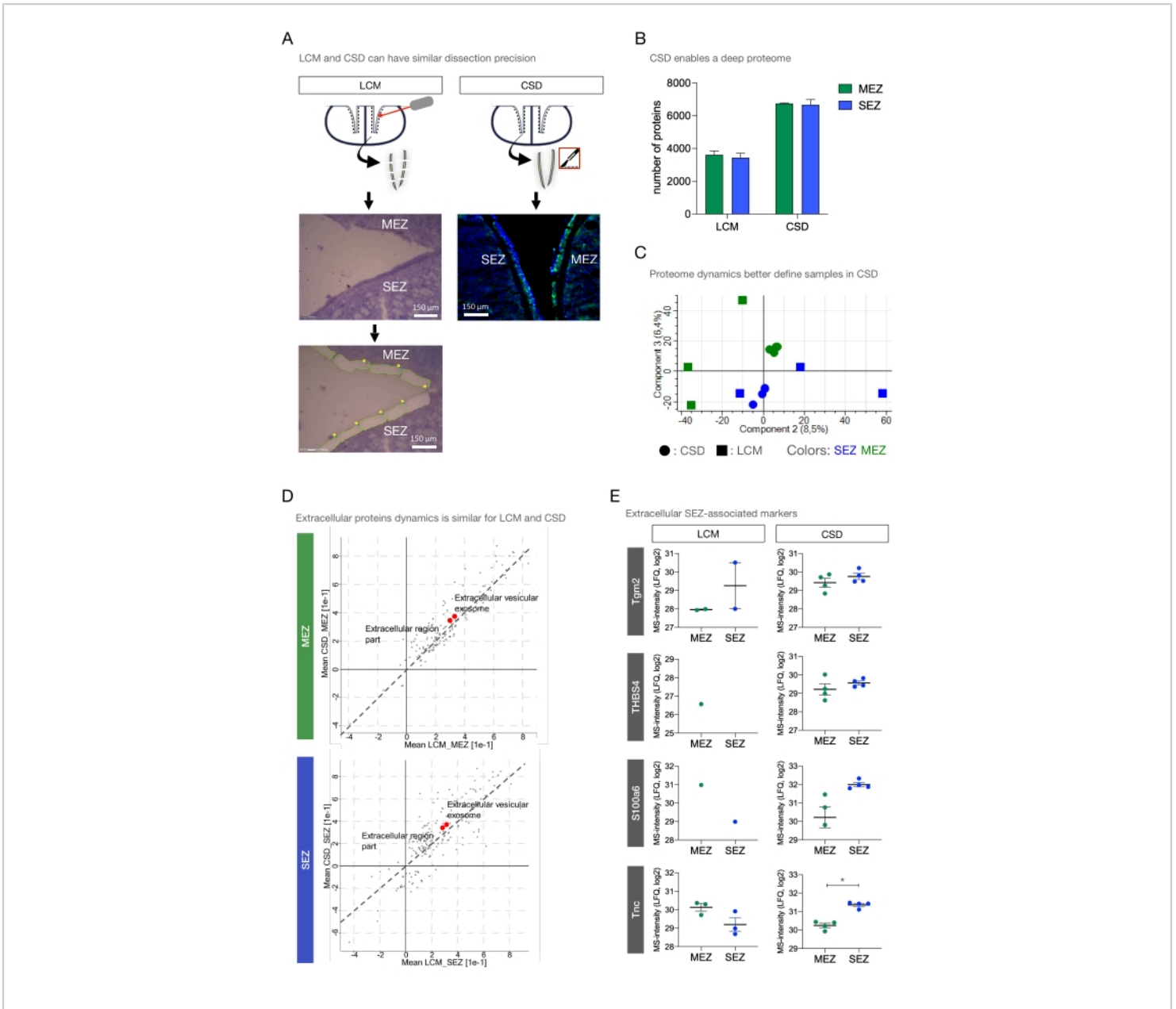


Figure 3: Improved extracellular protein quantification with cryo-section-dissection compared to LCM. (A) Cresyl violet staining of a lateral ventricle before and after laser capture of the SEZ and MEZ (left). For comparison, the CSD incision of the SEZ and MEZ (right). Scale bars = 150 μm. **(B)** Comparison of the number of detected proteins in the SEZ and MEZ samples from CSD and LCM. Data are presented as mean ± SD. **(C)** Principal component analysis of the SEZ and MEZ samples comparing CSD and LCM (component 2: 8.5% of the variance; component 3: 6.4%). **(D)** 2D annotation enrichment of the cryo-section- and laser-dissected MEZ (Top) and SEZ (Bottom). The GO terms extracellular organelle and extracellular region part are significantly enriched (red dots). **(E)** Abundances of extracellular SEZ-associated marker proteins in SEZ and MEZ for LCM (Tnc: $p = 0.3789$) and the CSD samples (Tgm2: $p = 0.2940$; S100a6: $p = 0.0218$; THBS4:

$p = 0.3941$; Tnc: $p = 0.0004$). Abbreviations: CSD = cryo-section dissection; LCM = laser-capture-microdissection; SEZ = subependymal zone; MEZ = medial ependymal zone; GO = gene ontology; Tnc = Tenascin-C; Tgm2 = transglutaminase 2; S100a6 = S100 calcium-binding protein A6; THBS4 = thrombospondin-4; LFQ = label-free quantitation. [Please click here to view a larger version of this figure.](#)

Discussion

The CSD method made it possible to precisely extract SEZ tissue and generate a reliable proteome with significant depth using MS. CSD displays a clear advantage compared to wholemount dissection in terms of greatly reduced striatal contamination of SEZ samples and extracellular protein enrichment. As it is also possible to detect a similar number of proteins in individual samples (~6,500 proteins per sample) with CSD and wholemount dissection, the additional time for CSD is well worth the effort. LCM provides more precise SEZ dissection but reached a lower proteome depth, with only 3,500 proteins per sample despite using the same MS protocol as CSD (library matching and label-free quantification). Importantly, variability was much greater, probably due to the eightfold longer preparation time per sample. PCA of the samples obtained by LCM and CSD reveals a clear separation of both methods with tight region-specific clusters robustly separated from each other. In contrast, the LCM samples displayed a more scattered distribution, which is probably in part due to the length of preparation. It is unclear whether collecting far more samples over a longer period would have yielded a proteome of equal robustness and depth with LCM. Calculating an estimate, collecting a similar sample volume as done for CSD would take 5-8 times longer with LCM, even up to 15 times longer if samples provided for the peptide spectra libraries were included, and much of it under thawed conditions. Furthermore, considering the additional perturbations of the tissue necessary for LCM (background staining, laser dissection), LCM provided little, if any, gain over CSD. Hence,

CSD can be deemed more suitable for extracellular proteome research, specifically for the SEZ.

Notably, if the region of interest is smaller than the SEZ (e.g., investigating only the ependymal cell layer), a free-hand approach falls behind the accuracy of the LCM. For example, using CSD to separate the ependymal from the subependymal layer is difficult as the ependymal layer is only a cell diameter wide, and the demarcation towards the subependymal layer is not visible for the naked eye in fresh frozen tissue. Hence, LCM will be a better choice than CSD if a precise dissection on a scale below 50 μm is more important than undisturbed tissue or keeping the dissection time short. For regions with a width of 50 μm and more, however, the precision of CSD is comparable to that of LCM for ECM protein analysis.

CSD has already proven to be useful by contributing to the investigation of the functional role of the ECM in the neurogenic niche²⁵. Hence, the continued application of CSD in the SEZ for various protein and proteome investigations (or even single-nucleus RNA sequencing) might lead to the detection of further neurogenesis regulators, stem cell activation markers, and a deeper understanding of SEZ stem cell niche physiology. Considering the decline of neurogenesis in the aging SEZ³⁷, a concise analysis of ECM changes of the SEZ of aged vs. young mice might promote the understanding of the exact niche mechanisms fostering NSC development and maintenance^{38,39}. Furthermore, the influence of inflammation and injury on SEZ neurogenesis is well established^{40,41,42,43}. The enrichment of blood-

derived fibrinogen in the SEZ after cortical brain injury and its influence on SEZ astroglialogenesis and scar formation⁴⁴ highlights the potential influence of trauma-induced microenvironment changes on the SEZ stem cell physiology. Hence, investigating the SEZ-ECM proteome in association with brain injury using CSD could help elucidate the mechanisms by which injury and inflammation affect neurogenesis. Importantly, the method could also be applicable to human brain neurogenic niches in health and disease as fresh frozen tissue can often be obtained from surgeries. Furthermore, given the species differences in adult neurogenesis, it would also be fascinating to apply the CSD method to other species, e.g., in association to striatal neurogenesis. Moreover, with other protein detection methods, differences in locally produced growth factors can be investigated accurately and efficiently using CSD for the SEZ and MEZ (e.g., ELISA).

Lastly, the dissection procedure could potentially be modified for accurate extraction of other brain regions, also for research questions not related to neurogenesis. For instance, CSD includes a brief semi-thawing step, during which compact myelin is visible as white areas distinct from the more translucent residual brain tissue. With a simple modification of the method, this feature would allow the precise dissection of only corpus callosum compact myelin tissue, which could be subjected to proteomic analysis of injury-related changes. A suggestion of a protocol modification that would allow the corpus callosum dissection is to omit steps 1.5-1.9 of the protocol and proceed directly to preparing the coronal sections instead of opening the ventricles to make the SEZ and MEZ accessible. Then, place the sections on dry ice, briefly lift and semi-thaw the slices, and simply remove the corpus callosum with a scalpel. This preparation should now

be ready for any analysis requiring an efficient dissection of native corpus callosum tissue.

In summary, this study presents a micro-dissection method that could be used for reliable ventricular neurogenic niche proteome analysis. The data underline the compatibility and utility of the CSD method together with MS-based proteomic analysis of the SEZ microenvironment. The combination of precision, efficiency, and minimal tissue perturbation render the CSD a valuable extension of existing methods.

Disclosures

The authors declare no competing interests

Acknowledgments

We wish to sincerely thank Mathias Mann for allowing us to perform large parts of the experiments in his laboratory, Fabian Coscia for help with LCM and proteome analysis, Tatiana Simon-Ebert for wholemount dissections, and Korbinian Mayr and Igor Paron for their technical help. We gratefully acknowledge funding from the German Research Council to MG (SFB870, TFR274), the EU (Ernet S-700982-5008-001), the ERC (aERC "NeuroCentro" to MG), the Swedish Society for Medical Research (SSMF, to JK) postdoctoral grant, and KI foundations and Funds (2020-01351, to JK).

References

1. Goodman, T., Hajihosseini, M. K. Hypothalamic tanycytes-masters and servants of metabolic, neuroendocrine, and neurogenic functions. *Frontiers in Neuroscience*. **9**, 387 (2015).

2. Chaker, Z. et al. Hypothalamic neurogenesis persists in the aging brain and is controlled by energy-sensing IGF-I pathway. *Neurobiology of Aging*. **41**, 64-72 (2016).
3. Kuhn, H. G., Toda, T., Gage, F. H. Adult hippocampal neurogenesis: a coming-of-age story. *Journal of Neuroscience*. **38** (49), 10401-10410 (2018).
4. Obernier, K., Alvarez-Buylla, A. Neural stem cells: origin, heterogeneity and regulation in the adult mammalian brain. *Development*. **146** (4), dev.156059 (2019).
5. Obernier, K. et al. Adult neurogenesis is sustained by symmetric self-renewal and differentiation. *Cell Stem Cell*. **22** (2), 221-234.e8 (2018).
6. Bordiuk, O. L., Smith, K., Morin, P. J., Semenov, M. V. Cell proliferation and neurogenesis in adult mouse brain. *PLoS One*. **9** (11), e111453 (2014).
7. Doetsch, F., Garcia-Verdugo, J. M., Alvarez-Buylla, A. Cellular composition and three-dimensional organization of the subventricular germinal zone in the adult mammalian brain. *Journal of Neuroscience*. **17** (13), 5046-5061 (1997).
8. Lim, D. A., Alvarez-Buylla, A. The adult ventricular-subventricular zone (V-SVZ) and olfactory bulb (OB) neurogenesis. *Cold Spring Harbor Perspectives in Biology*. **8** (5), a018820 (2016).
9. Sato, K. Effects of microglia on neurogenesis. *Glia*. **63** (8), 1394-1405 (2015).
10. Tavazoie, M. et al. A specialized vascular niche for adult neural stem cells. *Cell Stem Cell*. **3** (3), 279-288 (2008).
11. Sirko, S. et al. Chondroitin sulfates are required for fibroblast growth factor-2-dependent proliferation and maintenance in neural stem cells and for epidermal growth factor-dependent migration of their progeny. *Stem Cells*. **28** (4), 775-787 (2010).
12. Mercier, F. Fractones: extracellular matrix niche controlling stem cell fate and growth factor activity in the brain in health and disease. *Cellular and Molecular Life Sciences: CMLS*. **73** (24), 4661-4674 (2016).
13. Mercier, F., Kitasako, J. T., Hatton, G. I. Anatomy of the brain neurogenic zones revisited: fractones and the fibroblast/macrophage network. *Journal of Comparative Neurology*. **451** (2), 170-188 (2002).
14. Nascimento, M. A., Sorokin, L., Coelho-Sampaio, T. Fractone bulbs derive from ependymal cells and their laminin composition influence the stem cell niche in the subventricular zone. *Journal of Neuroscience*. **38** (16), 3880-3889 (2018).
15. Chen, G. et al. In vivo reprogramming for brain and spinal cord repair. *eNeuro*. **2** (5), ENEURO.0106-15.2015 (2015).
16. Zhang, Q., Chen, W., Tan, S., Lin, T. Stem cells for modeling and therapy of Parkinson's disease. *Human Gene Therapy*. **28** (1), 85-98 (2017).
17. Wei, C., Xiong, S., Cheng, L. Reprogramming of fibroblasts to neural stem cells by a chemical cocktail. *Methods in Molecular Biology*. **2117**, 265-270 (2020).
18. Tian, Z., Zhao, Q., Biswas, S., Deng, W. Methods of reactivation and reprogramming of neural stem cells for neural repair. *Methods*. **133**, 3-20 (2018).
19. Heinrich, C. et al. Sox2-mediated conversion of NG2 glia into induced neurons in the injured adult cerebral cortex. *Stem Cell Reports*. **3** (6), 1000-1014 (2014).
20. Masserdotti, G. et al. Transcriptional mechanisms of proneural factors and REST in regulating neuronal

- reprogramming of astrocytes. *Cell Stem Cell*. **17** (1), 74-88 (2015).
21. Seidenfaden, R., Desoeuvre, A., Bosio, A., Virard, I., Cremer, H. Glial conversion of SVZ-derived committed neuronal precursors after ectopic grafting into the adult brain. *Molecular and Cellular Neurosciences*. **32** (1–2), 187-198 (2006).
 22. Lepko, T. et al. Choroid plexus-derived miR-204 regulates the number of quiescent neural stem cells in the adult brain. *EMBO Journal*. **38** (17), e100481 (2019).
 23. Silva-Vargas, V., Maldonado-Soto, A. R., Mizrak, D., Codega, P., Doetsch, F. Age-dependent niche signals from the choroid plexus regulate adult neural stem cells. *Cell Stem Cell*. **19** (5), 643-652 (2016).
 24. Angelidis, I. et al. An atlas of the aging lung mapped by single cell transcriptomics and deep tissue proteomics. *Nature Communications*. **10** (1), 963 (2019).
 25. Kjell, J. et al. Defining the adult neural stem cell niche proteome identifies key regulators of adult neurogenesis. *Cell Stem Cell*. **26** (2), 277-293.e8 (2020).
 26. Mirzadeh, Z., Doetsch, F., Sawamoto, K., Wichterle, H., Alvarez-Buylla, A. The subventricular zone en-face: wholemount staining and ependymal flow. *Journal of Visualized Experiments: JoVE*. (39), 1938 (2010).
 27. Kulak, N. A., Geyer, P. E., Mann, M. Loss-less nano-fractionator for high sensitivity, high coverage proteomics. *Molecular & Cellular Proteomics: MCP*. **16** (4), 694-705 (2017).
 28. Tyanova, S., Temu, T., Cox, J. The MaxQuant computational platform for mass spectrometry-based shotgun proteomics. *Nature Protocols*. **11** (12), 2301-2319 (2016).
 29. Cox, J., Mann, M. MaxQuant enables high peptide identification rates, individualized p.p.b.-range mass accuracies and proteome-wide protein quantification. *Nature Biotechnology*. **26** (12), 1367-1372 (2008).
 30. Cox, J. et al. Accurate proteome-wide label-free quantification by delayed normalization and maximal peptide ratio extraction, termed MaxLFQ. *Molecular & Cellular Proteomics: MCP*. **13** (9), 2513-2526 (2014).
 31. Perez-Riverol, Y. et al. The PRIDE database and related tools and resources in 2019: improving support for quantification data. *Nucleic Acids Research*. **47** (D1), D442-D450 (2019).
 32. Tomassy, G. S. et al. Distinct profiles of myelin distribution along single axons of pyramidal neurons in the neocortex. *Science*. **344** (6181), 319-324 (2014).
 33. Sharma, K. et al. Cell type- and brain region-resolved mouse brain proteome. *Nature Neuroscience*. **18** (12), 1819-1831 (2015).
 34. Datta, S. et al. Laser capture microdissection: Big data from small samples. *Histology and Histopathology*. **30** (11), 1255-1269 (2015).
 35. Kerever, A. et al. Novel extracellular matrix structures in the neural stem cell niche capture the neurogenic factor fibroblast growth factor 2 from the extracellular milieu. *Stem Cells*. **25** (9), 2146-2157 (2007).
 36. Cox, J., Mann, M. 1D and 2D annotation enrichment: a statistical method integrating quantitative proteomics with complementary high-throughput data. *BMC Bioinformatics*. **13** (Suppl 16), S12 (2012).
 37. Daynac, M., Morizur, L., Chicheportiche, A., Mouthon, M.-A., Boussin, F. D. Age-related neurogenesis decline in the subventricular zone is associated with specific cell

cycle regulation changes in activated neural stem cells.

Scientific Reports. **6**, 21505 (2016).

38. Navarro Negredo, P., Yeo, R. W., Brunet, A. Aging and rejuvenation of neural stem cells and their niches. *Cell Stem Cell*. **27** (2), 202-223 (2020).
39. Smith, L. K., White, C. W., Villeda, S. A. The systemic environment: at the interface of aging and adult neurogenesis. *Cell and Tissue Research*. **371** (1), 105-113 (2018).
40. Neuberger, E. J., Swietek, B., Corrubia, L., Prasanna, A., Santhakumar, V. Enhanced dentate neurogenesis after brain injury undermines long-term neurogenic potential and promotes seizure susceptibility. *Stem Cell Reports*. **9** (3), 972-984 (2017).
41. Fisch, U., Brégère, C., Geier, F., Chicha, L., Guzman, R. Neonatal hypoxia-ischemia in rat elicits a region-specific neurotrophic response in SVZ microglia. *Journal of Neuroinflammation*. **17** (1), 26 (2020).
42. Götz, M., Sirko, S., Beckers, J., Imler, M. Reactive astrocytes as neural stem or progenitor cells: In vivo lineage, In vitro potential, and Genome-wide expression analysis. *Glia*. **63** (8), 1452-1468 (2015).
43. Kernie, S. G., Parent, J. M. Forebrain neurogenesis after focal Ischemic and traumatic brain injury. *Neurobiology of Disease*. **37** (2), 267-274 (2010).
44. Pous, L. et al. Fibrinogen induces neural stem cell differentiation into astrocytes in the subventricular zone via BMP signaling. *Nature Communications*. **11** (1), 630 (2020).

2.2 Aim of the study II – Constituting the proteome of the SEZ neurogenic niche

The aim of this project was to generate proteome data of the SEZ neural stem cell niche, use the proteome to detect candidate niche regulators and provide a bioinformatical resource to other researchers.

“Defining the Adult Neural Stem Cell Niche Proteome Identifies Key Regulators of Adult Neurogenesis.”

Jacob Kjell, Judith Fischer-Sternjak, Amelia J. Thompson, **Christian Friess**, Matthew J. Sticco, Favio Salinas, Jürgen Cox, David C. Martinelli, Jovica Ninkovic, Kristian Franze, Herbert B. Schiller, and Magdalena Götz

For this publication as co-author, I dissected the sub- and medial ependymal zone for mass spectrometry analysis using the Cryo-section Dissection. I was involved in filtering the proteome data for candidate proteins and performed immunohistochemistry analysis to confirm and further specify the location of the candidate proteins in the SEZ. Furthermore, I was involved in editing and reviewing the manuscript together with the other authors.

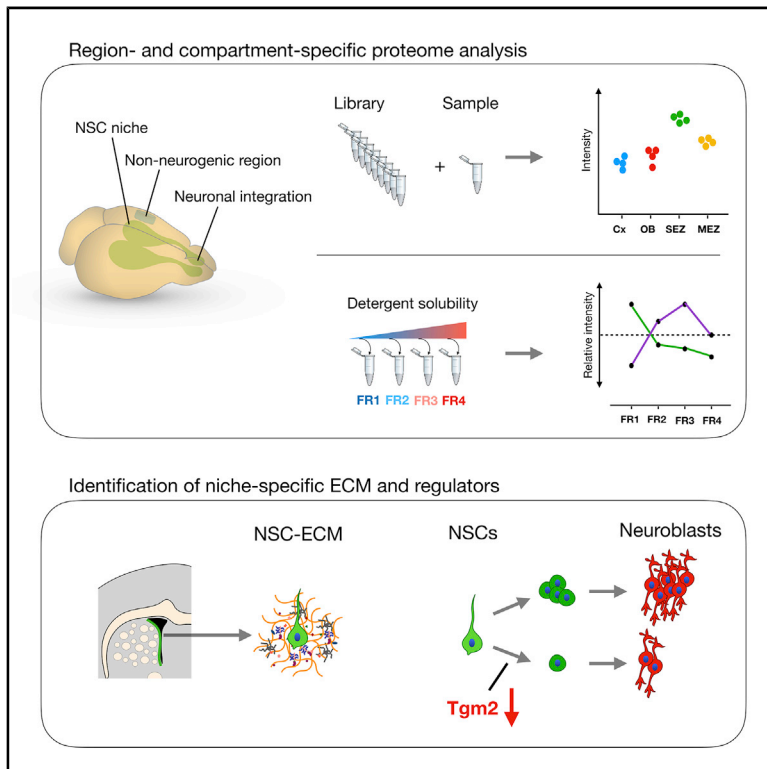
The paper is published on Cell Stem Cell (26), February 6, 2020, pages 277-293, <https://doi.org/10.1016/j.stem.2020.01.002>

As open access paper and author of this Cell Stem Cell article, I have the right to include it in a thesis or dissertation, provided it is not published commercially.

Cell Stem Cell

Defining the Adult Neural Stem Cell Niche Proteome Identifies Key Regulators of Adult Neurogenesis

Graphical Abstract



Authors

Jacob Kjell, Judith Fischer-Sternjak, Amelia J. Thompson, ..., Kristian Franze, Herbert B. Schiller, Magdalena Götz

Correspondence

magdalena.goetz@helmholtz-muenchen.de

In Brief

The physical properties of stem cell niches are thought to mediate important regulatory functions. Here we provide a proteomic resource of the neural stem cell niche in comparison to gliogenic brain parenchyma, highlighting stiffness and the enzyme transglutaminase 2 as key regulators of neurogenesis.

Highlights

- Proteomics define the NSC niche-specific extracellular matrix
- Detergent-solubility profiling reveals extracellular matrix architecture
- Transglutaminase 2 regulates neurogenesis
- Stiffness is increased in the neurogenic niches of the brain



Defining the Adult Neural Stem Cell Niche Proteome Identifies Key Regulators of Adult Neurogenesis

Jacob Kjell,^{1,2,9} Judith Fischer-Sternjak,^{1,2} Amelia J. Thompson,³ Christian Friess,¹ Matthew J. Sticco,⁴ Favio Salinas,⁵ Jürgen Cox,⁵ David C. Martinelli,⁴ Jovica Ninkovic,^{2,6,8} Kristian Franze,^{3,10} Herbert B. Schiller,^{5,7,10} and Magdalena Götz^{1,2,8,10,11,*}

¹Division of Physiological Genomics, Biomedical Center, Ludwig-Maximilians-Universität, München, Germany

²Institute for Stem Cell Research, Helmholtz Zentrum München, Germany

³Department of Physiology, Development and Neuroscience, Cambridge University, Cambridge, UK

⁴Department of Neuroscience, University of Connecticut Health Center, Farmington, CT, USA

⁵Department of Proteomics and Signal Transduction, Max-Planck Institute of Biochemistry, Martinsried, Germany

⁶Division of Cell Biology and Anatomy, Biomedical Center, Ludwig-Maximilians-Universität, München, Germany

⁷Institute of Lung Biology and Disease, Member of the German Center for Lung Research, Helmholtz Zentrum München, Germany

⁸SYNERGY, Excellence Cluster Systems Neurology, Ludwig-Maximilians-Universität, München, Germany

⁹Present address: Department of Clinical Neuroscience, Karolinska Institutet, Stockholm, Sweden

¹⁰Senior authors

¹¹Lead Contact

*Correspondence: magdalena.goetz@helmholtz-muenchen.de

<https://doi.org/10.1016/j.stem.2020.01.002>

SUMMARY

The mammalian brain contains few niches for neural stem cells (NSCs) capable of generating new neurons, whereas other regions are primarily gliogenic. Here we leverage the spatial separation of the subependymal zone NSC niche and the olfactory bulb, the region to which newly generated neurons from the sub-ependymal zone migrate and integrate, and present a comprehensive proteomic characterization of these regions in comparison to the cerebral cortex, which is not conducive to neurogenesis and integration of new neurons. We find differing compositions of regulatory extracellular matrix (ECM) components in the neurogenic niche. We further show that quiescent NSCs are the main source of their local ECM, including the multi-functional enzyme transglutaminase 2, which we show is crucial for neurogenesis. Atomic force microscopy corroborated indications from the proteomic analyses that neurogenic niches are significantly stiffer than non-neurogenic parenchyma. Together these findings provide a powerful resource for unraveling unique compositions of neurogenic niches.

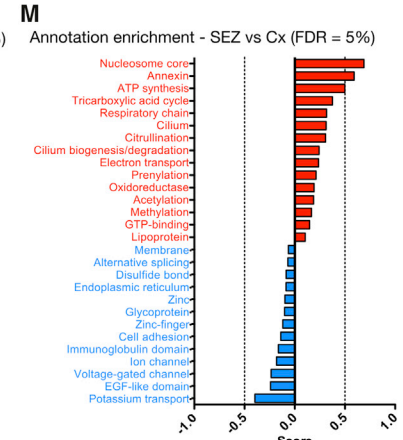
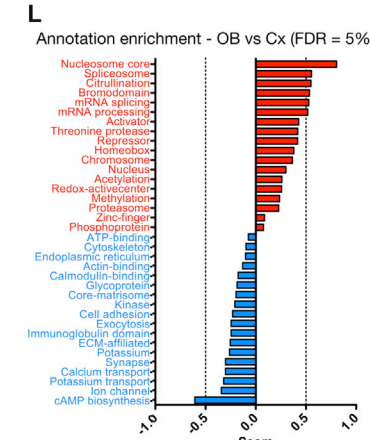
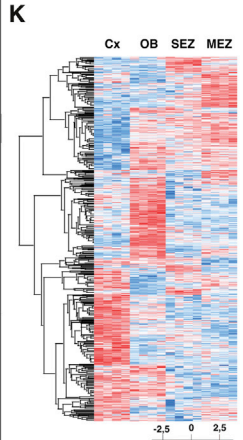
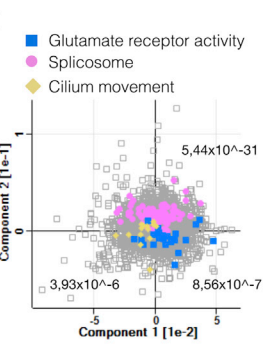
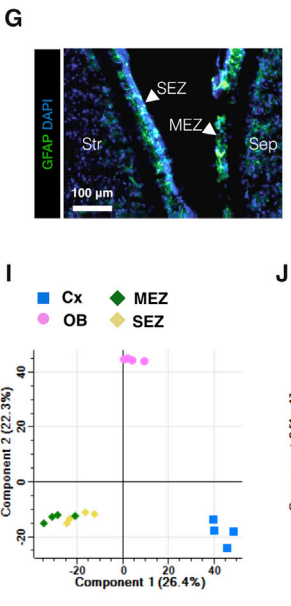
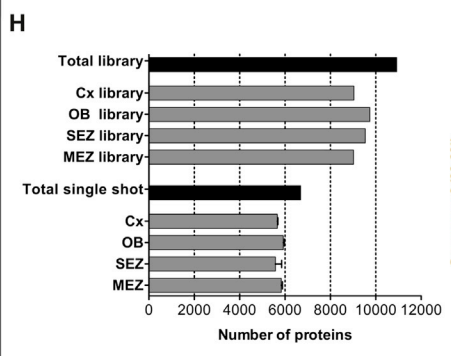
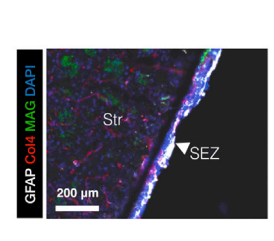
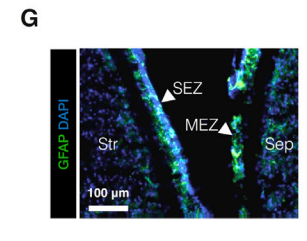
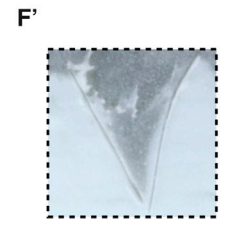
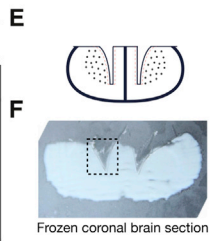
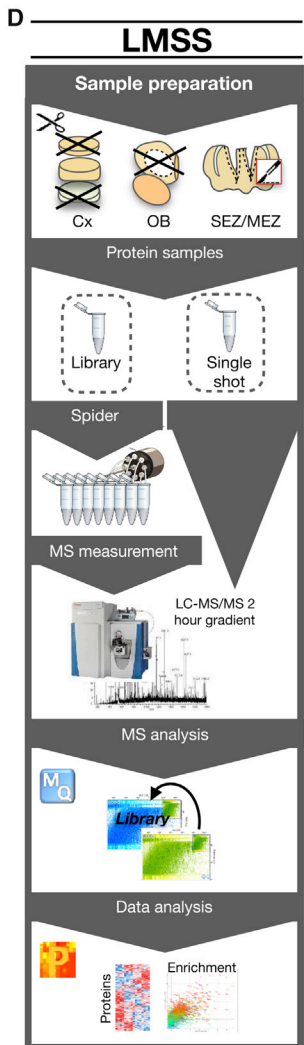
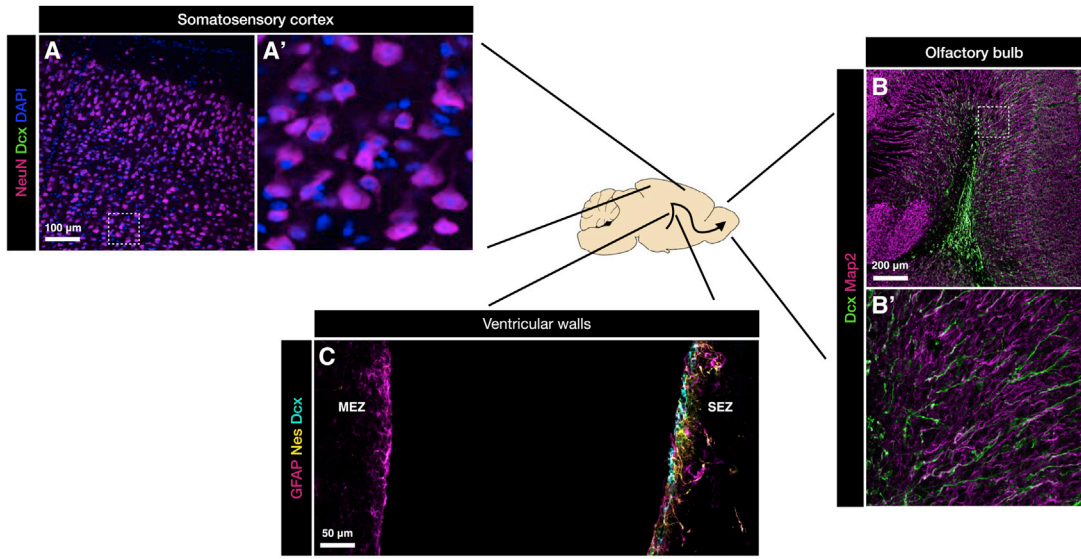
INTRODUCTION

Adult stem cell niches provide complex regulatory architectures that maintain the stem cell population and prevent terminal differentiation (Crane et al., 2017; Donnelly et al., 2018; Gonzales and Fuchs, 2017; Meran et al., 2017; Vining and Mooney, 2017). In the adult mammalian brain, the neural stem cell (NSC) niches are unique in supporting neurogenesis (Conover and Todd, 2017; Ruddy and Morshead, 2018), as only gliogenesis takes

place in the remainder of the brain (see e.g., Götz et al., 2016; Lim and Alvarez-Buylla, 2016). The brain parenchyma outside these niches (e.g., neocortex; Figure 1A) even limits the neurogenic potential of transplanted NSCs or neuroblasts (Barker et al., 2018; Englund et al., 2002; Fricker et al., 1999; Seidenfaden et al., 2006; Winkler et al., 1998). The largest NSC niche, the subependymal zone (SEZ), generates neuroblasts that migrate to the distant olfactory bulb (OB), where they differentiate and integrate (Figures 1B and 1C) (Lim and Alvarez-Buylla, 2016). This spatial separation allows the determination of the composition of the NSC niche (SEZ) that maintains the stem cells and generation of neuroblasts in comparison to the OB niche as an environment fostering neuronal differentiation and integration of new neurons.

The SEZ, located at the lateral wall of the lateral ventricles that are lined by ependymal cells, harbors nestin+ quiescent NSCs that can be activated and give rise to transit-amplifying progenitors (TAPs) that then generate doublecortin (Dcx)-positive neuroblasts (Figure 1C). The medial side of the lateral ventricle, the medial sub-ependymal zone (MEZ), also shares ependymal cell lining and access to the cerebrospinal fluid (CSF). As it contains many fewer NSCs and Dcx+ neuroblasts (Figure 1C) than the SEZ, this region provides a useful comparative tissue to identify specific components of the NSC and neurogenesis-associated environment. Individual proteins and ECM structures (Kerever et al., 2007) have been described as specific for the NSC niches in the adult murine brain, such as the ECM proteins Tenascin-C (Tnc) and Thrombospondin 4 (Thbs4) that both may regulate aspects of migration (Faissner et al., 2017; Garcion et al., 2001; Girard et al., 2014; Kazanis et al., 2007) or the matrix-associated protein Plexin-b2 that regulates proliferation and migration (Saha et al., 2012). However, no comprehensive proteomic analysis of this important niche has yet been performed. Likewise, in the OB, two matrix proteins, Reelin (Reln) and Tenascin-R (Tnr), have been reported to regulate the change from tangential to radial neuroblast migration (Figure 1B) (David et al., 2013; Hack et al., 2002), and, besides neuronal activity, little is known about factors allowing the integration of new neurons into pre-existing





(legend on next page)

networks in the adult brain (Hardy and Saghatelian, 2017; Lledo and Valley, 2016).

In contrast to the above-described niches, the mature brain parenchyma allows neither neurogenesis nor integration of new neurons in the absence of injury (Frisén, 2016). It contains a specialized extracellular matrix called “perineuronal nets” (PNNs) that is built up around neurons late in development and serves to restrict neuronal plasticity (Deepa et al., 2006). As the NSC niche contains no neurons, and hence no PNNs, its ECM composition is expected to differ from the brain parenchyma, but the actual composition is largely unknown, as are potential differences in ECM composition between the OB and brain parenchyma.

The ECM, the “matrisome,” consists of core ECM proteins often forming ECM structures, such as the basement membrane (BM) and associated ECM proteins, many with primarily protein-regulatory functions. The latter is essential for the enrichment and function of many growth factors and other signaling factors and, hence, is of key interest to mediate regulatory functions of a local niche. The proteins associated with the structural ECM can be enriched through detergent de-cellularization (Naba et al., 2012), but this has not yet been done in the NSC niches.

In contrast to the paucity of proteome data, the transcriptomes of SEZ NSCs, their progeny, and the surrounding niche cells are well studied (Beckervordersandforth et al., 2010; Codega et al., 2014; Kalamakis et al., 2019; Llorens-Bobadilla et al., 2015). However, gene expression analysis has proven inadequate to fully describe the proteome, including the tissue matrix environment (Angelidis et al., 2019; Schiller et al., 2015). For example, neurogenic and neuronal mRNAs are upregulated in NSCs and progenitors, but translation is inhibited to avoid premature differentiation and allow amplification of the lineage, a phenomenon referred to as “lineage priming” (Baser et al., 2019; Beckervordersandforth et al., 2010; Götz et al., 2016; Lepko et al., 2019). Moreover, proteins may be derived from the CSF that is contributing to the maintenance of the SEZ stem cell niche (Lepko et al., 2019; Silva-Vargas et al., 2016). Determining the composition of the pro-

teome, including the matrisome of the neurogenic niches, is thus important, particularly given the influence of the ECM composition on mechanical tissue properties, which regulate fate decisions of adult stem cells, such as muscle or mesenchymal SCs (Engler et al., 2006; Gilbert et al., 2010; Vining and Mooney, 2017). Neural crest SCs have been found to differentiate into smooth muscle cells on stiffer substrates and glial cells on softer substrates (Zhu et al., 2019), consistent with CNS tissue belonging to the softest tissues in our body (Franze et al., 2013). This softness of CNS tissue is most likely due to low expression of certain structural matrix constituents, such as collagen I, and the soft nuclear matrix of neurons, given their low content of lamin A (Swift et al., 2013). Tissue stiffness has been shown to potentially influence neurite outgrowth (Koser et al., 2016; Stukel and Willits, 2018), and NSCs possess mechanosensitive ion channels whose activity affects their self-renewal and differentiation (Pathak et al., 2014; Petrik et al., 2018). However, the mechanical properties of the adult stem cell niche are currently unknown.

Here we set out to provide a first in-depth characterization of what makes the composition and architecture of the adult brain’s neurogenic niche uniquely different from the non-neurogenic brain parenchyma.

RESULTS

High-Resolution Proteome Defines Niche-Specific Features

For ultra-deep proteomic assessment of the neurogenic niches, we used library-matched single shot (LMSS) proteomics (see STAR Methods). Cerebral cortex (Cx) gray matter (GM, omitting the white matter [WM] and meninges) was compared with the OB (also omitting the meninges), the SEZ, and the MEZ (Figure 1D). To obtain SEZ and MEZ samples, we performed cryo-micro-dissections on 100- μ m-thick tissue sections after removing cortex with corpus callosum and choroid plexus (10 sections per sample) (Figures 1E, 1F, and 1F’). The combination of methods allowed very high precision and proteome-measurement depth

Figure 1. High-Resolution Proteome of the Somatosensory Cortex and Neurogenic Niches

(A–C) The schematic drawing indicates a sagittal section of the adult murine brain with example photomicrographs of the regions used in this analysis—the non-neurogenic somatosensory cortex (A), the olfactory bulb (OB), where new neurons (labeled for doublecortin [Dcx]) integrate (B), and the lateral sub-ependymal zone (SEZ) where most NSCs reside, whereas only a few are located in the medial sub-ependymal zone (MEZ) (C). Sections were immunostained as indicated in the panels and are confocal z stacks.

(D) Experimental workflow using loss-less nano-fractionation for library-matched single shot measurements.

(E) Schematic of the high-precision cryo-dissection of the SEZ and the MEZ.

(F) Picture of a 50- μ m frozen coronal section (white, ventral down) with cortex, corpus callosum, and choroid plexus removed. (F’) shows magnification of the dissected region visible as a thin gray line.

(G) Photomicrographs of cryo-dissected SEZ and MEZ (separated from striatum [Str] and septum [Sep]) stained for GFAP and DAPI (left panel) and cryo-dissected SEZ stained for GFAP, collagen 4 (Col4), myelin-associated glycoprotein (MAG), and DAPI (right panel).

(H) Number of proteins quantified in the library sample measurements and the library-matched single shot (LMSS) sample measurements for each region. Data are shown as mean \pm standard deviation ($n = 1$ library sample per region, $n = 4$ single shot samples per region). See also Figures S1A–S1D.

(I) Principal component analysis (PCA) for each brain region. Components 1 and 2 separate the main regions. The SEZ and the MEZ are similar in these components.

(J) Colors indicate three categories that are enriched, respectively, in the Cx, the OB, and both the SEZ and the MEZ (FDR is presented for each category).

(K) Heatmap of 4,786 proteins found to be of different abundance comparing the four brain regions ($n = 4$ per region). Intensities are based on label-free quantification (LFQ) intensities after unsupervised hierarchical clustering (ANOVA with Benjamin-Hochberg post hoc test, FDR = 0.05).

(L) The datasets were annotated with Uniprot keywords and the matrisome annotation (see STAR Methods). Enriched features of the OB in comparison to the Cx were then scored (0 to 1) and are displayed in a bar graph (1D-annotation enrichment, FDR = 0.05). Conversely, features with a negative score (0 to -1) are enriched in the Cx compared to the OB.

(M) Enriched features of the SEZ in comparison to the Cx were analyzed in the same manner (1D-annotation enrichment, FDR = 0.05).

Scale bars as indicated in the panels.

of the small SEZ and MEZ regions, avoiding the myelin-associated-glycoprotein-rich (MAG+) brain parenchyma (Figure 1G).

We identified a total of 10,923 proteins in the library samples (four pooled tissue samples from each region) and 6,690 in LMSS samples ($n = 4$ per region) (Figure 1H; Table S1). Among the library-exclusive proteins, transcription factors ($p = 1.68 \times 10^{-6}$), cytokines, and neurogenesis-associated mitogens (e.g., interleukin-18, insulin growth factor, Vegf- α , etc.) were significantly enriched. As these are low-abundance proteins, *in vivo* proteome measurements of such factors have previously been unattainable. Our library measurements demonstrate that the mitogens and transcription factors known to be required for neurogenesis (e.g., Pax6) (Ninkovic et al., 2013) can be revealed and quantified *in vivo* with a proteome depth of 10,000 proteins (Figures S1A–S1D; Table S1).

The principal component analysis (PCA) of the four regions revealed that the SEZ and the MEZ have a more similar proteome than the other two regions (Figure 1I). An enriched common category was cilium movement ($p = 3.93 \times 10^{-6}$) (Figure 1J), highlighting that proteins from a single cell layer, the ependymal cells lining the ventricle, can be detected: e.g., Tektin (Tek1), a protein exclusive to ependymal cells and NSCs at the SEZ (<https://shiny.mdc-berlin.de/SVZapp/>).

In total, 4,786 proteins had a differential abundance among the four regions (ANOVA, FDR = 0.05) (Figure 1K). To identify features enriched in the neurogenic niche, we analyzed differences in protein abundance for either the OB or the SEZ in comparison to the Cx. Proteins were annotated with Uniprot keywords and the improved ECM annotation (<http://matrisome.org>; see STAR Methods). Enriched features of the OB included several nuclear and gene-regulatory processes (1D-annotation enrichment, FDR = 0.05) (Figures 1L and S1F; Table S2). This suggested that the OB has a larger proportion of gene-regulatory proteins, possibly because of the large population of maturing neuroblasts. Processes less pronounced in the OB compared to the Cx included synapse-associated features and core-matrisome proteins.

Proteins enriched in the SEZ, like in the OB, were associated with gene regulation and also oxidative phosphorylation (Figures 1M and S1E; Table S2), which is consistent with the fact that NSCs are largely glycolytic and the metabolism has to change as they differentiate into neuroblasts (Beckervordersandforth, 2017; Knobloch and Jessberger, 2017). Annexin-family proteins were found enriched in the SEZ compared to the Cx (Figure 1M), a notable observation given their importance in regulating the proliferation and migration of cancer cells (Lauritzen et al., 2015). Core matrisome proteins demonstrated the highest abundance in Cx ($p \leq 0.0001$, Kruskal-Wallis test with Dunn's multiple comparison test) (Figure 2A), and several proteins of the PNNs had higher abundance in the Cx and the MEZ compared to the SEZ and the OB (Figures 1L and 1M). None of the proteoglycans associated with migration during developmental neurogenesis, such as neurocan, aggrecan, or versican (Long and Huttner, 2019; Maeda, 2015), were an enriched component of the matrisome at the SEZ; instead, aggrecan was enriched in the OB in line with an association to neuroblasts (Figures 2B, 2C, and S2A–S2C). These data validate the quality of the dataset and provide a rich resource that can be accessed as a web-based database (<https://pawelsm.github.io/neuronichen1/> or <https://neuronicheproteome.org>).

Identification of Niche-Specific Marker Proteins

The abundance of neurogenesis-associated proteins was lower in the MEZ compared to the SEZ but still detectable, further supporting the depth of our analysis. One such protein is Tnc, the neurogenic niche-associated ECM protein discussed above (Roll and Faissner, 2014) that was enriched in the SEZ versus the MEZ, as expected (Figures 2A and 2B). We then compared the relative abundance of proteins in the SEZ, the MEZ, and the OB to the Cx as a control. These region-specific comparisons determined, S100a6 and C1q13 among others, to be distinctly enriched among matrisome-associated proteins of the SEZ (Figures 2B, 2C, S2B, and S2C). We therefore aimed to determine which cells produce these SEZ-enriched proteins. Immunostaining for S100a6 was high in the SEZ and comparably absent in the MEZ (Figure 2D) and low to absent in astrocytes in the Cx parenchyma (Figures S3G and S3H), in agreement with our analysis. Excitingly, however, S100a6 staining labeled NSCs (slow dividing nestin+ cells in the SEZ; Figures S3B, S3C, and S3F), but not neuroblasts (Dcx+; Figures 2D, 2G, and S3A–S3C). Likewise, S100a6 staining also extends into the rostral migratory stream (RMS), co-localizing with GFAP+ cells, but not Dcx+ neuroblasts (Figures S3I and S3K). It is worth noting that NSCs, expressing GFAP, have been identified also at these more rostral positions (Alonso et al., 2008). Moreover, we also found S100a6+ GFAP+ cells in the WM (Figures S3E and S3J), consistent with the presence of some NSCs there (Lim and Alvarez-Buylla, 2016). Thus, S100a6 not only labels NSCs in the dentate gyrus (DG) (Yamada and Jinno, 2014) but more broadly allows distinguishing NSCs from astrocytes, which is important as especially reactive astrocytes and NSCs share most of the so-called “astrocyte markers” (Beckervordersandforth et al., 2010; Götz et al., 2015).

Interestingly, single-cell RNA sequencing (scRNA-seq) data from the SEZ (Kalamakis et al., 2019) also showed enrichment of S100a6 specifically in a primed-quiescent subtype of NSCs, qNSC2 (Figure S6A), identifying these cells as the main source for the specific enrichment of S100a6 in the SEZ. Most notably, this proved to be the case for most mRNAs encoding for matrix proteins that are highest in quiescent NSCs, whereas activated NSCs, TAPs, and neuroblasts express very few ECM components (Figure S6A). Thus, NSCs contribute to the composition of their own niche (see also Faissner et al., 2017).

Some proteins enriched in the SEZ were also enriched at mRNA levels as seen by *in situ* hybridizations in the Allen Brain Atlas (Figures 2I and S4J). The systematic comparison of RNA and protein enrichment in the SEZ compared to the Cx and the OB, however, showed profound differences (Figures S6B and S6C; Table S5). For example, some RNAs were expressed at significantly higher levels in the SEZ compared to the Cx, but the respective proteins were lower abundance or not much different between the SEZ compared to the Cx (Figure S6B; Table S6). This is to be expected from the “lineage priming” as introduced above (Beckervordersandforth et al., 2010; Götz et al., 2016; Lepko et al., 2019) and would lead to “false positives” if relying on RNA data only. Even more misleading could be the class of proteins that we found enriched in the SEZ compared to the Cx, which had lower mRNA levels in SEZ compared to the Cx (Figure S6B). For example, the C1q13 protein is enriched at protein level in the SEZ, but mRNA is lower in the

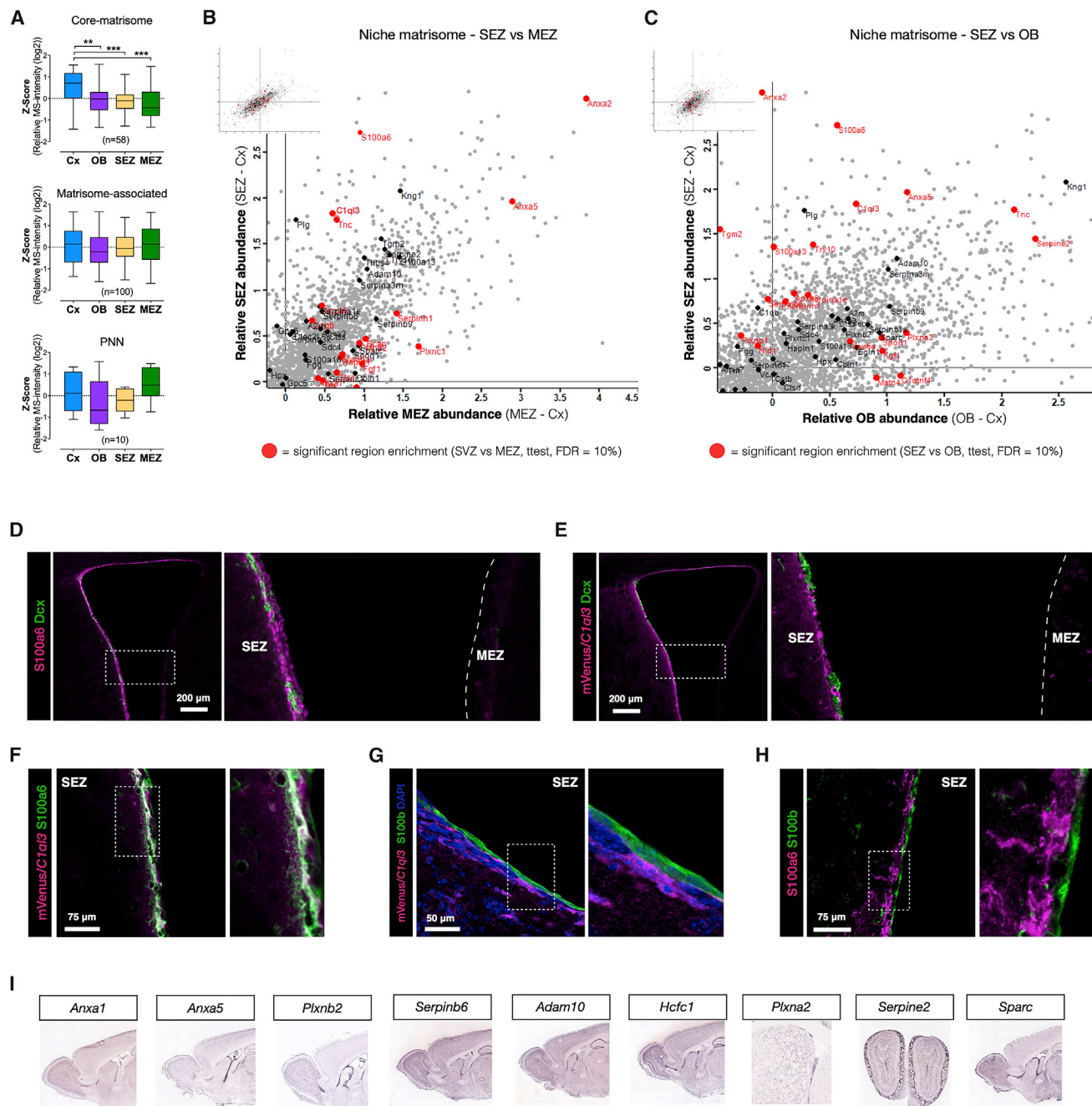


Figure 2. Niche-Specific ECM and NSC Markers

(A) Distribution plots of each brain region in the different categories of the matrisome as indicated. Average LFQ intensities for each protein were Z scored and displayed in whisker plots (ANOVA, Kruskal-Wallis test with Dunn's multiple comparison test, * $p = 0.05$, ** $p = 0.01$, and *** $p = 0.001$).

(B) Scatterplot with the matrisome (black) and matrisome significantly different (FDR ≤ 0.1) comparing the SEZ and the MEZ (red) highlighted.

(C) Scatterplot with the relative SEZ and OB values and significant differences (FDR ≤ 0.1) between intensities for the SEZ and the OB. Both plots highlight S100a6 and C1ql3 as enriched in the SEZ. See also [Figures S2B](#) and [S2C](#).

(D–H) Photomicrographs of the ventricle and the SEZ and the MEZ from coronal brain sections of C57BL/6J mouse or mVenus/C1ql3 transcriptional reporter mouse immunostained as indicated. Note that S100a6 and C1ql3 are not found in Dcx+ neuroblasts or parenchymal astrocytes and, typically, neither in ependymal cells. Scale bars as indicated, and (D) and (E) are z stacks of confocal images, while (F)–(H) are single optical sections. See also [Figures S3](#) and [S4A–S4I](#).

(I) *In situ* hybridization shows mRNA expression in the SEZ. Image credit: Allen Institute for Brain Science.

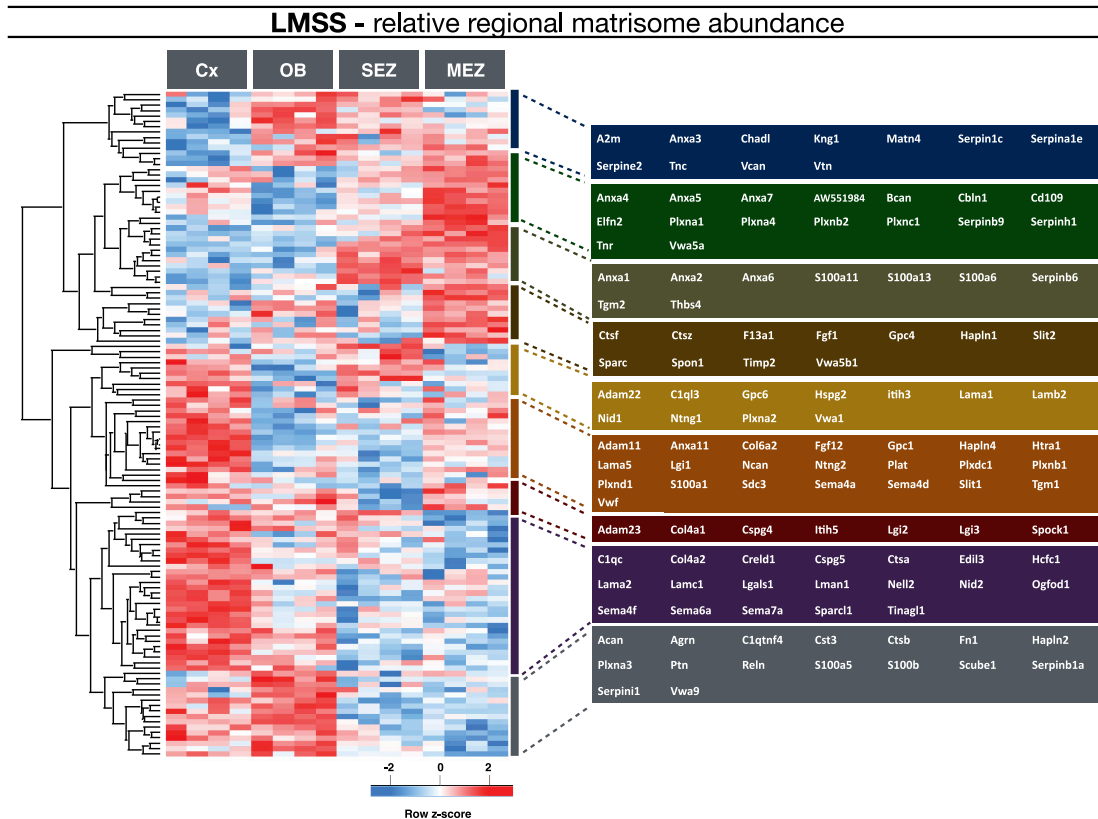


Figure 3. Regional Matrisome Distribution and Neurogenic Niche-Specific Matrisome

We compared 158 matrisome proteins and 78 of these had a significantly different distribution in the respective regions, of which the somatosensory cortex was found to be most abundant with extracellular matrix proteins. The heatmap displays unsupervised hierarchical clustering of the matrisome proteins with significantly different abundance when comparing the four brain regions (ANOVA with Benjamin-Hochberg post hoc test, FDR = 0.05). Members of different clusters (indicated by bars on the right of the heatmap) are listed on the further right of the heatmap in colored areas.

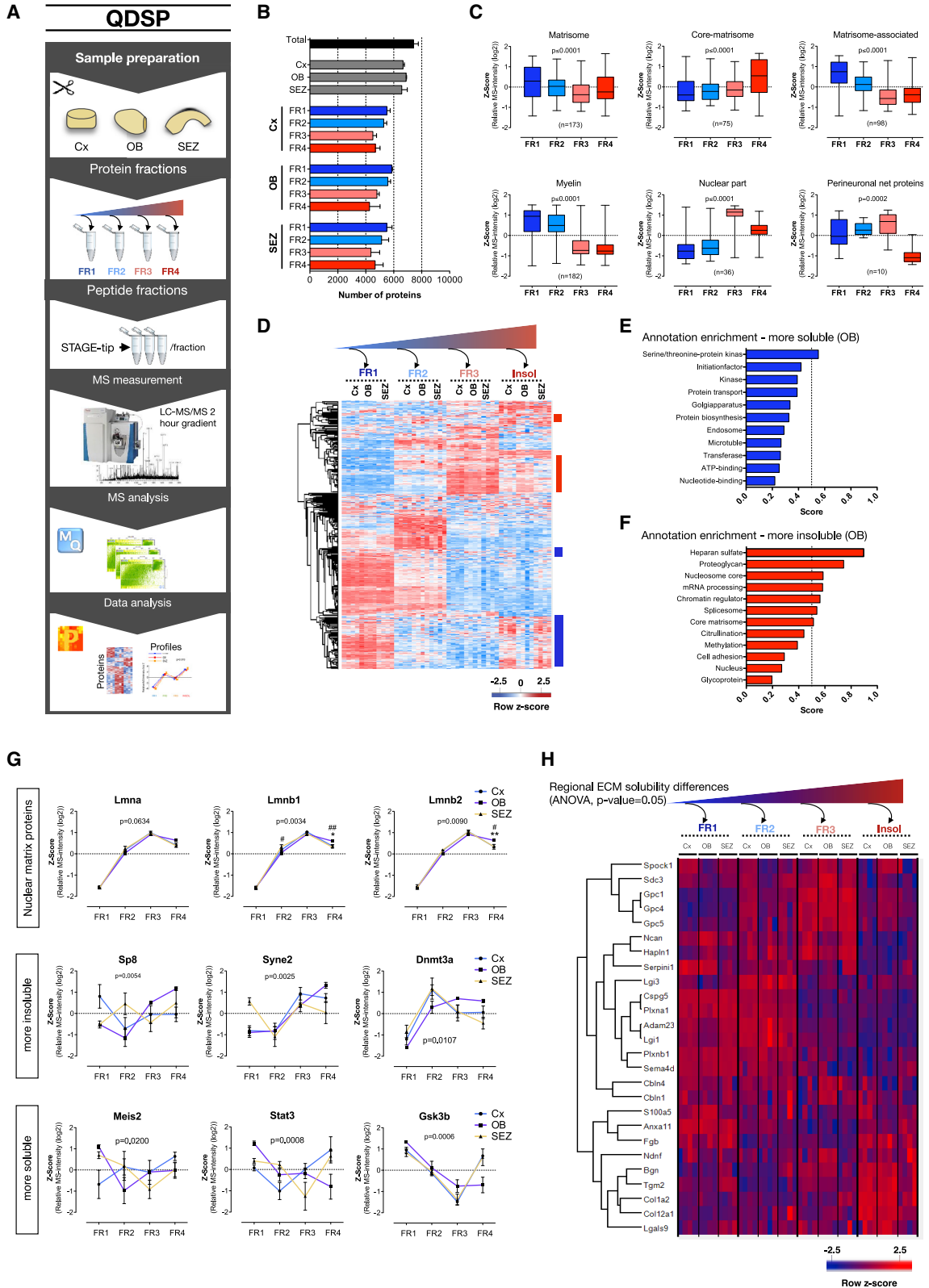
SEZ compared to the Cx. Moreover, C1ql3 was not detectable among the stem cell stages in the published scRNA-seq data (Figure S6C). This prompted us to examine the source of this protein in the SEZ.

To do so, we took advantage of the C1ql3-mVenus reporter mouse line (Martinelli et al., 2016). With this allele, any cell that expresses C1ql3 is marked by expression of cytoplasmic mVenus (not a fusion protein). In brain, C1ql3 has thus far been identified as a synaptic protein and, accordingly, mVenus+ cells in this reporter line in the brain parenchyma are mostly neurons (Martinelli et al., 2016). In the SEZ, however, C1ql3-mVenus+ cells were Dcx negative, i.e., not neuroblasts but nestin+ and S100a6+ NSCs (Figures 2E, 2F, S4A–S4C, and S4F). Conversely, we could not detect mVenus+ astrocytes in the brain parenchyma and the OB (Figures S4D, S4E, and S4G–S4I). Ependymal cells located at the ventricle and S100b+ did not contain S100a6 levels above background nor co-localized with C1ql3-mVenus (Figures 2G and 2H). Hence our analysis not only identified two SEZ-enriched NSC proteins whose role may extend beyond being niche-specific marker proteins but also showed a multitude of SEZ enriched proteins that were not detected by RNA analysis (Figures S6B and S6C).

Biochemical Profiling of the Neurogenic Niche-Specific Matrisome

Here we present an overview of the regional distribution of all matrisome proteins with significant abundance differences across conditions (Figure 3; unsupervised hierarchical clustering, Pearson correlation). The OB and the SEZ are particularly rich in serpins, vitronectin, and Tnc, whereas the SEZ and the MEZ share high levels of annexin and several S100 proteins (Figure 3). Interestingly, annexin and S100 proteins interact and regulate a variety of processes, including membrane fusion and repair (Jaiswal and Nylandsted, 2015). These may be of particular relevance in migrating cells present in both of these regions. Additional ECM-associated proteins in both the SEZ and the MEZ included the well-known Thrombospondin 4 (Thbs4) and the ECM cross-linking protein Transglutaminase 2 (Tgm2) that has so far not been described at protein level in the neurogenic niches (see below).

Matrisome proteins provide structural support and tether cell-surface proteins or soluble growth factors and thereby regulate their signaling functions. A way of experimentally enriching ECM proteins is to de-cellularize tissue using detergents and analyze the detergent-insoluble ECM components (Naba et al., 2012). However, such a method inherently loses ECM-affiliated



(legend on next page)

proteins that associate with weaker affinity with the ECM. In contrast, methods that use protein-abundance correlation across fractions of protein derived by stepwise centrifugation or differential detergent extraction can be used to assess biochemical properties of proteins, including their association strength with ECM, in a proteome-wide fashion. We therefore used the quantitative detergent solubility profiling (QDSP) method (Schiller et al., 2015) and sequentially separated Cx, OB, and SEZ tissue samples into four protein fractions.

Tissue proteins were separated by extraction with increasing stringency using consecutive extraction with four distinct detergent mixtures (Figure 4A), leading to the identification of 8,308 proteins (Figure 4B; Table S3). For comparison of protein solubility profiles, their intensities were Z scored within each region and relative protein abundance was compared in the four fractions by averaging the profile between regions to permit “brain” solubility profile comparisons for specific categories. As expected, we found “brain” core matrisome proteins, such as collagens and laminins, to be enriched in the fourth fraction and thus more insoluble, whereas matrisome-associated proteins, such as S100 proteins and serpins, were most abundant in the first fraction and thus more soluble ($p \leq 0.0001$, Kruskal-Wallis test) (Figures 4C, S5A, and S5B). Notably, the brain-specific ECM proteins associated with the PNNs (Figures 4C and S2G) form a soft structural matrix in the Cx, since they typically enrich in fraction three with much lower abundance in the insoluble fraction four ($p = 0.0002$, Kruskal-Wallis test). The PNN proteins neurocan (Ncan) and hyaluronan and proteoglycan link protein 1 (Hapln1) were distinctly more soluble in the OB compared to other regions (Figure S2G), an observation possibly related to the integration of new neurons into the network and a high degree of synaptogenesis.

Comparing all solubility profiles between the three regions, we found 1,208 proteins to have significantly different profiles (two-way ANOVA, $p \leq 0.05$) (Figure 4D). Unsupervised hierarchical cluster analysis revealed the OB to have many profiles that differ in their solubility from Cx and the SEZ, in particular in the fourth fraction. Since such solubility shifts may contain information concerning protein functions, we assessed the cellular features associated with proteins either more or less soluble (only fourth fraction) in the OB compared to the Cx (1D-annotation analysis, FDR = 0.05). Enriched features among the more insoluble proteins in the OB were associated with gene regulation and cell

adhesion, as well as core-matrisome proteins and proteoglycans (Figure 4F; Table S4). Lamin b1 and Lamin b2 were significantly more insoluble in the OB, suggesting that some or many cells have a nuclear matrix that is more insoluble (Figure 4G; Table S4). It should be noted that many, but not all, gene regulatory-associated proteins had a more insoluble profile in the OB, highlighting possible differences in nuclear architecture that remain to be explored. Along these lines, we observed that the presence of transcriptional and epigenetic regulators in different solubility fractions with tissue specificity, e.g., Sp8 and Dnmt3a, were less soluble, whereas Stat3, Meis2, and Gsk3b were more soluble in SEZ tissue (Figure 4G). Meis2 is an important regulator of neurogenesis in the SEZ (Kolb et al., 2018), prompting the suggestion that different solubility may reveal tissue-specific differences in transcriptional function. Another category in the more insoluble group of the OB included matrisome proteins, e.g., all three detected glypicans (Gpc1, Gpc4, and Gpc5) (Figure 4H). Thus, its less soluble ECM and nuclear lamina predict potentially higher tissue stiffness of the OB, a prediction that we tested and confirmed below.

Next, we focused on the solubility profiles of ECM components, providing a heatmap of the “brain” matrisome solubility profiles (Figure 5A; unsupervised hierarchical clustering, Pearson correlation). This highlights that familiar neurogenic niche ECM proteins are surprisingly soluble (Figures 5B and 5C). Interestingly, the solubility profile of C1q13 in the SEZ is distinctly different from the one in the OB and the Cx (Figure 5D), suggesting its localization in a different more soluble compartment compared to its normal synaptic membrane association. Indeed, matrisome proteins were generally more enriched in the soluble compartments of neurogenic niche-specific ECM-associated proteins ($p \leq 0.0001$, Kruskal-Wallis test) in the SEZ ($n = 26$) or the OB ($n = 19$) compared to the Cx in the LMSS data (FDR = 0.1) (Figure 5E). The solubility of proteins enriched in the Cx ($n = 40$) compared to either the SEZ or the OB (FDR = 0.1) in contrast had either a more membrane-associated or non-diffusible solubility profile. The structural ECM is thus not enriched in the neurogenic niche, including the typical “soft” structural brain ECM, although individual proteins with these properties can be found enriched in both the SEZ and the OB. Reln is uniquely insoluble in the OB (Figure 5C), whereas Tgm2 is one of the few proteins that was enriched in the SEZ (and the MEZ) that has a largely insoluble profile (Figure 5A).

Figure 4. Compartment Analysis with In-Depth Quantitative Proteomes of the Somatosensory Cortex and the Neurogenic Niches

- (A) With stepwise de-cellularization we determined insoluble and various diffusible grades of ECM and other cellular compartment-associated proteins.
- (B) Total number of quantified proteins for all regions (top, black and gray) and proteins quantified in each detergent fraction from each of the three brain regions (bottom, color). Each sample fraction is shown as mean \pm standard deviation ($n = 4$ in each brain region).
- (C) Solubility profile overview and distribution plot for the proteins in the displayed categories. Abundances were Z scored and then averaged for each protein in these categories shown in whisker plots with number of proteins in each category displayed in the graphs. Insoluble proteins distribute more toward fraction four and soluble proteins distribute toward fraction one (significance analyzed with Kruskal-Wallis test with Dunn’s multiple comparison test). See also Figures S2G, S5A, and S5B.
- (D) Heatmap of 1,216 proteins with significantly different solubility among our three regions (FDR ≥ 0.05).
- (E and F) Significantly enriched features among the more soluble (E) and insoluble (F) proteins in the OB when compared to the Cx using the relative difference of the LFQ intensities in the fourth fraction (1D-annotation enrichment, FDR = 0.05). The dataset was annotated with Uniprot keywords, matrisome, and a custom perineural nets annotation (see STAR Methods).
- (G) From the relatively more soluble and insoluble proteins in the OB, we display the quantitative profile of lamins of the nuclear matrix and neurogenesis-associated proteins (two-way ANOVA). Data are presented as mean \pm SEM.
- (H) Matrisome proteins with significantly different solubility profiles comparing the three brain regions (Z scored LFQ intensity values, two-way ANOVA, $p \geq 0.05$). Rows have undergone unsupervised hierarchical clustering.

QDSP - brain matrisome composition

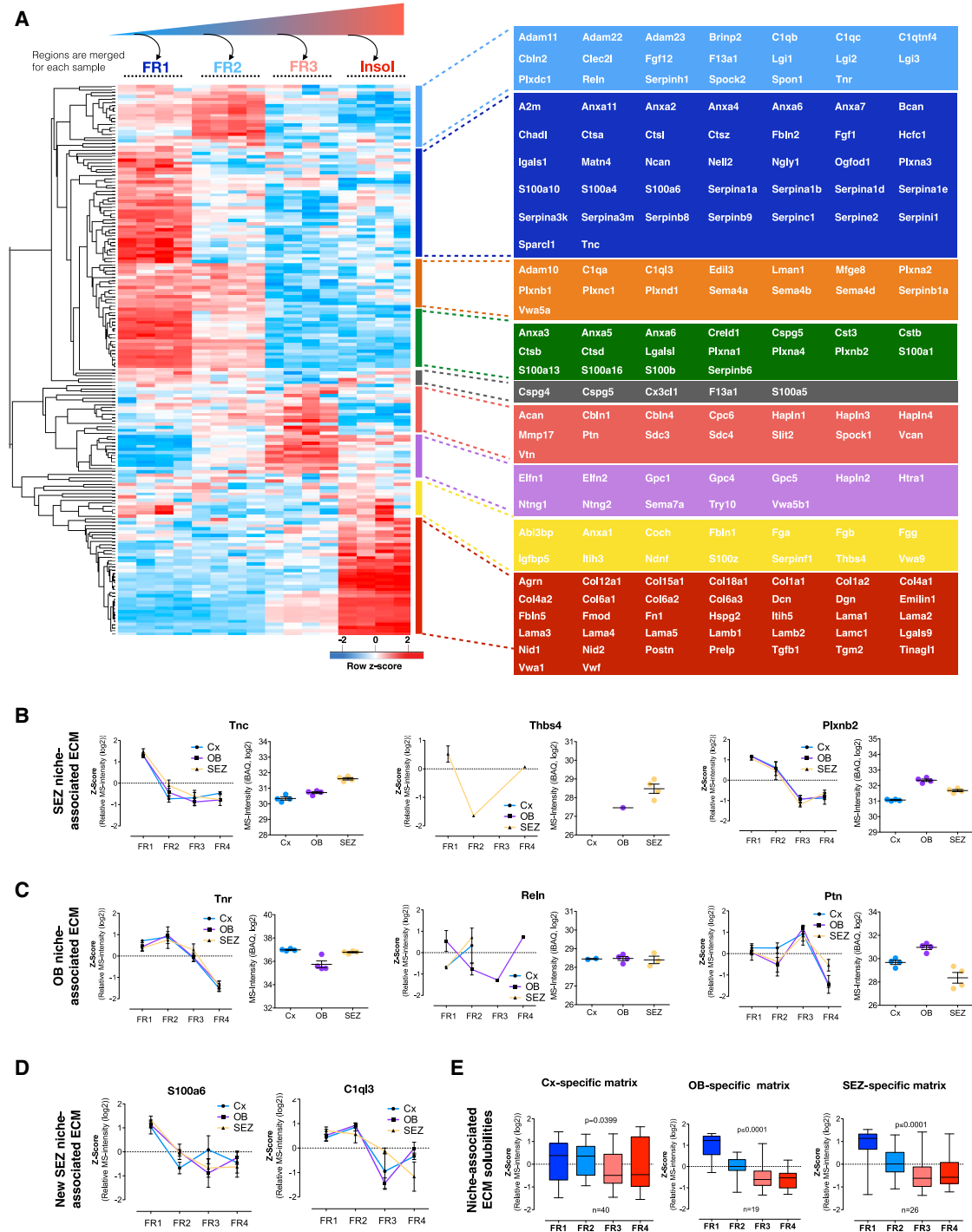


Figure 5. Brain- and Niche-Matrisome Composition

(A) The matrisome protein solubility profiles are displayed using unsupervised hierarchical clustering of the detergent solubility profiles derived from averaged Z scores from each brain region (the Cx, the OB, and the SEZ).

(B–D) Detergent solubility profiles for the SEZ-associated ECM proteins (B) Tenascin-C (Tnc), Thrombospondin-4 (Thbs4), and Plexin-b2 (Plxnb2); the OB-associated proteins (C) Tenascin-R (Tnr), Reelin (Reln), and Pleiotrophin (Ptn); and the two neurogenic niche-specific proteins (D) S100a6 and C1qf3 ($p = 0.0948$). Data are presented as mean \pm SEM.

(E) Solubility profiles for Cx-, SEZ-, and OB-enriched matrisome proteins shown in whisker plots (ANOVA, p values in graphs).

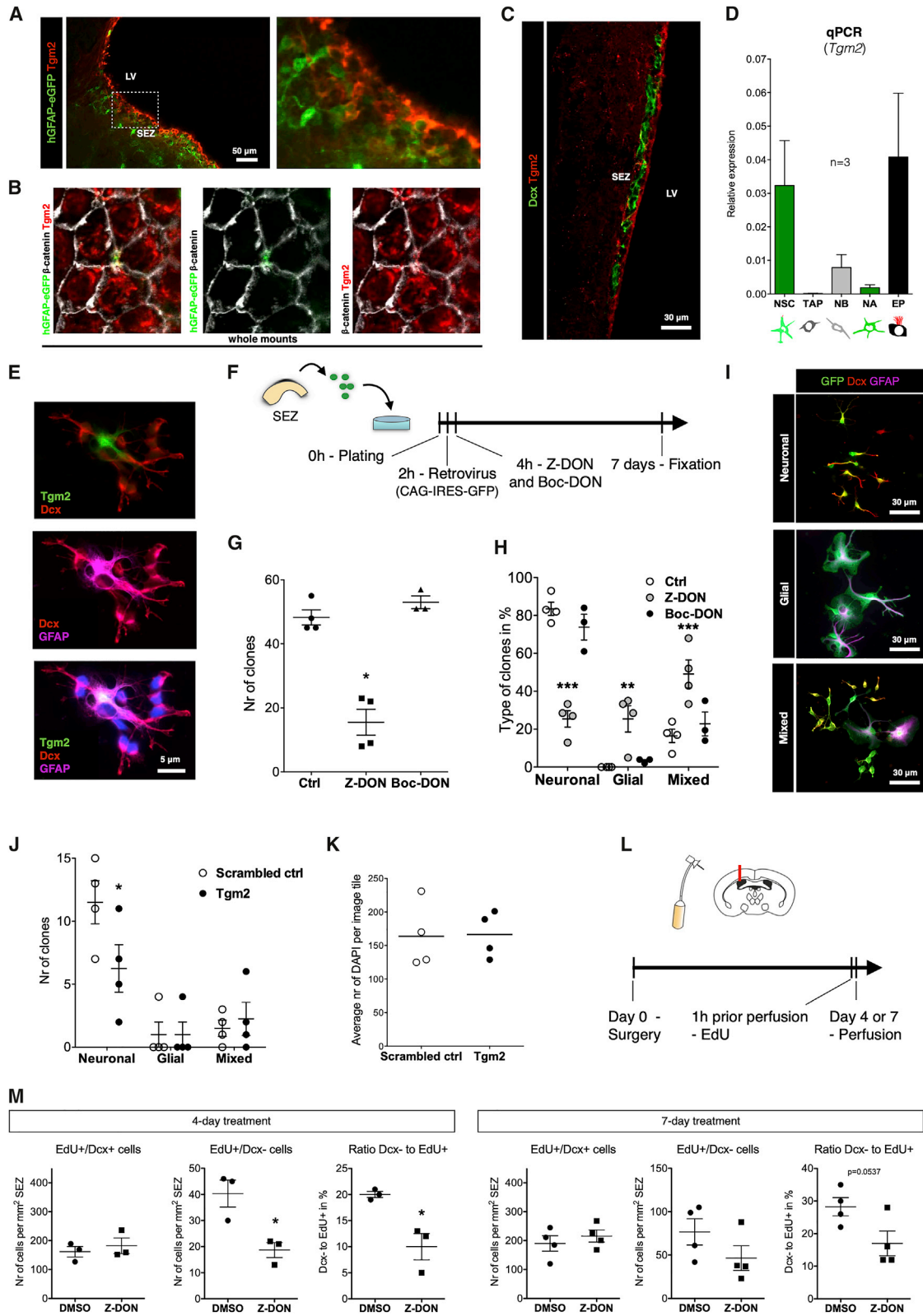


Figure 6. Transglutaminase 2 Promotes Neurogenesis

(A) NSCs were identified as hGFAP-GFP+ cells in the SEZ in sagittal sections counterstained with Tgm2 and inserted to the right indicated by the dashed line in the lower magnification picture on the left. Both NSCs and ependymal cells were labeled with Tgm2. LV, lateral ventricle.

(legend continued on next page)

Transglutaminase 2 Regulates Adult Neurogenesis

Given the specific enrichment and solubility profile of Tgm2 in both the SEZ and the MEZ (Figure S5D), we determined its cellular origin. Tgm2 immunoreactivity was found in ependymal cells (Figures 6A and 6B) and NSCs (hGFAP-GFP+; see Becker-vordersandforth et al., 2010; Codega et al., 2014) that extend an apical process to the ventricle (Figure 6B), but not in neuroblasts (Dcx+) (Figure 6C). Consistent with ependymal cells and NSCs containing the highest protein levels, these cells isolated by fluorescence-activated cell sorting (Beckervordersandforth et al., 2010; Fischer et al., 2011) also had high *Tgm2* mRNA levels, whereas TAPs and neuroblasts contained very low mRNA levels (Figure 6D). Notably, Tgm2 is the only family member detectable in the SEZ (Tgm1, Tgm3, Tgm5, and Tgm6 were not detectable). The expression of Tgm2 in ependymal cells explains its similar levels in the SEZ and the MEZ (Figure S5D), but its additional presence in NSCs implies possible autocrine or cell-intrinsic effects that we explored next.

To do so, we used primary SEZ cultures as described before (Costa et al., 2011); cells were cultured without growth factors and in the absence of matrix proteins (Figure 6F). Often a single GFAP+ NSC is surrounded by the Dcx+ neuroblast progeny (Figures 6E and 6I) with the former Tgm2+, whereas neuroblasts were negative, consistent with the data shown above (Figures 6C and 6D). To probe Tgm2 function in this culture system, we used 10 μ M of the Tgm2 inhibitor Z-DON. Cells were transduced 2 h after plating with retroviral vectors containing CAG-IRES-GFP at low titer to label few cells and allow detection of the progeny of a single cell as a distinct cluster of cells, i.e., a clone (Ortega et al., 2011). Notably, a single dose of Z-DON (at 4 h after plating) drastically reduced the number of clones (Figure 6G; comprising all clusters of GFP+ cells irrespective of their identity), suggesting a possible role of Tgm2 in promoting proliferation or survival. When we analyzed the composition of the clones, we noted a specific effect of the Tgm2 inhibitor on the clones comprising only neuroblasts (referred to as “neuronal clones” in Figures 6H and 6I) that are generated by proliferating TAPs or neuro-

blasts in these cultures (Costa et al., 2011). Conversely, NSC clones (containing one or few GFAP+ cells and Dcx+ neuroblasts, referred to as “mixed” in Figures 6H and 6I) or clones containing only GFAP+ cells (referred to as “glial” in Figures 6H and 6I) were favored by Tgm2 inhibition (Figure 6H).

Tgm2 has multiple modes of action, including intracellular and extracellular functions (Eckert et al., 2014; Lee and Park, 2017), and the above inhibitor blocks all of them. The inhibitor Boc-DON cannot enter the cells and hence specifically blocks extracellular Tgm2 but had no effects in these cultures (Figures 6G and 6H), suggesting that on this artificial glass substrate with high abundant media volume, extracellular functions of Tgm2 play no roles. Importantly, we confirmed the specific role of Tgm2 using Tgm2 small interfering RNA (siRNA) (Figure 6J). Notably, the reduced number of neuronal progeny after knockdown of Tgm2 was not due to cell death, as the control and knockdown condition had equal numbers of cells (Figure 6K).

Since Z-DON was as effective as siRNA *in vitro*, we sought to determine whether it would have a similar effect *in vivo*. Osmotic minipumps loaded with 100 μ M Z-DON in artificial CSF were implanted intra-ventricular in mice and inhibitor was administered for either 4 or 7 days. A pulse of EdU (1 h prior perfusion) allowed quantification of proliferating neuroblasts (Dcx+ and EdU+ cells) or TAPs (Dcx- and EdU+ cells) at the SEZ. Interestingly, blocking Tgm2 for 4 days affected mostly the number of TAPs, and this trend was largely maintained after 7 days of administering Z-DON (Figure 6M). This phenotype obtained *in vivo* is consistent with reduced clone numbers (Figure 6G) and effects on pure neuronal clones (Figures 6H and 6I) *in vitro*, as TAPs almost exclusively generate neuroblasts. Thus, the proteome analysis allowed the identification of Tgm2 in promoting neurogenesis from NSCs.

Higher Tissue Stiffness in Neurogenic Niches

The above-described tissue-specific distribution of potentially mechanically important proteins and the susceptibility of adult

(B) Whole-mount section of the SEZ showing an hGFAP-GFP+ Tgm2+ apical endfoot between ependymal cells delineated by β -catenin+ junctions.

(C) Single-plane confocal picture of the coronal section of the SEZ immunostained for Dcx and Tgm2 showing no double-positive cells.

(D) Tgm2 expression analysis by qRT-PCR in cells isolated from the SEZ by fluorescence-activated cell sorting (FACS). NSCs were identified by hGFAP-eGFP+ and the apical membrane marker CD133+, ependymal cells (EP) as hGFAP-GFP-/CD133+ and hGFAP-GFP+, and CD133-, PSA-NCAM-, EGFR- cells as niche astrocytes (NA). Note that NSCs and ependymal cells express high levels of *Tgm2* mRNA. The direct progeny of NSCs, the transit-amplifying progenitors (TAPs), isolated as EGFR+, CD133-, PSA-NCAM-, and neuroblasts, isolated as PSA-NCAM+ also hardly expressed Tgm2. Data are presented as mean \pm standard deviation.

(E) Primary culture from the SEZ stained as indicated showing that Tgm2+ cells were also GFAP+.

(F) Experimental setup for the primary SEZ culture and clonal analysis following Tgm2 inhibition with Z-DON (irreversible Tgm2 inhibitor) or Boc-DON (cell membrane impermeable and irreversible Tgm2 inhibitor).

(G) 10- μ M Z-DON treatment at 4 h after plating significantly reduced the number of retrovirally labeled cell clusters (clones, i.e., a cluster of cells sharing the cell of origin), whereas 100- μ M Boc-DON did not alter the number of clones. Data are presented as mean \pm SEM. * $p \leq 0.05$, two-tailed Mann-Whitney test.

(H) With Z-DON, but not Boc-DON, the proportion of GFP+ clones containing newly generated neuroblasts (Dcx+) was reduced, whereas the proportion of mixed and glial clones arising from NSCs was conversely increased. Data are presented as mean \pm SEM, two-way ANOVA with Bonferroni's multiple comparison test, ** $p \leq 0.01$ and *** $p \leq 0.001$.

(I) Examples of retrovirally labeled (CAG-IRES-GFP) clones composed of neuronal, glial, and mixed cell types stained as indicated. Scale bars as indicated.

(J) Primary SEZ cultures were treated with 10-nM siRNAs against Tgm2 and showed a reduced number of neuronal clones compared to the control (scrambled siRNA) ($n = 4$). Data are presented as mean \pm SEM, two-way ANOVA with Bonferroni's multiple comparison test, * $p \leq 0.05$.

(K) Countings of DAPI stainings from representative tiles ($n = 4$, with nine tiles counted in each n).

(L) Experimental setup for osmotic pump experiment with two time-points, 4 and 7 days, with continuous intra-ventricular infusion of 100- μ M Z-DON in artificial CSF.

(M) On the contralateral side of the infusion, we quantified EdU+ cells that were either Dcx+ or Dcx- at the SEZ. After 4 days Z-DON treatment, we found a significant reduction in TAPs (EdU+/Dcx-), whereas proliferating neuroblasts (EdU+/Dcx+) remained similar to control (Data are presented as mean \pm SEM. * $p \leq 0.05$, two-tailed t test). This trend continued after 7 days treatment (Data are presented as mean \pm SEM. $p = 0.0537$, two-tailed t test). Confocal image stacks from 6 sections were quantified per brain.

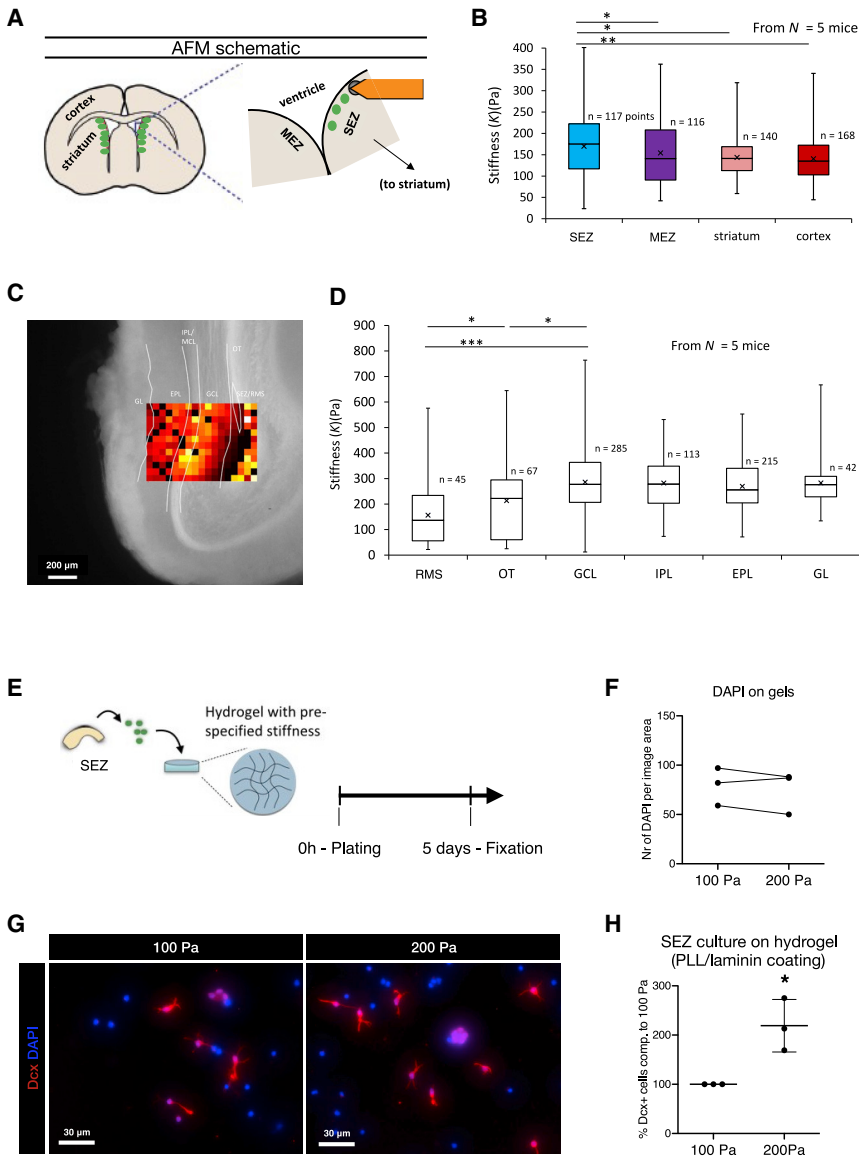


Figure 7. Higher Stiffness of the Neurogenic Niches

(A) Schematic drawing of the stiffness measurements on coronal slices (300 μ m) with AFM. (B) Stiffness was assessed in the SEZ, the MEZ, the striatum, and the Cx. Both ventricular regions are significantly stiffer than the Cx and the striatum that both have similar tissue stiffness. The SEZ was significantly stiffer than the MEZ. Data shown as whisker plots, * $p = 0.05$ and ** $p = 0.01$. (C) Representative tissue heatmap of OB measurements with scale bar as indicated. (D) In the OB, the end of the RMS was less stiff in comparison to the adjacent olfactory tract. The granule cell layer (GCL) was even stiffer still, as well as the internal and external plexiform layer (IPL/EPL) and the glomerular layer (GL). Data shown as whisker plots, Mann-Whitney test (two tailed), * $p = 0.05$ and *** $p = 0.001$. (E) Experimental setup for the primary SEZ culture plated on hydrogels with 100- or 200-Pa stiffness. (F) Number of DAPI cells was similar at the end of the 5-day experimental period. (G) Representative images of the Dcx+ cells at 5 days after plating. (H) Hydrogels with 200-Pa stiffness significantly increased the percentage of Dcx+ cells in comparison to the same primary SEZ culture on hydrogels with 100 Pa stiffness. Data are presented as mean \pm standard deviation. * $p = 0.05$, paired t test.

the stiffer 200-Pa substrate (Figures 7G and 7H), even though the outcome of this difference appears to depend on cell density (data not shown). In summary, these data support the concept that neurogenesis is responsive to such differences in stiffness.

Assessing the OB, we also found an increase in stiffness from the RMS toward the granule cell layer (GCL), which was stiffer throughout the OB parenchyma (Figures 7C and 7D). Thus, both neurogenic niches were significantly stiffer

than the brain parenchyma, suggesting that components of the proteome contribute to regulate these niche-specific mechanical properties, which affects neurogenesis.

NSCs to mechanical signals (Pathak et al., 2014; Petrik et al., 2018) prompted us to examine the stiffness of these regions in coronal slices using atomic force microscopy (AFM) (Figure 7A). The brain parenchymal regions, the cortex (GM) and the striatum, had a similar stiffness (Figure 7B). Both the SEZ and the MEZ regions were significantly stiffer (Figure 7B), and the SEZ, the main site of neurogenesis, was significantly stiffer than the MEZ, where few neuroblasts arise (Bordiuk et al., 2014) ($p \leq 0.05$, Mann-Whitney, two tailed). These data suggested a close correlation between higher tissue stiffness and more NSCs dedicated to adult neurogenesis. To examine the extent to which the stiffness differences of about 100 Pa are relevant for neurogenesis, we cultured the above-described primary SEZ cells on gels with the stiffness of 100 and 200 Pa. Cells were fixed and stained after 5 days, and no difference in total cell number was observed (Figures 7E and 7F). However, more than double the number of neuroblasts was detected on

than the brain parenchyma, suggesting that components of the proteome contribute to regulate these niche-specific mechanical properties, which affects neurogenesis.

DISCUSSION

Here we provide a comprehensive characterization of the neurogenic niche proteome compared to normal brain parenchyma and make the data available on an easy-to-use webpage (<https://pawelsm.github.io/neuronichen1/> or <https://neuronicheproteome.org>). Our two proteome datasets (LMSS and QDSP) allowed expanding the set of neurogenic niche-specific proteins and defining their region-specific compartment association. These data are an important complement to the RNA expression data, as RNA and protein enrichment are only partially congruent. This has been described in detail when comparing scRNA-seq and deep proteome data in the aging lung (Angelidis

et al., 2019) and was also apparent in our comparison of RNA and proteome data (Figure S6). The possible mechanisms for this are multiple. RNA stability and RNA-binding proteins may differ between brain regions, and the latter (including microRNAs [miRNAs]) may differentially regulate translation, leading to different abundances of newly produced proteins. Conversely, protein degradation may be regulated differently between regions, such that RNA could be enriched, but protein may be fast degraded and hence reduced. Likewise, especially for the matrisome proteins, the secretory pathways leading to their final localization in the ECM could be differentially regulated, causing a discrepancy between the mRNA coding for the protein and its amount in the ECM. Lastly, the location of the SEZ at the ventricle puts NSCs in direct contact with the CSF, and several factors released by the choroid plexus into the CSF have already been identified to regulate adult neurogenesis (Lepko et al., 2019; Silva-Vargas et al., 2016), including miRNAs (Lepko et al., 2019) or proteins (Silva-Vargas et al., 2016). In the latter case, we would detect the protein in our proteome analysis, but no RNA would be found, which is the case for many. Interestingly, especially proteins of the matrisome enriched in the SEZ were not enriched at RNA levels (Figure S7A), consistent with data obtained in lung (Angelidis et al., 2019). Prominent categories of proteins enriched in the OB compared to the cortex, not enriched at RNA level, were related to splicing (Figure S7B). Therefore, this proteome analysis provides an important resource, as proteins play key roles in the function of this unique niche.

Specific Matrisome of the NSC Niche

Various soluble factors are the most explored cell-extrinsic signals that regulate the adult NSC. Indeed, many matrix-associated proteins are more soluble in the neurogenic niches, and we even found several core-matrix proteins to be more soluble in the neurogenic niches compared to other brain regions and tissues (Figure S5C). This includes Hapln1, Tnc, and Thbs4. In addition to binding other core-matrisome proteins, such as collagens and fibronectin, Tnc interacts with a diverse set of ligands, such as growth factors (e.g., Wnt3a and transforming growth factor β [Tgf- β]) and receptors (e.g., Toll-like receptor 4 [TLR-4] and Rptp β) (De Laporte et al., 2013; Midwood et al., 2016). Thbs4 may act as, e.g., a voltage-gated ion-channel blocker or have intracellular functions (Brody et al., 2015; Girard et al., 2014; Lana et al., 2016; Narouz-Ott et al., 2000). The other niche-specific ECM proteins with a soluble profile include serpins, S100 proteins, and annexins that form a core interaction hub in the SEZ-enriched matrisome (Figure S7C). Soluble ECM proteins such as these may stem from the various cell types in the brain or blood (Geyer et al., 2016). However, we found no evidence for a general increase in blood proteins from allegedly leaky vessels (Tavazoie et al., 2008) in the SEZ tissue (Figures S2D and S2E) but rather expression of these genes (e.g., serpinb6, annexin 1, and annexin 5) by cells in the SEZ (Figure 2I), mostly qNSCs (Figure S6A). Another interesting protein in this category enriched in both the SEZ and the OB is Kininogen 1 (Kng1). Kng1 is a precursor for bradykinin (Figures 2B and 2C), which has been found to promote neurogenesis versus gliogenesis *in vitro* (Pillat et al., 2016). Interaction analysis of the niche-specific matrix protein in the SEZ highlights annexin-S100 protein interactions and calcium-binding and catalytic activity regulation, whereas in the OB, several serpins have known inter-

actions with other negative regulators of endopeptidase activity (Figures S7C and S7D).

Notably, the SEZ-enriched matrisome unraveled here differs profoundly from the enrichments found recently by RNA-seq of NSC niches in the developing Cx of murine or human samples (Fietz et al., 2012). Although RNA and proteome discrepancies may contribute, it is important to note that some of the crucial core matrisome proteins regulating embryonic SVZ expansion and cortex folding are not enriched in the adult NSC niche (Long et al., 2018; Long and Huttner, 2019). Indeed, many of the SEZ-enriched proteins are upregulated at early postnatal stages when the adult NSC niche forms (F.V., P.S., and M. Götz, unpublished data). Thus, as in many other organs, the niche maintaining adult stem cells differs profoundly from the niche regulating expansion in development.

S100a6 and C1ql3 were both soluble ECM-associated proteins that we found enriched in NSCs of the SEZ. Interestingly, S100a6 also marks NSCs in the DG (Yamada and Jinno, 2014) and is hence common to NSCs across regions. S100a6 has extracellular and intracellular functions (Donato et al., 2017); some of the latter are calcium dependent and involved in promoting proliferation in various cancer cells (Lerchenmüller et al., 2016; Li et al., 2015). This may explain its higher levels in late-stage quiescent NSCs compared to postmitotic parenchymal astrocytes. Moreover, S100a6 may be involved in the signal transduction cascade of flow- or stretch-sensitive channels, such as the epithelial sodium channel that is also absent from non-proliferating astrocytes but present in NSCs and increases the frequency of Ca signals when promoting proliferation (Petrik et al., 2018).

In brain, C1ql3 has thus far only been identified as a synapse-associated protein (Chew et al., 2017; Martinelli et al., 2016; Matsuda et al., 2016). Here we found it enriched with a specific solubility profile in the SEZ-niche and identified NSCs as the major source. Thus, C1ql3 also allows the discrimination of NSCs from parenchymal astrocytes, an urgent need given the labeling of NSCs by most astrocyte markers (see also Beckervordersandforth et al., 2010). Notably, C1ql3 is enriched in the SEZ only at the protein level and was hence not identified as a NSC marker in RNA analysis (Figure S6B). C1ql3's differential solubility at the SEZ suggests its localization in a different compartment that is unrelated to its reported synapse function in other brain regions. Outside the brain, extracellular C1ql3 has been reported to control cellular glucose homeostasis (Wei et al., 2011), which makes C1ql3 interesting as a potential regulator of NSC metabolism and perhaps part of the metabolism-enriched machinery we identified in the SEZ (Figure 1M). In order to further demonstrate the functional relevance of the proteome differences detected in this resource, we showed that the niche-candidate Tgm2 regulates proliferation and neurogenesis *in vitro* and *in vivo*. Tgm2 is a multifunctional enzyme and may regulate neurogenesis by intracellular and extracellular mechanisms *in vivo*. Worth noting is its predominant insoluble profile in the SEZ. Most importantly, it serves to substantiate the relevance of proteins found to be enriched in the SEZ.

Specific Matrisome of the OB, the Niche for Neuronal Integration

A key aspect of adult neurogenesis is the integration of the new neurons into pre-existing circuitry. However, the niche

conditions allowing this integration in the DG and the OB are not characterized. PNNs in the brain parenchyma have spurred much interest because of their role in plasticity (Sorg et al., 2016). Overall, many of the PNN-associated proteins are present at a lower degree in the SEZ and the OB compared to the Cx and the MEZ. In the OB, we found two PNN proteins (Hapln1 and Ncan) to be substantially more soluble than in the Cx and the SEZ, which suggests that these proteins may contribute less to PNNs in the OB compared to the Cx and hence constitute a composition of PNN proteins that may be involved in allowing constant synaptic plasticity in the OB. Indeed, Hapln1 is crucial for the formation of new PNNs and is key in mediating plasticity (Carulli et al., 2010). Ncan can act as repellent signal for PSA-NCAM and EphA3 signaling and may be integral to neuroblast migration and circuitry integration (Sullivan et al., 2018). We could further corroborate the absence of a typical PNN composition in the OB by staining with Wisteria floribunda agglutinin (WFA), a lectin-binding carbohydrate of the PNN, e.g., in the Cx, although it does not mark any nets around neurons of the OB (Figure S4K). The limited matrix association of PNN-associated proteins in the OB and the absence of typical PNNs makes them key candidates for the OB's distinct capacity to permit the integration of new neurons into the pre-existing circuitry.

Unique Stiffness of the Neurogenic Niches

An ECM that increases tissue stiffness typically contains insoluble proteins, such as the BM proteins, including collagens and laminins (Swift et al., 2013). Our solubility profiles show that the neuron-associated ECM clearly has a different composition and architecture compared to the insoluble BM proteins, and our data suggest it has very little contribution to tissue stiffness. Conversely, we found more insoluble ECM components that may relate to the increased stiffness of the SEZ, such as Laminin-b2 (Lamb2), Nidogen-1 (Nid1), and Perlecan (Hspg2) in the SEZ compared to the MEZ (Figure S2B), which suggests that the SEZ contains more or larger BM structures. This is in line with previous observations suggesting the specific BM structures in the SEZ, referred to as fractones, as sites for growth-factor accumulation (Kerever et al., 2007). Moreover, the higher expression of the ECM cross-linker Tgm2 originating from ependymal cells and NSCs may further contribute to the increased mechanical stiffness of this niche, besides its possible intracellular functions shown here *in vitro*. Transglutaminases have previously been shown to stiffen tissue (Majkut et al., 2013), and increased substrate stiffness promotes neurogenesis *in vitro* shown here and previously (Pathak et al., 2014).

We found no general enrichment of the insoluble ECM in the OB parenchyma, except for Reln, which suggests unique interconnections here that may be linked to its role in promoting neuroblast chain-migration detachment (Hack et al., 2002). Nevertheless, the OB was the stiffest among the investigated brain regions. The OB is altogether a cell dense region and cell density is known to correlate with tissue stiffness (Koser et al., 2015; Thompson et al., 2019). However, we also found all lamins of the nuclear matrix to be enriched in the OB, and lamin A correlates with tissue stiffness (Swift et al., 2013) (Figure S2F). The lamins were also more insoluble in the OB, which suggests they may have a different composition or associate to cytoskeletal proteins through proteins such as Nesprin-2 (Syne2), which

had similar distinct solubility characteristics in the OB. Nesprin-2 regulates nuclear movement during neurogenesis (Zhang et al., 2009) and may hence be involved in neuroblast migration in the OB. Cell migration is also regulated by tissue stiffness, and durotaxis (migration toward stiff substrate) has been described for several stem cells (Choi et al., 2012; Vincent et al., 2013). Moreover, the nuclear envelope can act as a mechanosensor (Donnaloja et al., 2019), highlighting the importance of nuclear envelope and cytoskeletal interactions. Importantly, stiffness has been found to regulate NSC differentiation *in vitro* (Saha et al., 2008), and we showed here the relevance of the 100-Pa difference measured *in vivo* exerting effects on neurogenesis *in vitro*. Thus, the unique properties of the SEZ niche are functionally relevant. Therefore, the niche-specific proteome described here provides a rich resource for a deeper understanding of the unique properties of this NSC niche in comparison to other adult stem cell niches.

STAR★METHODS

Detailed methods are provided in the online version of this paper and include the following:

- KEY RESOURCES TABLE
- LEAD CONTACT AND MATERIALS AVAILABILITY
- EXPERIMENTAL MODEL AND SUBJECT DETAILS
 - WT Mice (Proteomics, Cell Culture, Osmotic Pumps, IHC, and AFM) and hGFAP-eGFP mice (FACS, IHC)
 - C1ql3 Reporter Mice
 - Primary SEZ Culture
- METHOD DETAILS
 - Sample Preparation for Proteome Analysis
 - Mass Spectrometry
 - Immunohistochemistry
 - Fluorescence-activated Cell Sorting
 - qPCR
 - Clonal Analysis in Primary SEZ Cultures
 - Hydroxy-Acrylamid Gel Preparation for Cell Culture
 - Osmotic Pump Preparation and Surgery
 - Stiffness Measurements
 - Microarray Analysis
- QUANTIFICATION AND STATISTICAL ANALYSIS
 - Mass Spectrometric Data Analysis
 - Bioinformatic Analysis and Statistics
 - Bioinformatic Analysis of LMSS Dataset
 - Bioinformatic Analysis of QDSP Dataset
 - Analysis and Presentation of AFM Data
 - Bioinformatic Analysis Microarray Data
- DATA AND CODE AVAILABILITY

SUPPLEMENTAL INFORMATION

Supplemental Information can be found online at <https://doi.org/10.1016/j.stem.2020.01.002>.

ACKNOWLEDGMENTS

We wish to deeply thank Matthias Mann for allowing us to perform the proteome part of this study in his lab. We thank Fabian Coscia and Fabian Hosp for their help with the proteomics and Christoph Schaab for QDSP graphs. We are

very grateful to Andrea Steiner-Mezzadri, Tatiana Simon-Ebert, Korbinian Mayr, and Igor Paron for their technical help. We also thank David Petrik for providing the mouse brain sections from EdU-treated mice and Stefanie Hauck for feedback on the manuscript.

We also gratefully acknowledge funding from the German Research Council (SFB870, SPP1751, and SPP1738 to M.G. and J.N.), the EU (Eranet S-700982-5008-001 to M.G.) and the ERC (Consolidator Grant 772426 to K.F. and Advanced Grant 340793 to M.G.), and the Swedish Society for Medical Research (SSMF) postdoctoral grant (to J.K.).

AUTHOR CONTRIBUTIONS

M.G. conceived the project. J.K., H.B.S., M.G., and K.F. conceptualized and planned the project. J.K., J.F.-S., H.B.S., K.F., A.J.T., and M.G. designed experiments. J.K. performed all experiments and analyzed all results other than the following: J.F.-S. performed Tgm2 experiments including FACS sorting, whole-mount stainings, qPCR, and sample collection for the microarrays; J.N. performed osmotic minipump implantation and microarray analysis; A.J.T. performed AFM and its analysis and conceptualized these experiments with K.F.; C.F. performed SEZ cryo-dissections and SEZ stainings; M.J.S. and D.C.M. provided C1q3-mVenus reporter mice. J.K. and M.G. wrote the paper with feedback from the co-authors.

DECLARATION OF INTERESTS

The authors declare no competing interests.

Received: February 22, 2019

Revised: October 24, 2019

Accepted: January 2, 2020

Published: February 6, 2020

REFERENCES

- Alonso, M., Ortega-Pérez, I., Grubb, M.S., Bourgeois, J.P., Charneau, P., and Lledo, P.M. (2008). Turning astrocytes from the rostral migratory stream into neurons: a role for the olfactory sensory organ. *J. Neurosci.* *28*, 11089–11102.
- Angelidis, I., Simon, L.M., Fernandez, I.E., Strunz, M., Mayr, C.H., Greiffo, F.R., Tsitsiridis, G., Ansari, M., Graf, E., Strom, T.M., et al. (2019). An atlas of the aging lung mapped by single cell transcriptomics and deep tissue proteomics. *Nat. Commun.* *10*, 963.
- Barker, R.A., Götz, M., and Parmar, M. (2018). New approaches for brain repair—from rescue to reprogramming. *Nature* *557*, 329–334.
- Baser, A., Skabkin, M., Kleber, S., Dang, Y., Gülcüler Balta, G.S., Kalamakis, G., Göpferich, M., Ibañez, D.C., Schefzik, R., Lopez, A.S., et al. (2019). Onset of differentiation is post-transcriptionally controlled in adult neural stem cells. *Nature* *566*, 100–104.
- Beckervordersandforth, R., Tripathi, P., Ninkovic, J., Bayam, E., Lepier, A., Stempfhuber, B., Kirchhoff, F., Hirrlinger, J., Haslinger, A., Lie, D.C., et al. (2010). In vivo fate mapping and expression analysis reveals molecular hallmarks of prospectively isolated adult neural stem cells. *Cell Stem Cell* *7*, 744–758.
- Beckervordersandforth, R. (2017). Mitochondrial Metabolism-Mediated Regulation of Adult Neurogenesis. *Brain plasticity* *3*, 73–87.
- Bollmann, L., Koser, D.E., Shahapure, R., Gautier, H.O., Holzapfel, G.A., Scarcelli, G., Gather, M.C., Ulbricht, E., and Franze, K. (2015). Microglia mechanics: immune activation alters traction forces and durotaxis. *Front. Cell. Neurosci.* *9*, 363.
- Bordiuk, O.L., Smith, K., Morin, P.J., and Semënov, M.V. (2014). Cell proliferation and neurogenesis in adult mouse brain. *PLoS ONE* *9*, e111453.
- Brody, M.J., Schips, T.G., Vanhoutte, D., Kanisicak, O., Karch, J., Maliiken, B.D., Blair, N.S., Sargent, M.A., Prasad, V., and Molkentin, J.D. (2015). Dissection of Thrombospondin-4 Domains Involved in Intracellular Adaptive Endoplasmic Reticulum Stress-Responsive Signaling. *Mol. Cell. Biol.* *36*, 2–12.
- Carulli, D., Pizzorusso, T., Kwok, J.C., Putignano, E., Poli, A., Forostyak, S., Andrews, M.R., Deepa, S.S., Glant, T.T., and Fawcett, J.W. (2010). Animals lacking link protein have attenuated perineuronal nets and persistent plasticity. *Brain* *133*, 2331–2347.
- Chew, K.S., Fernandez, D.C., Hattar, S., Südhof, T.C., and Martinelli, D.C. (2017). Anatomical and Behavioral Investigation of C1q3 in the Mouse Suprachiasmatic Nucleus. *J. Biol. Rhythms* *32*, 222–236.
- Choi, Y.S., Vincent, L.G., Lee, A.R., Kretschmer, K.C., Chirasatitsin, S., Dobke, M.K., and Engler, A.J. (2012). The alignment and fusion assembly of adipose-derived stem cells on mechanically patterned matrices. *Biomaterials* *33*, 6943–6951.
- Codega, P., Silva-Vargas, V., Paul, A., Maldonado-Soto, A.R., Deleo, A.M., Pastrana, E., and Doetsch, F. (2014). Prospective identification and purification of quiescent adult neural stem cells from their in vivo niche. *Neuron* *82*, 545–559.
- Conover, J.C., and Todd, K.L. (2017). Development and aging of a brain neural stem cell niche. *Exp. Gerontol.* *94*, 9–13.
- Costa, M.R., Ortega, F., Brill, M.S., Beckervordersandforth, R., Petrone, C., Schroeder, T., Götz, M., and Berninger, B. (2011). Continuous live imaging of adult neural stem cell division and lineage progression in vitro. *Development* *138*, 1057–1068.
- Cox, J., Hein, M.Y., Lubner, C.A., Paron, I., Nagaraj, N., and Mann, M. (2014). Accurate proteome-wide label-free quantification by delayed normalization and maximal peptide ratio extraction, termed MaxLFQ. *Mol. Cell. Proteomics* *13*, 2513–2526.
- Cox, J., and Mann, M. (2008). MaxQuant enables high peptide identification rates, individualized p.p.b.-range mass accuracies and proteome-wide protein quantification. *Nat. Biotechnol.* *26*, 1367–1372.
- Crane, G.M., Jeffery, E., and Morrison, S.J. (2017). Adult haematopoietic stem cell niches. *Nat. Rev. Immunol.* *17*, 573–590.
- David, L.S., Schachner, M., and Saghatelian, A. (2013). The extracellular matrix glycoprotein tenascin-R affects adult but not developmental neurogenesis in the olfactory bulb. *J. Neurosci.* *33*, 10324–10339.
- De Laporte, L., Rice, J.J., Tortelli, F., and Hubbell, J.A. (2013). Tenascin C Promiscuously Binds Growth Factors via Its Fifth Fibronectin Type III-Like Domain. *PLoS One* *8*, e62076.
- Deepa, S.S., Carulli, D., Galtrey, C., Rhodes, K., Fukuda, J., Mikami, T., Sugahara, K., and Fawcett, J.W. (2006). Composition of perineuronal net extracellular matrix in rat brain: a different disaccharide composition for the net-associated proteoglycans. *J. Biol. Chem.* *281*, 17789–17800.
- Donato, R., Sorci, G., and Giambanco, I. (2017). S100A6 protein: functional roles. *Cell. Mol. Life Sci.* *74*, 2749–2760.
- Donnalaja, F., Jacchetti, E., Soncini, M., and Raimondi, M.T. (2019). Mechanosensing at the Nuclear Envelope by Nuclear Pore Complex Stretch Activation and Its Effect in Physiology and Pathology. *Front. Physiol.* *10*, 896.
- Donnelly, H., Salmeron-Sanchez, M., and Dalby, M.J. (2018). Designing stem cell niches for differentiation and self-renewal. *J. R. Soc. Interface* *15*, 20180388.
- Eckert, R.L., Kaartinen, M.T., Nurminskaya, M., Belkin, A.M., Colak, G., Johnson, G.V., and Mehta, K. (2014). Transglutaminase regulation of cell function. *Physiol. Rev.* *94*, 383–417.
- Engler, A.J., Sen, S., Sweeney, H.L., and Discher, D.E. (2006). Matrix elasticity directs stem cell lineage specification. *Cell* *126*, 677–689.
- Englund, U., Fricker-Gates, R.A., Lundberg, C., Björklund, A., and Victorin, K. (2002). Transplantation of human neural progenitor cells into the neonatal rat brain: extensive migration and differentiation with long-distance axonal projections. *Exp. Neurol.* *173*, 1–21.
- Faissner, A., Roll, L., and Theocharidis, U. (2017). Tenascin-C in the matrisome of neural stem and progenitor cells. *Mol. Cell. Neurosci.* *81*, 22–31.
- Fietz, S.A., Lachmann, R., Brandl, H., Kircher, M., Samusik, N., Schröder, R., Lakshmanaperumal, N., Henry, I., Vogt, J., Riehn, A., et al. (2012). Transcriptomes of germinal zones of human and mouse fetal neocortex suggest a role of extracellular matrix in progenitor self-renewal. *Proc. Natl. Acad. Sci. USA* *109*, 11836–11841.

- Fischer, J., Beckervordersandforth, R., Tripathi, P., Steiner-Mezzadri, A., Ninkovic, J., and Götz, M. (2011). Prospective isolation of adult neural stem cells from the mouse subependymal zone. *Nat. Protoc.* *6*, 1981–1989.
- Franze, K., Janmey, P.A., and Guck, J. (2013). Mechanics in neuronal development and repair. *Annu. Rev. Biomed. Eng.* *15*, 227–251.
- Fricker, R.A., Carpenter, M.K., Winkler, C., Greco, C., Gates, M.A., and Björklund, A. (1999). Site-specific migration and neuronal differentiation of human neural progenitor cells after transplantation in the adult rat brain. *J. Neurosci.* *19*, 5990–6005.
- Frisén, J. (2016). Neurogenesis and Gliogenesis in Nervous System Plasticity and Repair. *Annu. Rev. Cell Dev. Biol.* *32*, 127–141.
- Garcion, E., Faissner, A., and French-Constant, C. (2001). Knockout mice reveal a contribution of the extracellular matrix molecule tenascin-C to neural precursor proliferation and migration. *Development* *128*, 2485–2496.
- Geyer, P.E., Kulak, N.A., Pichler, G., Holdt, L.M., Teupser, D., and Mann, M. (2016). Plasma Proteome Profiling to Assess Human Health and Disease. *Cell Syst.* *2*, 185–195.
- Gilbert, P.M., Havenstrite, K.L., Magnusson, K.E., Sacco, A., Leonardi, N.A., Kraft, P., Nguyen, N.K., Thrun, S., Lutolf, M.P., and Blau, H.M. (2010). Substrate elasticity regulates skeletal muscle stem cell self-renewal in culture. *Science* *329*, 1078–1081.
- Girard, F., Eichenberger, S., and Celio, M.R. (2014). Thrombospondin 4 deficiency in mouse impairs neuronal migration in the early postnatal and adult brain. *Mol. Cell. Neurosci.* *61*, 176–186.
- Gonzales, K.A.U., and Fuchs, E. (2017). Skin and Its Regenerative Powers: An Alliance between Stem Cells and Their Niche. *Dev. Cell* *43*, 387–401.
- Götz, M., Sirko, S., Beckers, J., and Imler, M. (2015). Reactive astrocytes as neural stem or progenitor cells: In vivo lineage, in vitro potential, and Genome-wide expression analysis. *Glia* *63*, 1452–1468.
- Götz, M., Nakafuku, M., and Petrik, D. (2016). Neurogenesis in the Developing and Adult Brain—Similarities and Key Differences. *Cold Spring Harb. Perspect. Biol.* *8*, a018853.
- Hack, I., Bancila, M., Loulier, K., Carroll, P., and Cremer, H. (2002). Reelin is a detachment signal in tangential chain-migration during postnatal neurogenesis. *Nat. Neurosci.* *5*, 939–945.
- Hardy, D., and Saghatelian, A. (2017). Different forms of structural plasticity in the adult olfactory bulb. *Neurogenesis (Austin)* *4*, e1301850.
- Hertz, H. (1881). Über die Berührung fester elastischer Körper. *J. Reine Angew. Math.* *92*, 156–171.
- Hutter, J.L., and Bechhoefer, J. (1993). Calibration of atomic-force microscope tips. *Rev. Sci. Instrum.* *64*, 1868–1873.
- Jaiswal, J.K., and Nylandsted, J. (2015). S100 and annexin proteins identify cell membrane damage as the Achilles heel of metastatic cancer cells. *Cell Cycle* *14*, 502–509.
- Kalamakis, G., Brüne, D., Ravichandran, S., Bolz, J., Fan, W., Ziebell, F., Stiehl, T., Catalá-Martínez, F., Kupke, J., Zhao, S., et al. (2019). Quiescence modulates stem cell maintenance and regenerative capacity in the aging brain. *Cell* *176*, 1407–1419.e14.
- Kazanis, I., Belhadi, A., Faissner, A., and French-Constant, C. (2007). The adult mouse subependymal zone regenerates efficiently in the absence of tenascin-C. *J. Neuroscience* *27*, 13991–13996.
- Kerever, A., Schnack, J., Vellinga, D., Ichikawa, N., Moon, C., Arikawa-Hirasawa, E., Efrid, J.T., and Mercier, F. (2007). Novel extracellular matrix structures in the neural stem cell niche capture the neurogenic factor fibroblast growth factor 2 from the extracellular milieu. *Stem Cells* *25*, 2146–2157.
- Knobloch, M., and Jessberger, S. (2017). Metabolism and neurogenesis. *Curr. Opin. Neurobiol.* *42*, 45–52.
- Kolb, J., Anders-Maurer, M., Müller, T., Hau, A.C., Grebbin, B.M., Kallenborn-Gerhardt, W., Behrends, C., and Schulte, D. (2018). Arginine Methylation Regulates MEIS2 Nuclear Localization to Promote Neuronal Differentiation of Adult SVZ Progenitors. *Stem Cell Reports* *10*, 1184–1192.
- Koser, D.E., Moeendarbary, E., Hanne, J., Kuerten, S., and Franze, K. (2015). CNS cell distribution and axon orientation determine local spinal cord mechanical properties. *Biophys. J.* *108*, 2137–2147.
- Koser, D.E., Thompson, A.J., Foster, S.K., Dwivedy, A., Pillai, E.K., Sheridan, G.K., Svoboda, H., Viana, M., Costa, L.D., Guck, J., et al. (2016). Mechanosensing is critical for axon growth in the developing brain. *Nat. Neurosci.* *19*, 1592–1598.
- Kulak, N.A., Pichler, G., Paron, I., Nagaraj, N., and Mann, M. (2014). Minimal, encapsulated proteomic-sample processing applied to copy-number estimation in eukaryotic cells. *Nat. Methods* *11*, 319–324.
- Kulak, N.A., Geyer, P.E., and Mann, M. (2017). Loss-less nano-fractionator for high sensitivity, high coverage proteomics. *Mol. Cell. Proteomics* *16*, 694–705.
- Lana, B., Page, K.M., Kadurin, I., Ho, S., Nieto-Rostro, M., and Dolphin, A.C. (2016). Thrombospondin-4 reduces binding affinity of [(3)H]-gabapentin to calcium-channel $\alpha 2\delta$ -1-subunit but does not interact with $\alpha 2\delta$ -1 on the cell-surface when co-expressed. *Sci. Rep.* *6*, 24531.
- Lauritzen, S.P., Boye, T.L., and Nylandsted, J. (2015). Annexins are instrumental for efficient plasma membrane repair in cancer cells. *Semin. Cell Dev. Biol.* *45*, 32–38.
- Lee, C.S., and Park, H.H. (2017). Structural aspects of transglutaminase 2: functional, structural, and regulatory diversity. *Apoptosis* *22*, 1057–1068.
- Lepko, T., Pusch, M., Müller, T., Schulte, D., Ehses, J., Kiebler, M., Hasler, J., Huttner, H.B., Vandembroucke, R.E., Vandendriessche, C., et al. (2019). Choroid plexus-derived miR-204 regulates the number of quiescent neural stem cells in the adult brain. *EMBO J.* *38*, e100481.
- Lerchenmüller, C., Heißenberg, J., Damilano, F., Bezzeridis, V.J., Krämer, I., Bochaton-Piallat, M.L., Hirschberg, K., Busch, M., Katus, H.A., Peppel, K., et al. (2016). S100A6 Regulates Endothelial Cell Cycle Progression by Attenuating Antiproliferative Signal Transducers and Activators of Transcription 1 Signaling. *Arterioscler. Thromb. Vasc. Biol.* *36*, 1854–1867.
- Li, Y., Wagner, E.R., Yan, Z., Wang, Z., Luther, G., Jiang, W., Ye, J., Wei, Q., Wang, J., Zhao, L., et al. (2015). The Calcium-Binding Protein S100A6 Accelerates Human Osteosarcoma Growth by Promoting Cell Proliferation and Inhibiting Osteogenic Differentiation. *Cell. Physiol. Biochem.* *37*, 2375–2392.
- Lim, D.A., and Alvarez-Buylla, A. (2016). The Adult Ventricular-Subventricular Zone (V-SVZ) and Olfactory Bulb (OB) Neurogenesis. *Cold Spring Harb. Perspect. Biol.* *8*, a018820–a018834.
- Lledo, P.M., and Valley, M. (2016). Adult Olfactory Bulb Neurogenesis. *Cold Spring Harb. Perspect. Biol.* *8*, a018945.
- Llorens-Bobadilla, E., Zhao, S., Baser, A., Saiz-Castro, G., Zwadlo, K., and Martín-Villalba, A. (2015). Single-Cell Transcriptomics Reveals a Population of Dormant Neural Stem Cells that Become Activated upon Brain Injury. *Cell Stem Cell* *17*, 329–340.
- Long, K.R., Newland, B., Florio, M., Kalebic, N., Langen, B., Kolterer, A., Wimberger, P., and Huttner, W.B. (2018). Extracellular matrix components HAPLN1, Lumican and collagen I cause hyaluronic acid-dependent folding of the developing human neocortex. *Neuron* *99*, 702–719.e6.
- Long, K.R., and Huttner, W.B. (2019). How the extracellular matrix shapes neural development. *Open Biol.* *9*, 180216.
- Maeda, N. (2015). Proteoglycans and neuronal migration in the cerebral cortex during development and disease. *Front. Neurosci.* *9*, 98.
- Majkut, S., Idema, T., Swift, J., Krieger, C., Liu, A., and Discher, D.E. (2013). Heart-specific stiffening in early embryos parallels matrix and myosin expression to optimize beating. *Curr. Biol.* *23*, 2434–2439.
- Martinelli, D.C., Chew, K.S., Rohlmann, A., Lum, M.Y., Ressler, S., Hattar, S., Brunger, A.T., Missler, M., and Südhof, T.C. (2016). Expression of C1q3 in Discrete Neuronal Populations Controls Efferent Synapse Numbers and Diverse Behaviors. *Neuron* *91*, 1034–1051.
- Matsuda, K., Budisantoso, T., Mitakidis, N., Sugaya, Y., Miura, E., Kakegawa, W., Yamasaki, M., Konno, K., Uchigashima, M., Abe, M., et al. (2016). Transsynaptic Modulation of Kainate Receptor Functions by C1q-like Proteins. *Neuron* *90*, 752–767.

- Meran, L., Baulies, A., and Li, V.S.W. (2017). Intestinal Stem Cell Niche: The Extracellular Matrix and Cellular Components. *Stem Cells Int.* 2017, 7970385.
- Midwood, K.S., Chiquet, M., Tucker, R.P., and Orend, G. (2016). Tenascin-C at a glance. *J. Cell Sci.* 129, 4321–4327.
- Mirzadeh, Z., Doetsch, F., Sawamoto, K., Wichterle, H., and Alvarez-Buylla, A. (2010). The subventricular zone en-face: wholemount staining and ependymal flow. *J. Vis. Exp.* 6, 1938.
- Moeendarbary, E., Weber, I.P., Sheridan, G.K., Koser, D.E., Soleman, S., Haenzi, B., Bradbury, E.J., Fawcett, J., and Franze, K. (2017). The soft mechanical signature of glial scars in the central nervous system. *Nat. Commun.* 8, 14787.
- Naba, A., Clauser, K.R., Hoersch, S., Liu, H., Carr, S.A., and Hynes, R.O. (2012). The matrisome: in silico definition and in vivo characterization by proteomics of normal and tumor extracellular matrices. *Mol. Cell Proteomics* 11, M111.014647.
- Narouz-Ott, L., Maurer, P., Nitsche, D.P., Smyth, N., and Paulsson, M. (2000). Thrombospondin-4 binds specifically to both collagenous and non-collagenous extracellular matrix proteins via its C-terminal domains. *J. Biol. Chem.* 275, 37110–37117.
- Ninkovic, J., Steiner-Mezzadri, A., Jawerka, M., Akinci, U., Masserdotti, G., Petricca, S., Fischer, J., von Holst, A., Beckers, J., Lie, C.D., et al. (2013). The BAF complex interacts with Pax6 in adult neural progenitors to establish a neurogenic cross-regulatory transcriptional network. *Cell Stem Cell* 13, 403–418.
- Nolte, C., Matyash, M., Pivneva, T., Schipke, C.G., Ohlemeyer, C., Hanisch, U.K., Kirchhoff, F., and Kettenmann, H. (2001). GFAP promoter-controlled EGFP-expressing transgenic mice: a tool to visualize astrocytes and astrogliosis in living brain tissue. *Glia* 33, 72–86.
- Ortega, F., Costa, M.R., Simon-Ebert, T., Schroeder, T., Götz, M., and Berninger, B. (2011). Using an adherent cell culture of the mouse subependymal zone to study the behavior of adult neural stem cells on a single-cell level. *Nat. Protoc.* 6, 1847–1859.
- Pathak, M.M., Nourse, J.L., Tran, T., Hwe, J., Arulmoli, J., Le, D.T., Bernardis, E., Flanagan, L.A., and Tombola, F. (2014). Stretch-activated ion channel Piezo1 directs lineage choice in human neural stem cells. *Proc. Natl. Acad. Sci. USA* 111, 16148–16153.
- Perez-Riverol, Y., Csordas, A., Bai, J., Bernal-Llinares, M., Hewapathirana, S., Kundu, D.J., Inuganti, A., Griss, J., Mayer, G., Eisenacher, M., et al. (2019). The PRIDE database and related tools and resources in 2019: improving support for quantification data. *Nucleic Acids Res.* 47, D442–D450.
- Petrik, D., Myoga, M.H., Grade, S., Gerkau, N.J., Pusch, M., Rose, C.R., Grothe, B., and Götz, M. (2018). Epithelial Sodium Channel Regulates Adult Neural Stem Cell Proliferation in a Flow-Dependent Manner. *Cell Stem Cell* 22, 865–878.e8.
- Pillat, M.M., Lameu, C., Trujillo, C.A., Glaser, T., Cappellari, A.R., Negraes, P.D., Battastini, A.M.O., Schwindt, T.T., Muotri, A.R., and Ulrich, H. (2016). Bradykinin promotes neuron-generating division of neural progenitor cells through ERK activation. *J. Cell Sci.* 129, 3437–3448.
- Roll, L., and Faissner, A. (2014). Influence of the extracellular matrix on endogenous and transplanted stem cells after brain damage. *Front. Cell. Neurosci.* 8, 219.
- Ruddy, R.M., and Morshead, C.M. (2018). Home sweet home: the neural stem cell niche throughout development and after injury. *Cell Tissue Res.* 371, 125–141.
- Saha, K., Keung, A.J., Irwin, E.F., Li, Y., Little, L., Schaffer, D.V., and Healy, K.E. (2008). Substrate modulus directs neural stem cell behavior. *Biophys. J.* 95, 4426–4438.
- Saha, B., Ypsilanti, A.R., Boutin, C., Cremer, H., and Chédotal, A. (2012). Plexin-B2 regulates the proliferation and migration of neuroblasts in the postnatal and adult subventricular zone. *J. Neurosci.* 32, 16892–16905.
- Schiller, H.B., Fernandez, I.E., Burgstaller, G., Schaab, C., Scheltema, R.A., Schwarzmayr, T., Strom, T.M., Eickelberg, O., and Mann, M. (2015). Time- and compartment-resolved proteome profiling of the extracellular niche in lung injury and repair. *Mol. Syst. Biol.* 11, 819.
- Seidenfaden, R., Desoeuvre, A., Bosio, A., Virard, I., and Cremer, H. (2006). Glial conversion of SVZ-derived committed neuronal precursors after ectopic grafting into the adult brain. *Mol. Cell. Neurosci.* 32, 187–198.
- Silva-Vargas, V., Maldonado-Soto, A.R., Mizrak, D., Codega, P., and Doetsch, F. (2016). Age-Dependent Niche Signals from the Choroid Plexus Regulate Adult Neural Stem Cells. *Cell Stem Cell* 19, 643–652.
- Sorg, B.A., Berretta, S., Blacktop, J.M., Fawcett, J.W., Kitagawa, H., Kwok, J.C.F., and Miquel, M. (2016). Casting a Wide Net: Role of Perineuronal Nets in Neural Plasticity. *J. Neurosci.* 36, 11459–11468.
- Stukel, J.M., and Willits, R.K. (2018). The interplay of peptide affinity and scaffold stiffness on neuronal differentiation of neural stem cells. *Biomed. Mater.* 13, 024102.
- Sullivan, C.S., Gotthard, I., Wyatt, E.V., Bongu, S., Mohan, V., Weinberg, R.J., and Maness, P.F. (2018). Perineuronal Net Protein Neurocan Inhibits NCAM/EphA3 Repellent Signaling in GABAergic Interneurons. *Sci. Rep.* 8, 6143.
- Swift, J., Ivanovska, I.L., Buxboim, A., Harada, T., Dingal, P.C., Pinter, J., Pajeroski, J.D., Spinler, K.R., Shin, J.W., Tewari, M., et al. (2013). Nuclear lamin-A scales with tissue stiffness and enhances matrix-directed differentiation. *Science* 341, 1240104.
- Tavazoie, M., Van der Veken, L., Silva-Vargas, V., Louissaint, M., Colonna, L., Zaidi, B., Garcia-Verdugo, J.M., and Doetsch, F. (2008). A specialized vascular niche for adult neural stem cells. *Cell Stem Cell* 3, 279–288.
- Thomas, P.D., Campbell, M.J., Kejarawal, A., Mi, H., Karlak, B., Daverman, R., Diemer, K., Muruganujan, A., and Narechania, A. (2003). PANTHER: a library of protein families and subfamilies indexed by function. *Genome Res.* 13, 2129–2141.
- Thompson, A.J., Pillai, E.K., Dimov, I.B., Foster, S.K., Holt, C.E., and Franze, K. (2019). Rapid changes in tissue mechanics regulate cell behaviour in the developing embryonic brain. *eLife* 8, e39356.
- Tyanova, S., Temu, T., Sinitcyn, P., Carlson, A., Hein, M.Y., Geiger, T., Mann, M., and Cox, J. (2016). The Perseus computational platform for comprehensive analysis of (prote)omics data. *Nat. Methods* 13, 731–740.
- Vincent, L.G., Choi, Y.S., Alonso-Latorre, B., del Álamo, J.C., and Engler, A.J. (2013). Mesenchymal stem cell durotaxis depends on substrate stiffness gradient strength. *Biotechnol. J.* 8, 472–484.
- Vining, K.H., and Mooney, D.J. (2017). Mechanical forces direct stem cell behaviour in development and regeneration. *Nat. Rev. Mol. Cell Biol.* 18, 728–742.
- Wei, Z., Peterson, J.M., and Wong, G.W. (2011). Metabolic regulation by C1q/TNF-related protein-13 (CTRP13): activation OF AMP-activated protein kinase and suppression of fatty acid-induced JNK signaling. *J. Biol. Chem.* 286, 15652–15665.
- Wierer, M., Prestel, M., Schiller, H.B., Yan, G., Schaab, C., Azghandi, S., Werner, J., Kessler, T., Malik, R., Murgia, M., et al. (2018). Compartment-resolved Proteomic Analysis of Mouse Aorta during Atherosclerotic Plaque Formation Reveals Osteoclast-specific Protein Expression. *Mol. Cell. Proteomics* 17, 321–334.
- Winkler, C., Fricker, R.A., Gates, M.A., Olsson, M., Hammang, J.P., Carpenter, M.K., and Björklund, A. (1998). Incorporation and glial differentiation of mouse EGF-responsive neural progenitor cells after transplantation into the embryonic rat brain. *Mol. Cell. Neurosci.* 11, 99–116.
- Yamada, J., and Jinno, S. (2014). S100A6 (calcylin) is a novel marker of neural stem cells and astrocyte precursors in the subgranular zone of the adult mouse hippocampus. *Hippocampus* 24, 89–101.
- Zhang, X., Lei, K., Yuan, X., Wu, X., Zhuang, Y., Xu, T., Xu, R., and Han, M. (2009). SUN1/2 and Syne/Nesprin-1/2 complexes connect centrosome to the nucleus during neurogenesis and neuronal migration in mice. *Neuron* 64, 173–187.
- Zhu, Y., Li, X., Janairo, R.R.R., Kwong, G., Tsou, A.D., Chu, J.S., Wang, A., Yu, J., Wang, D., and Li, S. (2019). Matrix stiffness modulates the differentiation of neural crest stem cells in vivo. *J. Cell. Physiol.* 234, 7569–7578.

STAR★METHODS

KEY RESOURCES TABLE

REAGENT or RESOURCE	SOURCE	IDENTIFIER
Antibodies		
Beta-catenin (1/2000)	BD bioscience	Cat# 610153; RRID:AB_397554
Collagen 4 (1/100)	Millipore	AB756P; RRID:AB_2276457
DCX (1/500)	Millipore	Cat# AB2253; RRID:AB_1586992
GFAP (rb) (1/500)	DAKO	Cat# Z0334; RRID:AB_10013382
GFAP (ms) (1/500)	Sigma	Cat# G3893; RRID:AB_477010
GFAP (goat) (1/500)	abcam	Cat# ab53554; RRID:AB_880202
GFP (1/1000)	Millipore	Cat# MAB3580; RRID:AB_94936
GFP (1/2000-4000)	Aves lab	Cat# GFP-1020; RRID:AB_10000240
MAG (1/400)	Millipore	Cat# MAB1567; RRID:AB_2137847
MAP2 (1/1000)	Sigma	Cat# M4403; RRID:AB_477193
Nestin (1/100)	Millipore	Cat# MAB353; RRID:AB_94911
NeuN (1/100)	Millipore	Cat# MAB377; RRID:AB_2298772
S100a6 (1/500)	Abcam	Cat# ab181975
S100B (ms) 1/500)	Sigma	Cat# S2532; RRID:AB_477499
Tgm2 (1/100)	Labvision	Cat# MS-224-B0; RRID:AB_62201
WFA (biotin conjugated) (1/500)	Sigma	Cat# L1516-2MG; RRID:AB_2620171
Secondary antibodies		
Alexa Fluor® secondary antibodies (488, 555, 647) (1/1000)	ThermoFisher Scientific	Cat# A-11001; RRID:AB_2534069
555 Alexa Fluor® conjugated streptavidin	ThermoFisher Scientific	Cat# S32355; RRID:AB_2571525
FACS antibodies		
CD133-PE (1/250)	eBioscience	Cat# 12-1331-82; RRID:AB_465849
EGF-Alexa Fluor 647 (1/300)	Molecular Probes	Cat# E-35351
Anti-PSA-NCAM-PE (1/250)	Miltenyi	Cat# 130-093-274; RRID:AB_1036069
Rat IgG1 K isotype control PE (1/250)	eBioscience	Cat# 12-4301-81; RRID:AB_470046
Mouse IgM-PE antibody (isotype control (1/250))	Miltenyi	Cat# 130-093-177; RRID:AB_871723
Chemicals, Peptides, Recombinant Proteins and Kits		
IGPAL-CA-630	Sigma	Cat# I8896
Phosphatase inhibitors	Roche	Cat# 04906837001
Benzonase	Merck	Cat# 70746-3
Protease inhibitors (+EDTA)	LifeTech	Cat# 78430
Sodium deoxycholate	Sigma	Cat# D6750
TCEP	Sigma	Cat# 646547
2-Chloroacetamide	Sigma	Cat# C0267
Ammonium acetate	Sigma	Cat# V800034
Formic acid	Sigma	Cat# 543804
Gaudinium	Sigma	Cat# G4505
Thio-urea	Sigma	Cat# T8656
SDS	Sigma	Cat# L4509
HEPES	Sigma	Cat# H3375
Trypsin	Sigma	Cat# T9201
Hyaluronidase	Sigma	Cat# H3884
DMEM/F12	Life Technologies	Cat# 21331020
B27 Supplement	Life Technologies	Cat# 17504044

(Continued on next page)

Continued

REAGENT or RESOURCE	SOURCE	IDENTIFIER
Poly-D-lysine hydrobromide	Sigma	Cat# P0899
GlutaMax	Life Technologies	Cat# 35050038
Trypsin-EDTA (0.05%)	ThermoFisher Scientific	Cat# 25300054
Poly-L-ornithin	Sigma	Cat# P4957
Laminin	Roche	Cat# 11243217001
TSA Tetramethylrhodamine kit	PerkinElmer	Cat# NEL702001KT
Acetonitrile	Sigma	Cat# 271004
Trifluoroacetic acid	Sigma	Cat# 302031
Micro BCA protein assay kit	ThermoFisher Scientific	Cat# 23235
Goat Serum	ThermoFisher Scientific	Cat# 16210072
RLT lysis buffer	QIAGEN	Cat# 79216
Triton X-100	Sigma	Cat# T8787
RLT lysis buffer	QIAGEN	Cat# 79216
RNeasy Micro Kit	QIAGEN	Cat# 74004
RNeasy Mini Kit	QIAGEN	Cat# 74104
SuperScript III	Invitrogen	Cat# 18080093
iQ SYBR Green Supermix	BIO-RAD	Cat# 1708880
IsoFlo	Abbott Laboratories	Cat# NDC 0044-5260-03
DMSO	Sigma	Cat# D2438-10ML
ZDON	Zedira	Cat# Z006
BocDON	Zedira	Cat# B003
EdU	ThermoFisher Scientific	Cat# E10187
Click-iT EdU Alexa fluor 647 Imaging kit	Invitrogen	Cat# C10340
HiPerFect® transfection reagent	QIAGEN	Cat# 301704
Allstars Negative control siRNA	QIAGEN	Cat# 1027280
FlexiTube GeneSolution for Tgm2	QIAGEN	Cat# GS21817
Glutaraldehyde	Sigma	Cat# G5882
(3-Aminopropyl) trimethoxysilane (APTMS)	Sigma	Cat# 281775
Acrylamide	Sigma	Cat# A4058
N-Hydroxyethyl-acrylamide	Sigma	Cat# 697931
Bis-acrylamide	Fisher Scientific	Cat# BP1404-250
Experimental Models: Organisms/Strains		
C57Bl6/J mice	In-house breeding	N/A
<i>C1ql3^{fllox}</i> ; <i>C1ql3^{tm1.1Sud}</i>	Martinelli et al., 2016	RRID: MGI_5779515
hGFAP-GFP mice (Tg(GFAP-EGFP)1Hket)	Nolte et al., 2001	MGI:6188855
Deposited Data		
Proteome dataset	ProteomeXchange Consortium at http://proteomecentral.proteomexchange.org	PXD016632
Supplementary tables (of in-article analyzed data)	The journal	N/A
Proteome dataset	https://pawelsm.github.io/neuronichen1/ or https://neuronicheproteome.org	N/A
Microarray dataset	Gene Expression Omnibus at https://www.ncbi.nlm.nih.gov/geo/	accession number GPL15692
Software and Algorithms		
MATLAB, including custom-written scripts to analyze AFM data	Mathworks: https://www.mathworks.com/products/matlab/Custom MATLAB scripts: https://github.com/FranzeLab	Version R2018b
Maxquant	http://www.coxdocs.org/doku.php?id=maxquant:start	Version 1.6.0.16

(Continued on next page)

Continued

REAGENT or RESOURCE	SOURCE	IDENTIFIER
Perseus	http://www.coxdocs.org/doku.php?id=perseus:start	Version 1.6.0.7
Prism	Graphpad	Version 5
Microarray analysis	GeneSpring GX v11.5.1 software package	Agilent Technologies
String	https://string-db.org/	N/A
ZEN imaging software	Carl Zeiss	N/A
Other		
CellHesion 200 AFM head	JPK Instruments	N/A
PetriDishHeater for maintaining constant temperature during AFM-based stiffness measurements	JPK Instruments	N/A
Tipless silicon cantilevers for AFM-based stiffness measurements	NanoWorld	Arrow TL-1
Spherical probes for AFM cantilevers	microParticles GMBH	37.28 μ m polystyrene beads, PS-R-37.0

LEAD CONTACT AND MATERIALS AVAILABILITY

Further information and requests for resources and reagents should be directed to and will be fulfilled by the Lead Contact, Prof. Magdalena Götz (magdalena.goetz@helmholtz-muenchen.de). This study did not generate new unique reagents.

EXPERIMENTAL MODEL AND SUBJECT DETAILS**WT Mice (Proteomics, Cell Culture, Osmotic Pumps, IHC, and AFM) and hGFAP-eGFP mice (FACS, IHC)**

All experimental procedures in this study done at LMU Muenchen were performed in accordance with German and European Union guidelines and were approved by the government of upper Bavaria. In addition, all procedures performed in Cambridge were carried out in accordance with the UK Animals (Scientific Procedures) Act 1986 and with university guidelines. For the proteomics experiments, only male C57BL/6J mice between 8-10 weeks were used, for osmotic pump experiments, only male C57Bl6/J mice between 10-12 weeks were used, and for AFM experiments, only male C57Bl6/J mice aged 8 weeks were used (to reduce any potential variability). For other experiments both male and female C57BL/6J mice were used between 8-12 weeks. For FACS and IHC experiments, we used both male and female 8-12 week old hGFAP-eGFP mice (Tg(GFAP-EGFP)1Hket, [Nolte et al., 2001](#)). Mice were fed *ad libitum* and housed with a 12/12 h light and dark cycle and kept under specific-pathogen-free (SPF) conditions.

C1q3 Reporter Mice

The analysis of *C1q3* gene expression was performed using the IRES-mVenus knockin reporter allele (*C1q3^{fllox}*; *C1q3^{tm1.1Sud}* RRID: MGI_5779515) described in ([Martinelli et al., 2016](#)). The background strain of the mice was C57BL/6. All procedures involving the use of mice at the University of Connecticut Health Center were approved by the Institutional Animal Care and Use Committee, and in accordance with guidelines set forth by the National Research Council of the National Academies Guide for the Care and Use of Laboratory Animals.

Primary SEZ Culture

The sub-ependymal zones (SEZ) of 8 - 12 weeks old C57BL/6J wild-type mice were dissected in Hank's Balanced Salt Solution (HBSS) with 10 mM HEPES (4-(2-hydroxyethyl)-1-piperazineethanesulfonic acid) and after removing the dissection medium incubated in 5 mL dissociation solution (HBSS containing 15 mM HEPES, 5.4 Glucose, 3.4 mg trypsin powder and 3.5 mg hyaluronidase powder) at 37°C for 15 min. The SEZ pieces were triturated 10 times using a 5 mL glass pipette and incubated for another 15 min at 37°C. 5 mL ice-cold solution 3 (solution 3: EBSS (Earle's Balanced Salt Solution) containing 20 mM HEPES and 0,04 g/mL BSA (Bovine Serum Albumin); pH 7.5) were added and solutions were mixed by pipetting 10 times with a 10 mL pipette. The cell suspension was filtrated through a 70- μ m cell strainer and centrifuged at 250 g for 5 min at 4°C. The supernatant was discarded and cells were resuspended in 10 mL ice-cold solution 2 (solution 2: HBSS containing 0.9 M Sucrose; pH 7.5) and centrifuged at 650 g for 10 min at 4°C. After discarding the supernatant, cells were resuspended in 2 mL ice-cold solution 3. 2 mL of the cell suspension were added to a 15 mL falcon tube with 12 mL ice-cold solution 3 and centrifuged at 350 g for 7 min at 4°C. The supernatant was carefully removed and cells were resuspended in B27-supplemented culture medium (culture medium: DMEM/F12 (1:1) with 1x GlutaMAX containing 1x B27 serum-free supplement, 100 units/mL penicillin, 100 mg/mL streptomycin, 8 mM HEPES) and seeded

(2 SEZs per well) onto poly-D-lysine - coated (PDL) coverslips in 24-well tissue culture plates (Ortega et al., 2011). Cells were kept in the incubator for 7d at 37°C and 5% CO₂, with the exception of cultures on hydrogels (see Hydroxy-Acrylamid Gel Preparation for Cell Culture) that were kept for 5 d.

METHOD DETAILS

Sample Preparation for Proteome Analysis

Library-Matched Single Shot (LMSS) Method. Mice were sacrificed by cervical dislocation and brains were subsequently extracted and put into cold phosphate buffered saline (PBS). The ventricular walls were laid bare by removing the dorsal ventricular wall and all tissue above it, as well as the choroid plexus. Brains were then snap-frozen on dry ice and cut into 100 μm sections on a cryostat (Leica CM1000S). The medial (MEZ) and lateral ventricular (SEZ) walls were then manually dissected under a light microscope (Leica MZ6). 8-10 sections from each animal were collected per sample (n = 8) and kept on dry ice until tissue lysis. Somatosensory cortex (Cx) samples were dissected by removing corpus callosum and top layer of cortex (including meninges). Olfactory bulb (OB) was dissected by cutting out the core of the OB approximately along the external plexiform layer. Both Cx and OB samples were subsequently snap-frozen on dry ice (n = 8). Tissues were lysed in buffer containing 0.1 M Tris-HCl (pH 8.5), 1% (w/v) Sodium Deoxycholate, 10 mM tris(2-carboxyethyl)phosphine hydrochloride (TCEP), and 40 mM 2-Chloroacetamide at 99°C for 10 min. The lysates were sonicated for 2 × 15 min (or until homogeneous) (Bioruptor, model UCD-200, Diagenode) and protein concentration was determined using the BCA method (Micro BCA protein assay kit) according to manufacturer instructions. 25 μg of protein was digested with LysC and trypsin overnight at 37°C. 250 μl Isopropanol with trifluoroacetic acid (TFA) (each sample contains 1% TFA) was added to each sample and then mixed strongly. Samples were desalted using the StageTip method with SDB-RPS (styrene-divinyl-benzene reverse phase sulfonate; 3M, #2241) filters (Kulak et al., 2014). Therefore, filters were activated with acetonitrile (ACN) and equilibrated with 30% methanol (MeOH) and 1% TFA. After washing with 0.2% TFA, the samples were added to the stage tips and then filters were washed again. Elution was done using 1% Ammonia and 80% ACN. Four of the peptide samples from each region were combined and used for the library proteome of each region. These pooled peptide samples were divided into 8 fractions with nano-fractionation using a high pH reversed-phase fractionator that switches the elution flow every 90 s using a rotating valve (Kulak et al., 2017). The four remaining single-shot samples from each region were analyzed without fractionation.

Quantitative Detergent Solubility Profile (QDSP) Method. Mice were sacrificed by cervical dislocation and brains were subsequently extracted and put into cold PBS. The OB was removed by dissection at its base. Somatosensory cortex (Cx) was dissected using a 2.5 mm biopsy punch and the white matter was removed. Both subependymal zones (SEZ and MEZ) were dissected (Ortega et al., 2011). All samples were homogenized using a (100 μl) dounce homogenizer (Wheaton #357844) in 100 μl PBS (with protease inhibitor cocktail and Ethylenediaminetetraacetic acid (EDTA)) and directly frozen in liquid nitrogen and stored at -80°C until tissue protein fractionation. Tissue lysates from 3 animals were pooled, resulting in 5 samples per region and then processed simultaneously (a total of 15 mice). Following centrifugation, we collected the supernatant (protein fraction 0) and then sequentially extracted proteins using the MS analysis adapted de-cellularization protocol of Schiller et al. (Schiller et al., 2015). Therefore, we resuspended the pellet in three buffers, each followed by a centrifugation for 20 min at 16,000 g. The samples were incubated in buffer 1 (150 mM NaCl, 50 mM Tris-HCl (pH 7.5), 5% glycerol, 1% IGEPAL, 1 mM MgCl₂, protease inhibitors (+EDTA), 1% benzonase, 1 × phosphatase inhibitors) and buffer 2 (150 mM NaCl, 50 mM Tris-HCl (pH 7.5), 5% glycerol, 1.0% IGEPAL, 0.5% sodium deoxycholate, 0.1% SDS, 1 × protease inhibitors (+EDTA), and 1% benzonase) for 20 min on ice, and in buffer 3 (500 mM NaCl, 50 mM Tris-HCl (pH 7.5), 5% glycerol, 1.0% IGEPAL, 2% sodium deoxycholate, 1% SDS, 1 × protease inhibitors (+EDTA), and 1% benzonase) for 20 min at RT. Each of the supernatant from the buffer treatment resulted in fraction 1, 2, and 3, with the residual insoluble material resulting in fraction 4. Fraction 0 and 1 were combined to generate our first fraction. All four fractions were precipitated in 80% acetone and sonicated for 5x30 s (Bioruptor, model UCD-200, Diagenode). Afterward, samples were incubated at -20°C for a minimum of 1 h and were then centrifuged. The precipitation was repeated once in order to remove any residual detergent. Alkylation/reduction buffer (100 mM Tris-HCl (pH 8.5), 6M GdmCl, 10 mM TCEP, and 50 mM 2-chloroacetamide) was added to the samples and then boiled at 99°C for 15 min, followed by sonication for 10 × 30 s. Protein concentration was determined using the BCA method (Micro BCA protein assay kit) according to manufacturer instructions. Enzymatic digestion was done in two steps. First, samples were incubated at 37°C for 2 h with LysC (1/50) and then with LysC (1/50) and Trypsin (1/25) overnight. Both digestions were aided by 10 × 30 s sonification. Samples were then acidified by adding 1% TFA followed by desalting using the StageTip method with SDB-RPS filters (Kulak et al., 2014). Therefore, filters were activated with acetonitrile (ACN) and equilibrated with 30% methanol (MeOH) and 1% TFA. After washing with 0.2% TFA, the samples were added to the stage tips and then filters were washed again. Each protein lysate was eluted into three peptide fractions using three buffers (buffer 1: 150 mM NH₄HCO₂, 40% acetonitrile, 0.5% Formic acid (FA); buffer 2: 150 mM NH₄HCO₂, 60% acetonitrile, 0.5% FA and buffer 3: 5% ammonia (from 25% stock solution) and 80% acetonitrile) resulting in a total of 12 fractions per sample.

Mass Spectrometry

For both the LMSS (including each library sample) and QDSP samples, we loaded approximately 2 μg of peptides in buffer A (0.1% (v/v) formic acid). We separated peptides by a 2 h gradient in a 50 cm long C18 column (75 μm inner diameter filled in house with ReproSil-Pur C18-AQ 1.9-μm resin (Dr. Maish GmbH)). Samples were eluted in 5%–60% buffer B (0.1% (v/v) formic acid, 80% (v/v) acetonitrile) at a flow rate of 250 nL/min using a nanoflow UHPLC (Easy nLC, Thermo Fisher Scientific) online coupled to the

mass spectrometer (Q Exactive HF Orbitrap, Thermo Fisher Scientific). Each gradient was followed by a wash with buffer B and recalibration with buffer A. Survey scans had a resolution of 70,000 at m/z 400 with a maximum injection time of 20 ms. Target value for the full scan MS spectra was 3×10^6 and isolation window of 1.6 m/z with 10 most abundant precursor ions chosen for fragmentation. MS/MS scans had a resolution of 17,500 at m/z 400 with a maximum injection time of 120 ms. Ion target value for the MS/MS scan was 1×10^5 .

Immunohistochemistry

Brain Sections. For obtaining brain sections, mice (hGFAP-eGFP, mVenus/C1q/3, or C57BL/6J) were anaesthetized by intraperitoneal injection of ketamine (100mg per kg of body weight) and xylazine (10mg per body weight) and then transcardially perfused first with PBS followed by 4% Paraformaldehyde (PFA). Brains were dissected and cut at 80–100 μm thickness at the vibratome (Leica VT1000S) or 30 μm at the cryostat (Leica CM3050S). Sections were stained with primary antibodies in PBS containing 0.1% Triton X-100 and 10% normal goat serum (NGS) overnight at 4°C, washed and incubated with secondary antibodies in PBS containing 10% NGS for 2 h at RT. mVenus/C1q/3 expression was detected using chicken anti-GFP (Aves, 1:4000).

Perfused brains from the osmotic pump experiments were sectioned coronally (20 μm) along the ventricles. Sections were stained for Dcx and EdU according to manufacturer instructions (Click-iT™). Photomicrographs of the SEZ contralateral to the pump implantation site for quantifications were acquired using confocal microscope LSM 710 (Zeiss).

Whole Mounts. Whole mounts of the SEZ from three months old hGFAP-eGFP transgenic mice were dissected (Mirzadeh et al., 2010) and fixed for 15 min with 2% PFA. After washing with PBS, the tissue was stained for 48 h with primary antibodies in PBS containing 0.1% Triton X-100 and 10% normal goat serum (NGS). Whole mounts were washed three times with PBS at room temperature and incubated with the secondary antibodies in PBS containing 10% NGS overnight at 4°C. After three washings in PBS, DAPI was added for 5 min and washed again. Primary antibodies used were: mouse IgG1 anti-Tgm2 (Labvision, 1:100), rabbit anti- β -catenin (Sigma, 1:2000) and chicken anti-GFP (Aves, 1:2000). Tyramide Signal Amplification was used to enhance the Tgm2 fluorescence signal according to the manufacturer instructions (TSA Tetramethylrhodamine kit, PerkinElmer). Photomicrographs were acquired using confocal microscope LSM 710 (Zeiss).

Primary SEZ Cultures. Primary SEZ cultures were fixed with 400 μl of 4% (wt/vol) PFA for 15 min at room temperature (RT) and afterward washed twice with PBS. The staining solution contained primary antibodies in PBS with 0.5% Triton X-100 and 10% NGS. Primary antibodies used were: mouse IgG1 anti-Tgm2 (Labvision, 1:100), chicken anti-GFP (Aves, 1:2000), rabbit anti-GFAP (Dako, 1:500), and guinea pig anti-Dcx (Millipore, 1:500). Cells were incubated with the primary antibodies at 4°C overnight, washed with PBS twice and incubated with secondary antibodies in PBS with 10% NGS for 2 h at RT. Photomicrographs were acquired using fluorescent microscope AXIO Imager.Z1 (Zeiss).

All primary and secondary antibodies used can be found in the KEY RESOURCES TABLE (including the used concentration).

Fluorescence-activated Cell Sorting

SEZ from heterozygous hGFAP-eGFP (Nolte et al., 2001) and C57BL/6J (WT) mice were dissected in dissection medium (HBSS containing 10mM HEPES) on ice and transferred into a 15 mL falcon tube containing 5 mL of solution 1 (solution 1 (HBSS-glucose), see above, 0.81% glucose, 15 mM HEPES in HBSS; pH 7.5). The tissue was mechanically dissociated by pipetting up and down ten times with a fire-polished glass Pasteur pipette. 100 μl of 0.05% trypsin was added to the sample, followed by an incubation step at 37°C for 15 min. Trituration was repeated after 15 min with a fire-polished Pasteur pipette and cells were incubated for additional 15 min. Final trituration was done ten times at the end of the incubation. 5 mL of ice-cold solution 3 (solution 3 (BSA-EBSS-HEPES) 20 mM HEPES, 0.04 g/mL BSA in EBSS; pH 7.5) was added and solutions were mixed by pipetting several times up and down. The cell suspension was filtrated using a 70- μm cell strainer and centrifuged at 180 g for 5 min at 4°C. The supernatant was removed and cells were resuspended in 10 mL of ice-cold solution 2 (solution 2 (saccharose-HBSS) 0.9 M saccharose) in HBSS; pH 7.5) and centrifuged at 510 g for 20 min at 4°C. The pellet was resuspended in 2 mL of ice-cold solution 3 and pured on top of 12 mL of ice-cold solution 3 and centrifuged at 290 g for 12 min at 4°C. Staining solution (0.02% sodium azide, 10%, FBS in PBS) was added to the pellet and cells were incubated with primary antibodies for 30 min at 4°C. After washing with PBS, cells were resuspended in PBS and sorted using the FACS Aria III (BD). Gates were set by the use of isotype controls (Fischer et al., 2011).

To collect neural stem cells (NSC), transient amplifying progenitors (TAP), neuroblasts (NB), ependymal cells (EC) and niche astrocytes (NA) we stained the cells as follows: tube 1, cells from hGFAP-eGFP mice with CD133-PE (1:250); tube 2, cells from hGFAP-eGFP mice with CD133-PE (1:250), EGF-Alexa Fluor 647 (1:300) and Anti-PSA-NCAM-PE (1:250) and tube 3, cells from hGFAP-eGFP mice with Anti-PSA-NCAM-PE (1:250). Controls to set the gates were prepared as follows: tube 4, cells from WT mice lacking any antibody; tube 5, cells from WT with rat IgG1 K isotype control PE (1:250); tube 6, cells from WT mice with mouse IgM-PE isotype control (1:250).

qPCR

FACS sorted cells were directly collected into RLT lysis buffer (QIAGEN) during the sorting procedure. Total RNA was isolated with the RNeasy MICRO kit (QIAGEN) according to the manufacturer's instructions. Quality and concentration of total RNA was examined with the Agilent Bioanalyzer. Subsequently, cDNA was synthesized with SuperScript III (Invitrogen) as per manufacturer's instructions. qPCR was performed on an Opticon (BIO-RAD) with iQ SYBR Green Supermix (BIO-RAD) and expression levels were normalized to GAPDH.

Clonal Analysis in Primary SEZ Cultures

The primary SEZ cultures were prepared for cluster analysis according to the protocol above (Ortega et al., 2011). The SEZ from two mice were pooled in order to provide an $n = 1$ and the cells were plated in two wells (24-well plate) onto poly-D-Lysin coated coverslips. An $n = 4$ was prepared and analyzed for these experiments. Low titer of CAG-IRES-GFP retrovirus was added at 2 h after plating. Tgm2 inhibitor Z-DON (Zedira) or Boc-DON (Zedira) was added 4 h after plating at a concentration of 10 μM and 100 μM , respectively. Control samples had the equivalent volume of DMSO as the Boc-DON samples added to them (2 $\mu\text{l/well}$). Cells were incubated at 37°C with 5% CO_2 for 7 days until fixation with 4% PFA for 15 min at RT. Immunocytochemistry was performed as described above. Cluster counting and analysis was performed after photomicrograph acquisition of the whole coverslips (Axio Imager M2m, Zeiss). siRNA experiments were performed in the same manner as the *in vitro* inhibitor experiments, except that the siRNA (QIAGEN) was added to the cultures immediately after plating together with an equal part Hitransfect (QIAGEN) (mixed 30 min prior to use). Each well was transfected with a total concentration of 10 nM siRNA containing four Tgm2 siRNAs (Flexitube, QIAGEN) or the same concentration of scrambled siRNA control (Allstar negative control, QIAGEN).

Hydroxy-Acrylamid Gel Preparation for Cell Culture

In order to prepare gels with different stiffness we used the method developed by Bollmann et al., 2015. Glass bottom Petri dishes were washed first with 70% Ethanol and then 0.1% sodium hydroxide (NaOH). The NaOH treated surface was treated with (3-Amino-propyl) trimethoxysilane (APTMS) for 3 min, washed and subsequently 0.5% glutaraldehyde was applied for 30 min. The gel solution was prepared by adding 500 μl 40% acrylamide, 65 μl 100% hydroxyl-acrylamide and 250 μl 2% bis-acrylamide. 89.4% and 88.8% PBS were added to the premix to obtain the desired shear moduli of 100 Pa and 200 Pa, respectively. The desired gel-stiffness was confirmed with Atomic force microscopy (AFM). Finally, gels were coated with Poly-L-ornithin (Sigma, P4957) for 2 h followed by Laminin coating (Roche, #11243217001) for another 2 h.

Osmotic Pump Preparation and Surgery

Osmotic pumps (model 2001, ALZET®) were prepared the day before surgery according to the vendors instructions. Pumps were filled with 100 μM Z-DON in artificial cerebrospinal fluid (aCSF) or DMSO in an equivalent concentration (0.4%) as in the treatment group. Pumps were kept in sterile PBS at 37°C until surgery. The experimental procedure was approved by the government of upper Bavaria. Mice were anaesthetized by intraperitoneal injection of fentanyl (0.05 mg/kg), midazolam (5 mg/kg), and medetomidine (0.5 mg/kg) and after the surgery the anesthesia was antagonized by injection of buprenorphine (0.1 mg/kg), atipamezole (2.5 mg/kg), and flumazenil (0.5 mg/kg). Intra ventricular osmotic pump implantation (Brain kit 2, ALZET®) was performed at the coordinates 1.2 mm laterally to and 0.5 mm posterior to the bregma (right side) (Lepko et al., 2019). The experimental endpoints were 4 ($n = 3$) and 7 days ($n = 4$) after surgery. 5 mg/mL EdU in saline was administered i.p. at a volume of 10 μl per gram of the mouse's weight 1 h prior perfusion. The mice were perfused with 4% PFA and the brains were post-fixed overnight.

Stiffness Measurements

Sample Preparation. Male C57BL6/J mice ($N = 5$ animals), aged 8 weeks, were anaesthetized using 5% isoflurane (IsoFlo, Abbott Laboratories) and euthanized by intraperitoneal injection of a lethal dose of pentobarbital (Pentoject, Animalcare UK), followed by cardiac perfusion with cold slicing aCSF. Brains were immediately dissected out into cold slicing aCSF, keeping the olfactory bulbs intact, and sections prepared for stiffness measurements using the *ex vivo* acute CNS slice protocol described previously in Koser et al. (2015) and Moeendarbary et al. (2017). Hence, each brain was embedded in 4% low melting point agarose (Sigma; in 1 \times PBS), the agarose block containing the tissue was glued onto a vibratome platform (Leica), and 300 μm thick coronal sections were cut in cold slicing aCSF. Sections containing the anatomical regions of interest were transferred to a collection chamber containing measuring aCSF at room temperature (approx. 20°C) and allowed to equilibrate for ~ 5 -10 min. Sections were then attached to 35 mm Petri dishes (TPP) using small dabs of superglue at the outer corners of the surrounding agarose, immediately covered with fresh measuring aCSF, and transferred to the AFM set-up for measurement. The time elapsed between euthanasia of the animals and the beginning of slicing was ~ 30 min.

The compositions of the buffers used in this protocol were as follows: for slicing aCSF, 191 mM sucrose, 0.75 mM K-gluconate, 1.25 mM KH_2PO_4 , 26 mM NaHCO_3 , 4 mM MgSO_4 , 1 mM CaCl_2 , 20 mM glucose, 2 mM kynurenic acid, 1 mM (+)-sodium L-ascorbate, 5 mM ethyl pyruvate, 3 mM myo-inositol, and 2 mM NaOH; and for measuring aCSF, 121 mM NaCl, 3 mM KCl, 1.25 mM NaH_2PO_4 , 25 mM NaHCO_3 , 1.1 mM MgCl_2 , 2.2 mM CaCl_2 , 15 mM glucose, 1 mM (+)-sodium L-ascorbate, 5 mM ethyl pyruvate, and 3 mM myo-inositol. Both solutions were freshly prepared before each experiment and bubbled with 95% O_2 and 5% CO_2 , beginning at least 30 min before first use and continuing throughout the procedure (Koser et al., 2015; Moeendarbary et al., 2017).

Atomic Force Microscopy (AFM) Setup. A JPK CellHesion 200 atomic force microscope (JPK Instruments) was mounted on an inverted optical microscope (AxioObserver.A1, Zeiss) with a motorized x-y stage (JPK Instruments). For stiffness measurements, the spring constant k of tipless silicon cantilevers (Arrow-TL1, NanoWorld) were determined using the thermal noise method (Hutter and Bechhoefer, 1993) and cantilevers with k of 0.01-0.04 N/m (for olfactory bulb (OB) measurements) or 0.05-0.07 N/m (for SEZ/MEZ measurements) were selected. Spherical monodisperse polystyrene beads (diameter = $37.28 \pm 0.34 \mu\text{m}$ (for olfactory bulb) or $19.3 \pm 0.34 \mu\text{m}$ (for SEZ/MEZ)) (microParticles GmbH) were used as probes and attached to the ends of the cantilevers using heat-curing glue (M-Bond 610, MicroMeasurements). The use of spherical probes ensured a consistent contact area with the sample surface and

prevented damage to the slices. A PetriDishHeater (JPK Instruments) was set up on the motorised stage and used to maintain samples at a set temperature of 34°C for the duration of AFM measurements.

AFM Measurements. Prepared sections were placed in the sample holder and allowed to equilibrate for ~5 min while brightfield images of the slices were collected with an Andor Zyla 4.2 CMOS camera (connected to a modified upright AxioZoom V.16 system (Zeiss)). Force-distance curves (set force: 10 nN, approach speed: 5 μm/s, sampling rate: 1,000 Hz) were either taken manually (for SEZ/MEZ measurements), or automatically every 30–40 μm apart in a raster scan (for OB), using a custom-written script (Koser et al., 2015, 2016) generating a ‘stiffness map’ of the area. For stiffness maps, images of the upper right and lower left corners of the measured area were also collected to identify the region of the slice mapped by the AFM.

Microarray Analysis

After dissecting the OB, SEZ and Cx the RNA was extracted using the RNeasy Mini Kit from QIAGEN following the manufacturer’s instructions. Sample preparation and microarray analysis was carried out by Arraystar applying the Agilent Array platform. The sample preparation and microarray hybridization were performed based on the manufacturer’s standard protocols with minor modifications (Agilent Low Input Quick Amp Labeling Kit). Briefly, the sample was amplified and transcribed into fluorescent cRNA along the entire length of the transcripts without 3’ bias utilizing a random priming method. The labeled cRNAs were hybridized onto the Mouse LncRNA Array v2.0 (8 × 60K, Arraystar). After having washed the slides, the arrays were scanned by the Agilent Scanner G2505B.

QUANTIFICATION AND STATISTICAL ANALYSIS

Mass Spectrometric Data Analysis

We processed the mass spectra using MaxQuant (<http://coxdocs.org/doku.php>) (Cox and Mann, 2008). Using the Andromeda search engine, the spectra were searched against the mouse Uniprot sequence database (<https://www.uniprot.org>). Cysteine carbamidomethylation was set as fixed modification while variable modifications included hydroxylation of proline and methionine oxidation. For both protein and peptide level we set FDR to 0.01 and only peptides with an amino-acid length of seven or more were considered. The peptide identifications among the library samples from the four brain regions (Cx, OB, SEZ, MEZ) in the LMSS dataset were used to additionally identify peptides in the single shot samples based on similar mass and retention time. The matching between runs feature (a feature of the Max quant software) thus allows identification of proteins in the single shot samples (that were identified in library samples) when precursor peptides were found in MS1, but not selected for fragmentation and identification in MS2. Single shots and library samples were also matched within themselves, which was also the case for samples in the QDSP dataset. The label-free protein quantification was restricted to proteins identified with at least two unique peptides. Label-free quantification (LFQ) algorithm was used for protein quantifications (Cox et al., 2014). LFQ intensities are normalized median mass spectra intensity values that allow this quantification to be performed with any peptide and protein fractionation while maintaining high accuracy (Cox et al., 2014). For a protein to be considered valid, two peptide ratios are needed. Among the QDSP samples, there was one sample with two of the brain regions that had protein fraction with very low protein content and several fractions with lower protein identification. Thus, we omitted the whole sample from further bioinformatics analysis. This resulted in 4 samples per region (each with their respective four solubility fractions).

Bioinformatic Analysis and Statistics

Bioinformatic analysis was performed primarily with the Perseus software (coxdocs.org/doku.php) (Tyanova et al., 2016). For all datasets, we have used log₂ LFQ intensities for analysis and comparisons. Plots of selected categories or individual proteins were done in Graphpad Prism (version 5).

Bioinformatic Analysis of LMSS Dataset

The presented library proteomes depth signifies number of identified proteins ($n = 1/\text{region}$). The presented library-matched single shot sample measurements are filtered for at least 3 values per region ($n = 4/\text{region}$). This filtering was also used for data imputation. Imputation of missing values was done by random selection according to a normal distribution with negative shift of 1.8 standard deviations from the mean and with a width of 0.3 standard deviations. These log₂ LFQ intensities values for all proteins were then used for PCA, statistical analysis, gene ontology analysis and heatmap presentations. Proteome comparisons of regions were done with one-way ANOVA and p values were used for filtering significant regional abundance differences after FDR correction. Heatmaps display proteins with an FDR of 0.05 (Figure 1K). 1D and 2D enrichment analysis of annotated terms was done in Perseus (Figures 1L, 1M, 4E, 4F, 1SE, and 1SF) with an FDR of 0.05 and full annotation enrichment lists can be found in Table S2, and 4. Gene ontology analysis for library exclusive proteins was done in Panther (pantherdb.org) (Thomas et al., 2003) (Figures S1B and S1C). Matrisome distribution plots (Wisker plots) comprise of z-scored mean LFQ intensities for proteins of the respective category (number of proteins for each category is presented in the respective graphs). This data was analyzed using Kruskal-Wallis test with Dunn’s multiple comparison test and $p \leq 0.05$ was considered significant. For t test comparisons between brain regions an FDR ≤ 0.1 was considered significant.

Bioinformatic Analysis of QDSP Dataset

The presented total number of proteins from all regions signifies number of identified proteins ($n = 4/\text{region}$). The total number of identifications from each region is instead filtered for at least 3 values in a region. We filtered the data for at least 8 values in a region prior intensity imputation. Imputation of missing values for the protein fractions of each region was done by random selection according to a normal distribution with negative shift of 1.7 standard deviations from the mean and with a width of 0.4 standard deviations. These log₂ LFQ intensities values for all fractions were then used for PCA, annotation enrichment analysis, category solubility profiles, and heatmap presentations. 1D enrichment analysis of annotated terms (Figures 4E and 4F) used an FDR of 0.05. Category solubility profile plots (Whisker plots) comprise of z-scored mean LFQ intensities for protein fractions of the respective category (number of proteins for each category is presented in the respective graphs). We present the mean value of the three regions in all “brain” solubility profiles for different categories (z-scoring was always done within regions). This data was analyzed using Kruskal-Wallis test with Dunn’s multiple comparison test and $p \leq 0.05$ was considered significant. Categories in the PCA were considered significant with a $\text{FDR} \leq 0.05$. Differences between brain region solubility profiles were determined using the z-scored LFQ intensities and two-way ANOVA with FDR correction (p value ≤ 0.05 was considered significant). The matrixome proteins with differential solubility (Figure 4H) (p value ≤ 0.05) were filtered from the analysis of all proteins (in heatmap, Figure 4D). In Figure S5C, we compared the brain matrixome data to previously published datasets (using the QDSP method) in aorta and lung tissue (Schiller et al., 2015; Wierer et al., 2018). The averaged solubility profiles here are comprised of an average from all experimental groups of each study.

Analysis and Presentation of AFM Data

Analysis of Raw AFM Data. First, the force-distance curves collected from AFM measurements were analyzed using a custom-written MATLAB script (described previously in Koser et al. [2015] and Koser et al. [2016]) to obtain the reduced apparent elastic modulus \mathbf{K} , a measure of tissue stiffness. Raw AFM data were fitted to the Hertz model,

$$\mathbf{F} = \frac{4}{3} \mathbf{K} \delta^{\frac{3}{2}} \sqrt{\mathbf{R}}$$

with the applied force \mathbf{F} , the reduced apparent elastic modulus $\mathbf{K} = E/(1-\nu^2)$, with E being the Young’s modulus and ν the Poisson’s ratio, \mathbf{R} the radius of the probe, and δ the indentation depth (Hertz, 1881). Force-distance curves were analyzed at the maximum applied force of 10 nN. Points where the AFM data was not analyzable were excluded from further analysis. Criteria for excluding individual force-distance curves were the inability to apply linear fits through the baseline of the curve, e.g., due to noise, and the inability to apply good-quality Hertz-fits to the indentation region. \mathbf{K} values were color-coded and converted to 8-bit scale colormaps, using the MATLAB ‘hot’ colormap pre-set. The resulting two-dimensional ‘stiffness maps’ were overlaid onto images of the samples using custom-written MATLAB scripts (Koser et al., 2015, 2016). Local brain region stiffness was statistically analyzed using Mann-Whitney test (two-tailed).

Bioinformatic Analysis Microarray Data

Agilent Feature Extraction software (version 10.7.3.1) was used to analyze acquired array images. Quantile normalization and subsequent data processing were carried out by Arraystar using the GeneSpring GX v11.5.1 software package (Agilent Technologies). After quantile normalization of the raw data, mRNAs that at least 6 out of 12 samples have flags in Present or Marginal (“All Targets Value”) were chosen for further data analysis. Differentially expressed mRNAs were identified through Volcano Plot filtering.

DATA AND CODE AVAILABILITY

The mass spectrometry proteomics data have been deposited to the ProteomeXchange Consortium via the PRIDE (Perez-Riverol et al., 2019) partner repository and the accession number for the proteomes reported in this paper is ProteomeXchange: PXD016632 (<http://proteomecentral.proteomexchange.org>). We also provide excel tables with the analyzed proteomics data for easy access. Furthermore, the two proteomes are available with pre-made graphs for each protein on the webpage <https://pawelsm.github.io/neuronichen1/> or <https://neuronicheproteome.org>. The microarray dataset is accessible at GEO: GPL15692. Custom-written scripts used for motorised stage control, processing of AFM raw data, and the generation and alignment of colormaps can be found at <https://github.com/FranzeLab>.

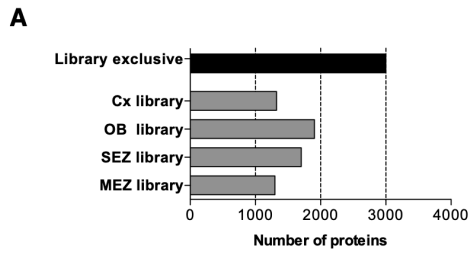
Cell Stem Cell, Volume 26

Supplemental Information

Defining the Adult Neural Stem Cell Niche Proteome

Identifies Key Regulators of Adult Neurogenesis

Jacob Kjell, Judith Fischer-Sternjak, Amelia J. Thompson, Christian Friess, Matthew J. Sticco, Favio Salinas, Jürgen Cox, David C. Martinelli, Jovica Ninkovic, Kristian Franze, Herbert B. Schiller, and Magdalena Götz



B

Protein Class	Number of proteins (of 2692)	Fold Enrichment	P-value
transcription factor	204	1.51	1.68E-06
Unclassified	1363	1.08	0.00E00
hydrolase	140	0.73	6.20E-03
RNA binding protein	88	0.65	1.54E-03
membrane traffic protein	40	0.52	5.40E-04
dehydrogenase	24	0.51	2.94E-02
ribosomal protein	18	0.41	1.60E-03

Protein
Dlx5
Dlx6
Foxj2
Foxp1
Foxp2
Pax6
Prox1
Rybpb
Smad1
Smad3
Sox2
Sox10
Sox11
Tbx21

C

Molecular Function	Number of proteins (of 2692)	Fold Enrichment	P-value
ubiquitin-protein ligase activity	47	1.80	2.20E-02
sequence-specific DNA binding transcription factor activity	162	1.58	2.74E-06
DNA binding	191	1.47	2.06E-05
receptor activity	114	1.40	4.66E-02
Unclassified	1356	1.06	0.00E00
catalytic activity	693	.87	9.28E-04
structural molecule activity	93	.67	3.05E-03
structural constituent of ribosome	16	.40	1.73E-03

Protein
CD47
Fzd5
Htra1a,b
Htra2a,c
Ifngr1
Ngfr
Ntsr1
Tgfbf1

D

Neurogenesis associated proteins

IL16	IL18	IL34
Igf1	Igf2	Igfbp6,7
Fzr1	Csf1	Pdgfra
Notch1	Notch2	Notch3
Rxra,g	Sirpa	Tgfb3
Uhrf1	Vegfa	Wnt4
Wnt5a	Wnt9a	

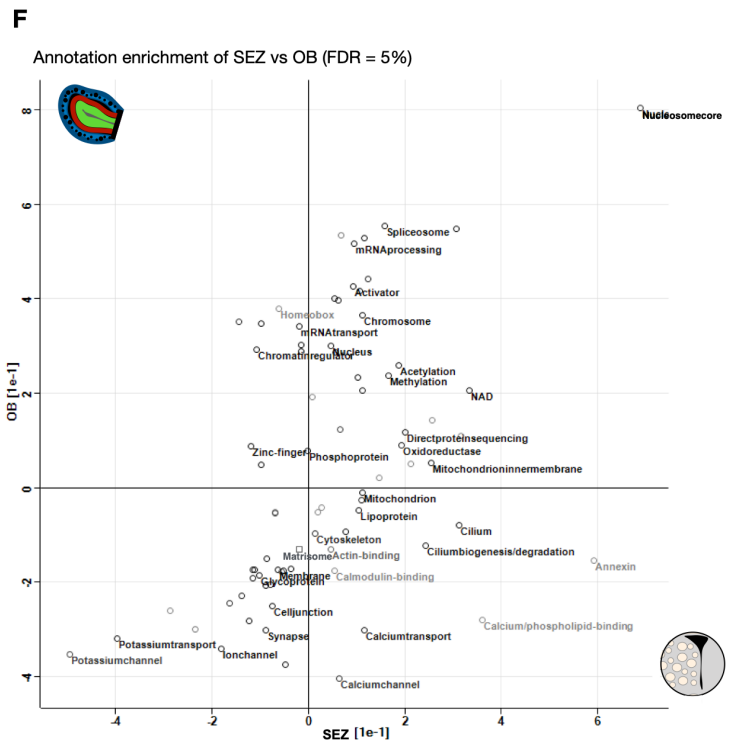
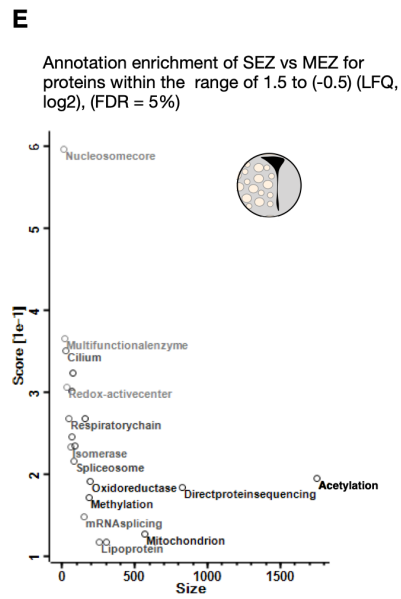


Figure S1, Related to Fig. 1H-M. Library-exclusive proteome is enriched in mitogens, cytokines, and transcription factors. The proteome depth achieved within the library measurements allowed greater detection of e.g. mitogens, cytokines, and transcription factors in vivo compared to single shot measurements. A) Number of proteins exclusive to the library measurements. B) Gene ontology of “protein class” with Panther (pantherdb.org) shows transcription factors significantly enriched among the library-exclusive proteins (red=positive enrichment, blue=negative enrichment) and C) gene ontology of “molecular function” shows receptor activity (e.g. growth factor receptors) significantly enriched among the library-exclusive proteins. D) Further examples of mitogens and cytokines exclusively detected in the library samples. E) The MEZ contains parts of the neurogenic niche (see discussion) and typically the neurogenic niche-associated proteins can be detected with lower LFQ intensities. Hence, we selected proteins with a similar abundance in SEZ and MEZ that had LFQ intensities within a range of 1.5 (log₂ fold) and -0,5 (log₂ fold) comparing SEZ to MEZ. This was used to bioinformatically remove potential non-neurogenic contamination. Subsequent enrichment analysis was performed as in Figure 1M. F) We compared the feature-enrichment of both OB and SEZ (input data was relative to Cx as in Figure 1L,M) and note that both enrich in nucleus and gene regulation (2D-annotation enrichment, FDR=0.05).

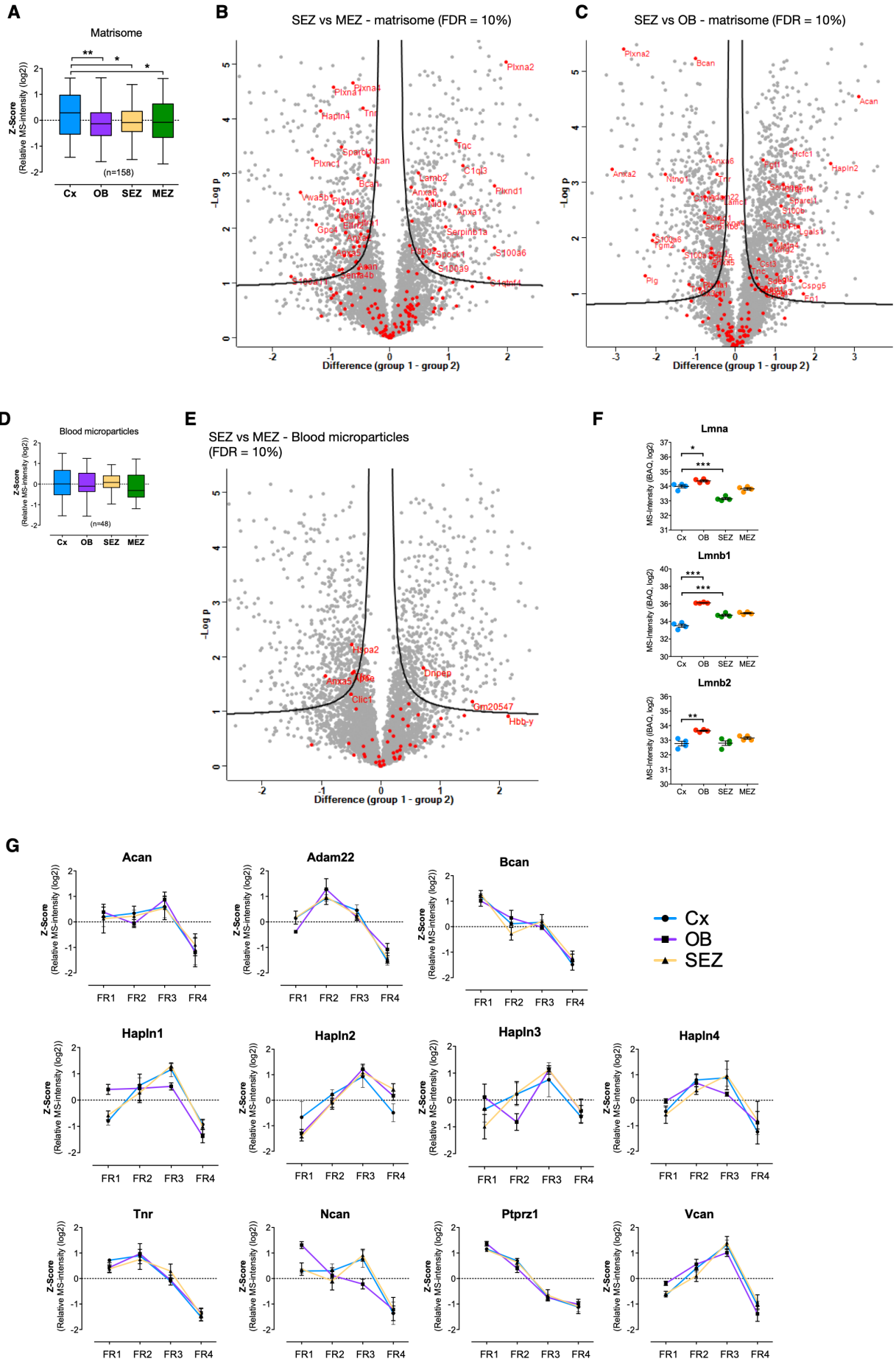


Figure S2, Related to Fig. 2. Niche matrisome, nuclear lamin, and perineuronal nets.

A) Distribution plots for the matrisome proteins of each brain region. Average LFQ intensities for each protein have been z-scored and are displayed in Whisker plots (ANOVA, Kruskal-Wallis test with Dunn's multiple comparison test, * $p=0.05$, ** $p=0.01$, and *** $p=0.001$). B) Volcano plots of SEZ and MEZ protein abundance values with matrisome proteins highlighted in red. Significance was analyzed using two-tailed t-test with FDR=0.1 ($S_0=0.1$). C) Abundance difference was analyzed in the same manner for SEZ and OB. D) Since the proteins of the blood microparticle category had similar abundance, blood proteins were not the reason for differences in regional matrisome distributions. Data shown as Whisker plots, ANOVA, * $p=0.05$, ** $p=0.01$, and *** $p=0.001$. E) Among the blood microparticle proteins, we find only a couple of significantly enriched proteins in the SEZ (and four in the MEZ) (two-tailed t-test, FDR=0.1, $S_0=0.1$). F) LFQ intensities of lamin-A, B1, and B2 from the LMSS experiment (ANOVA with Bonferroni's multiple comparison test, * $p=0.05$, ** $p=0.01$, and *** $p=0.001$). Data are presented as mean SEM. G) Each of the 11 proteins included in the PNN plot (Figure 2A) is shown here with individual solubility plots. Data is displayed as z-scored LFQ intensities of the four fractions of each protein and are presented as mean SEM.

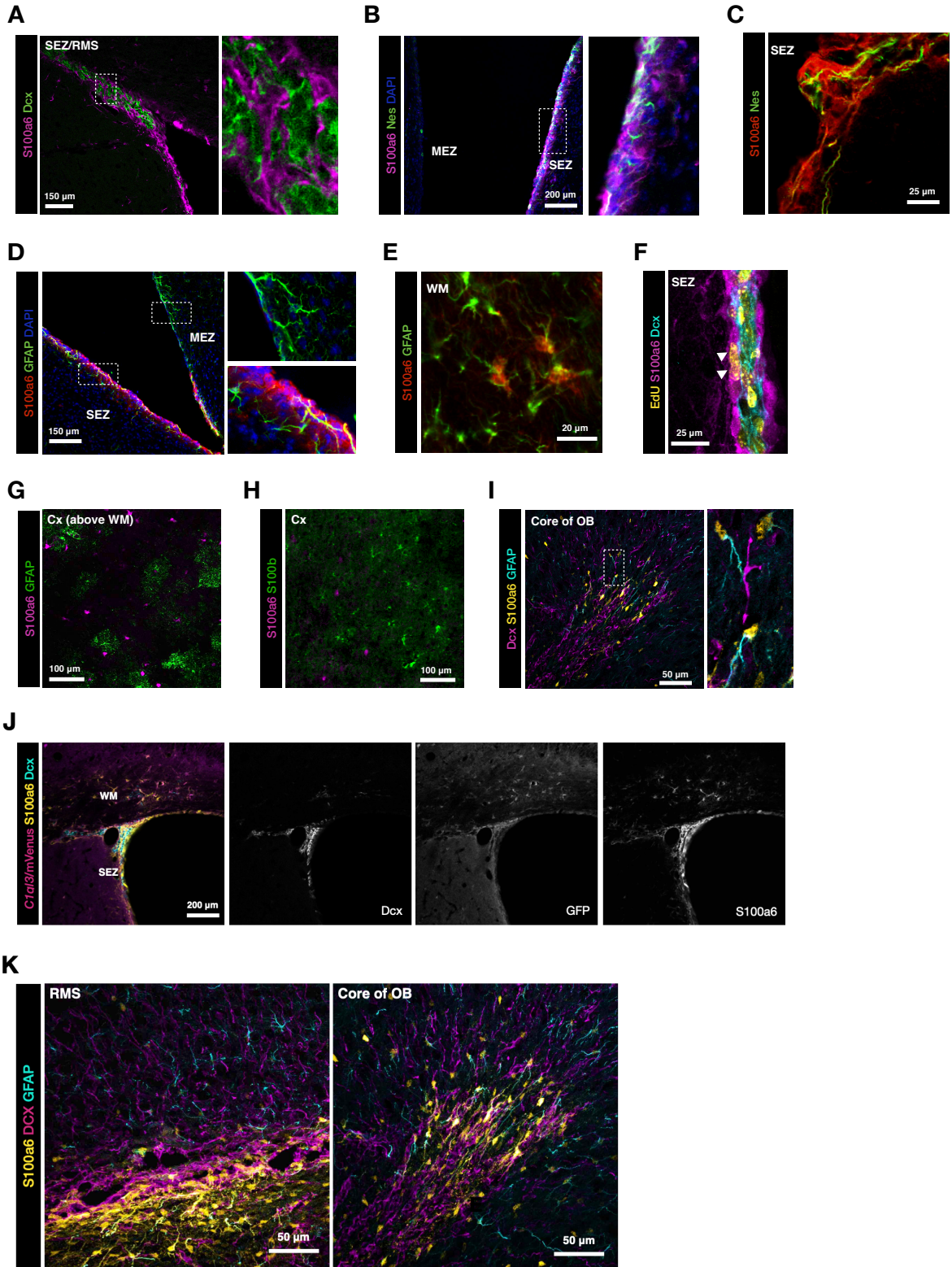


Figure S3, Related to Fig. 3. S100a6 in the neurogenic niches. A) Photomicrograph of immunostainings with S100a6 and Dcx highlight their proximity, but separate localization. B-C) S100a6 colocalizes with Nestin⁺ processes at the SEZ and D-E) colocalization with GFAP can be found at the SEZ (picture = confocal Z-stack) and in the white matter (WM, of corpus callosum). F) EdU was administered for 4 weeks and proliferation of S100a6⁺ cells was assessed. Note the EdU⁺/S100a6⁺ cells highlighted by arrowheads. G-H) S100a6 did not colocalize with GFAP nor S100b in Cx, instead, as shown in I) S100a6/GFAP colocalization could be found in the OB, in or in close proximity of the RMS. J) S100a6 and mVenus/C1q/3 (detected by GFP immunostaining) are colocalized in the WM consistent with the presence of some NSCs there, above the niche. K) Photomicrograph of immunostainings with S100a6, Dcx and GFAP in a sagittal section of the RMS/OB. As the neural stem cell niche ends, so do the majority of S100a6-high cells. S100a6-low cells (GFAP-positive cells) can be seen throughout the OB with somewhat higher density at the final length of the RMS in the OB (picture = stack composite). Scale bars as indicated in the panels. Figure S3D,J,K are Z-stacks of confocal pictures .

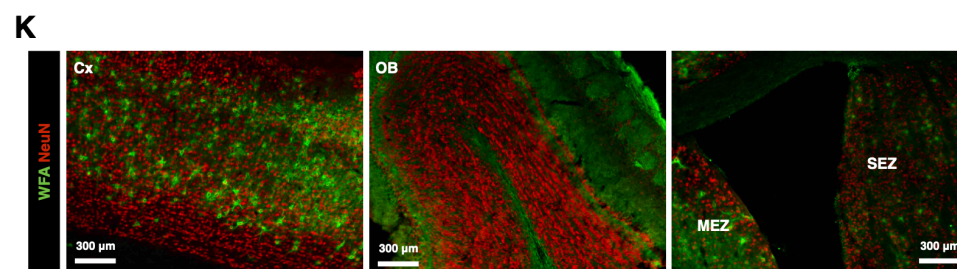
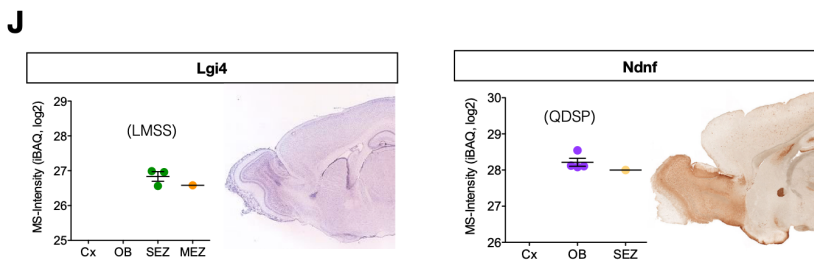
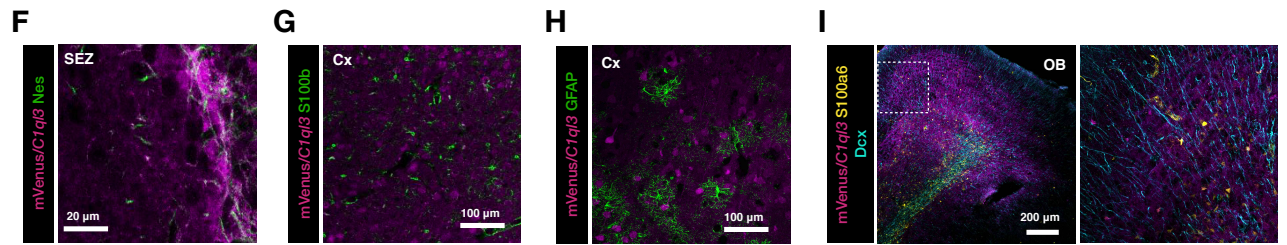
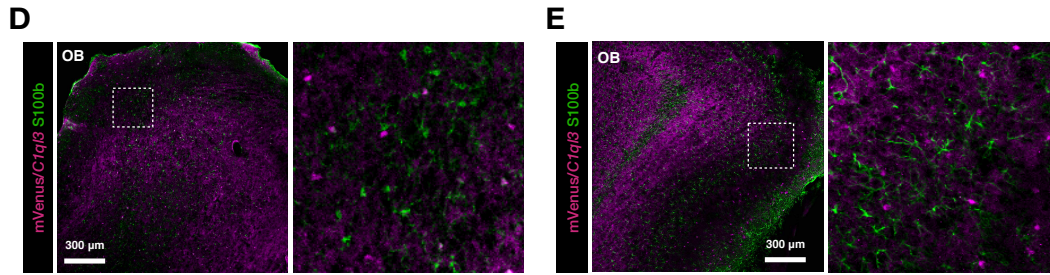
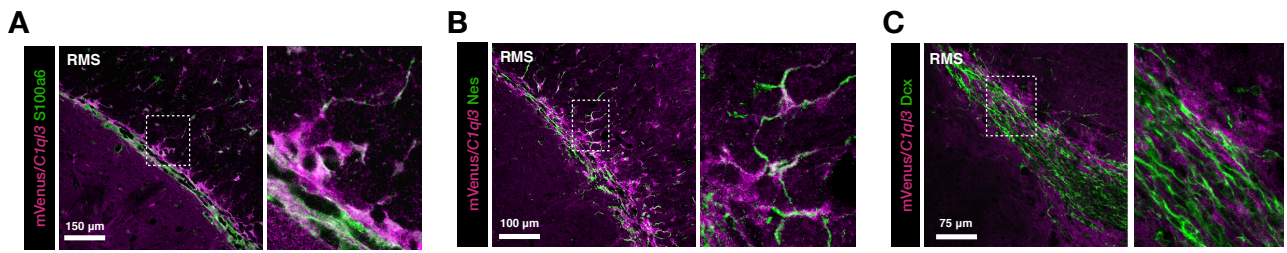


Figure S4, related to Figure 5. C1qI3, PNNs and additional new candidates at the neurogenic niches. At the beginning of the rostral migratory stream (RMS), we found mVenus/C1qI3 to colocalize with S100a6 (A) and Nestin (B). C) mVenus/C1qI3+ cells surround the Dcx+ neuroblasts also in the middle of the RMS. D) mVenus/C1qI3 was mostly diffuse in the OB, but also labeled some GFAP- and E) S100b- cells. F) Nestin+ processes in the SEZ are often mVenus/C1qI3 positive. G-H) In the Cx, mVenus/C1qI3 does not colocalize with either GFAP, nor S100b. I) Contrary to the SEZ, in the OB mVenus/C1qI3 does not colocalize with S100a6. Image is a confocal Z-stack. J) Matrisome proteins Leucine Rich Repeat LGI Family Member 4 (*Lgi4*) and Neuron Derived Neurotrophic Factor (*NDNF*) were only quantified in the LMSS data and the QDSP data, respectively. Data are presented as mean SEM. *Lgi4* seems enriched at the SEZ and *NDNF* seems enriched in the OB. *Lgi4* in situ-hybridization originates from Allen brain atlas. Image credit: Allen institute for Brain Science. *Ndnf* expression (EGFP) pictures originate from GENSAT gene expression atlas. Image credit: GENSAT project at Rockefeller. K) Perineuronal nets were stained using the lectin *Wisteria floribunda* (WFA) that binds N-acetylgalactosamine on carbohydrates. Perineuronal nets were identified in the Cx when immunostained with WFA and NeuN to label neurons (left panel), while none are stained in the OB (middle panel) and SEZ (right panel). Scale bars as indicated in the panels.

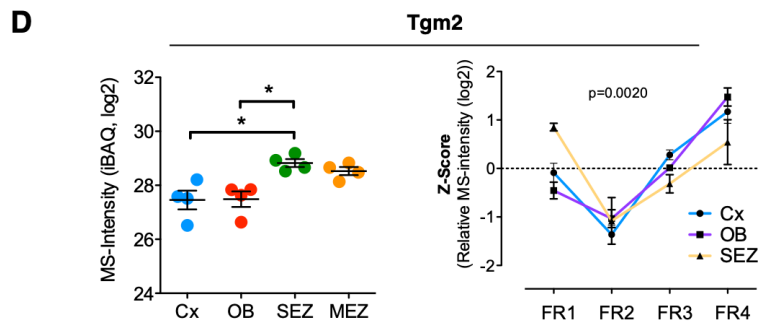
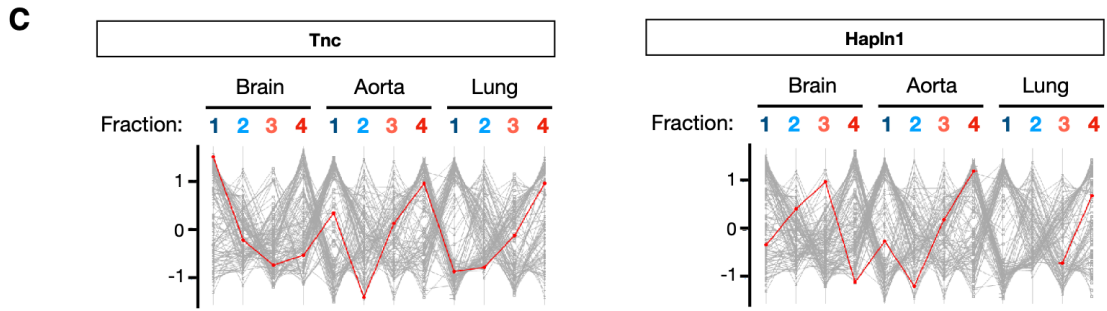
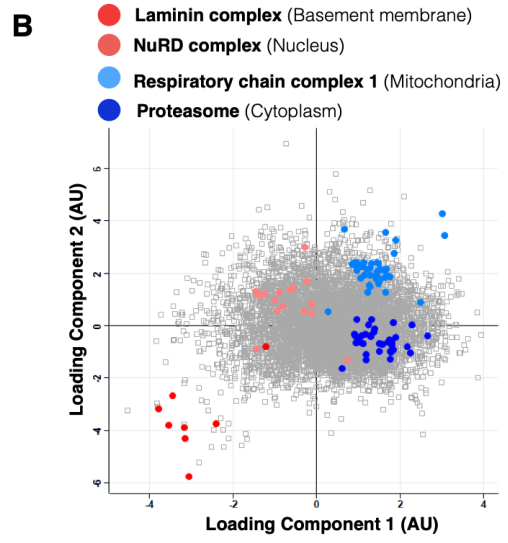
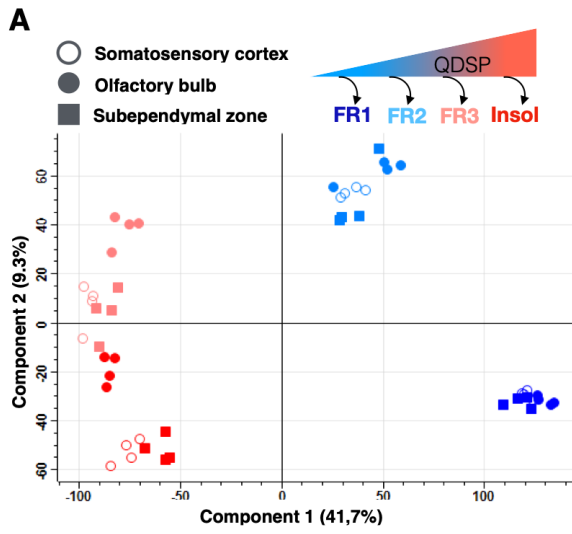
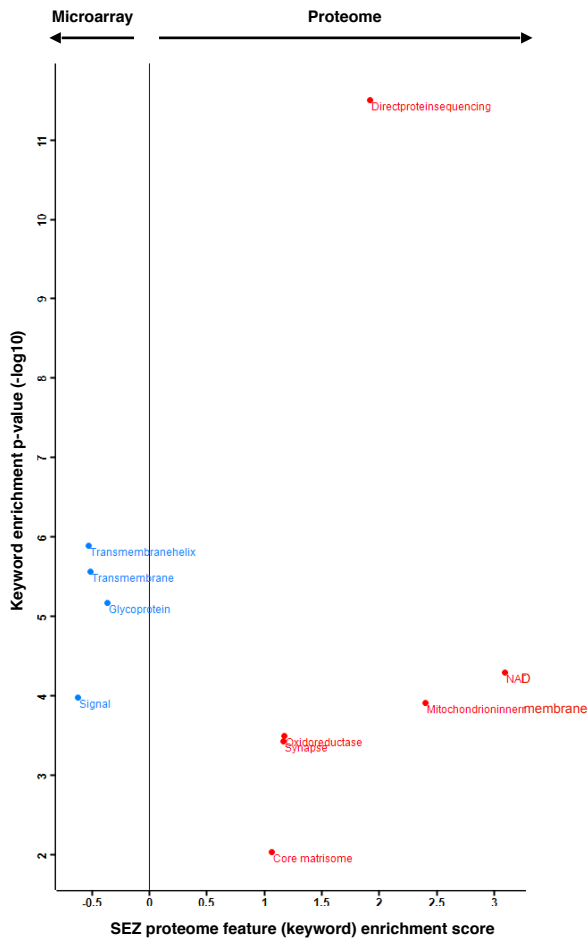


Figure S5, Related to Fig. 6. QDSP comparisons and Transglutaminase 2 measurements. A) Principal component analysis (PCA) for each brain region and detergent fraction. Component 1 and 2 separates the detergent fractions. B) In the scatterplot (of the PCA), we display four categories (in color) with significant enrichment for each of the four fractions ($FDR \leq 0.05$). C) We compared the brain matrixome data to previously published data sets using the QDSP method in aorta and lung tissue (Schiller et al. 2015, Wierer et al. 2018). Overall, many proteins have a similar profile in the different tissues, but some ECM proteins such as for example Tnc and Hapln1 have drastically different solubility profiles (more soluble in brain). The averaged data sets here are comprised of an average from all experimental groups of each study. D) Tgm2 proteome data from the LMSS data-set (left plot) (ANOVA with Bonferroni's multiple comparison test, * $p=0.05$) and the QDSP data-set (right plot) (z-scored, 2way-ANOVA). In the QDSP data-set both Cx and OB contain meninges (only perenchyma in the LMSS dataset). This may be a reason for difference in solubility between the OB/Cx and the SEZ, since Tgm2 can be found in the meninges. Data are presented as mean SEM.

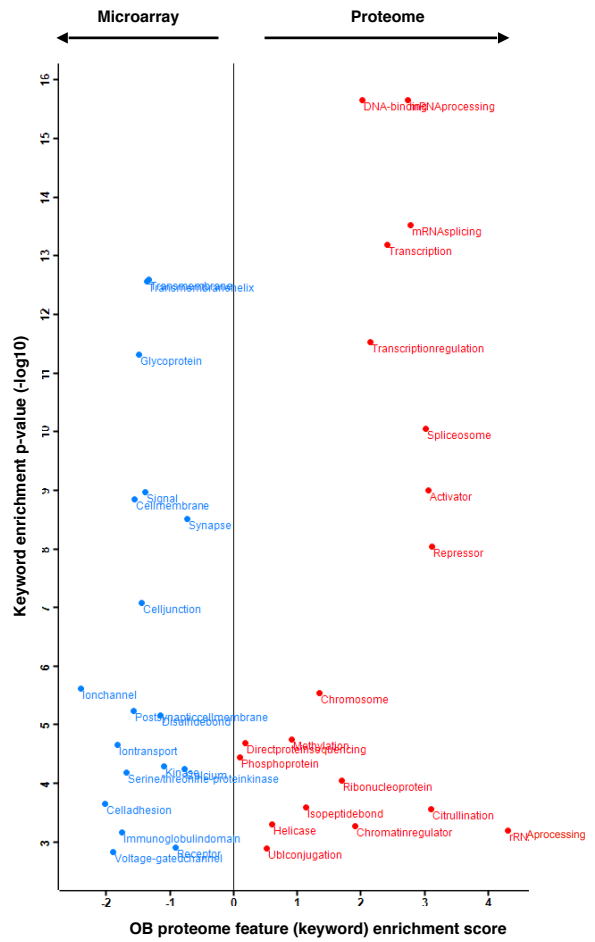
Figure S6, Related to Fig. 4. Comparison of the niche matrisome data with microarray and scRNAseq data. A) Kalamakis et al. (2019) used scRNAseq to analyse the neurogenic niche cells of the SEZ and determined cell-specific enrichment of the stem cell stage/subtype genes. The relative enrichment values from the scRNAseq was compared to the SEZ abundance normalized to Cx. Note that the niche-specific matrisome is abundantly expressed by quiescent neural stem cells (qNSCs), primarily the 2nd stage/subtype of the qNSCs. B-C) The microarray data originates from the same tissues as the proteome data (Cx, OB, and SEZ) and the data presented here had a cut-off of 2-fold difference to Cx. Both SEZ (B) and OB (C) was normalized to the Cx measurements from the respective data-sets and the relative matrisome abundance was compared as seen in the scatterplots (red = matrisome proteins/genes, grey = all proteins/genes). Significant regulation in the microarray data is defined by its p-value, and also as the fold change. The dashed line at 1 and -1 log₂ fold change highlights the minimum fold change for significant difference between SEZ and Cx. Note that while e.g. *Thbs4* in the SEZ correlates well between the proteome and microarray data, e.g. *C1ql3* was instead anti-correlated.

A

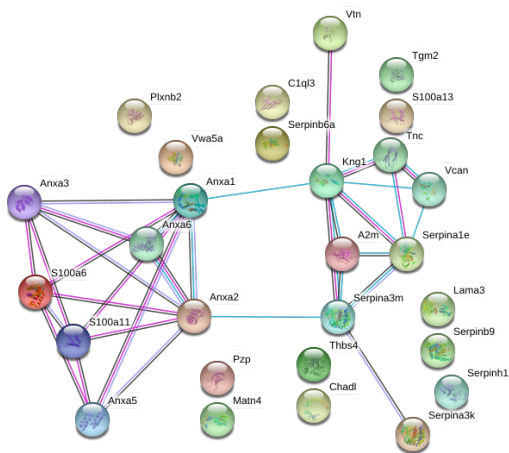
Relative enrichment of SEZ features in the proteome vs microarray data-set

**B**

Relative enrichment of OB features in the proteome vs microarray data-set

**C**

SVZ-enriched matrisome proteins in comparison to Cx
(p-value cut-off = 0.1)

**D**

OB-enriched matrisome proteins in comparison to Cx
(p-value cut-off = 0.1)

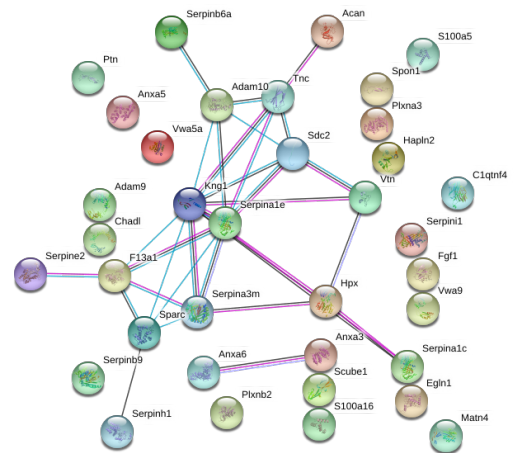


Figure S7, Related to Figure 4. Divergent -omics data features and niche-specific matrixome interactomes. A-B) The microarray data and proteome data in Fig. S6B,C was analysed for enriched features (2D-annotation enrichment, FDR=0.05, using the Uniport keyword annotation). The significantly enriched features are displayed with a relative score for the comparable enrichment in the proteome to the microarray in the SVZ (A) and the OB (B). (C-D) Enriched matrixome proteins ($p \leq 0.1$) of the SEZ in comparison to Cx (C) and OB in comparison to Cx (D) were analyzed in the STRING database (string-db.org) for known protein interactions.

3. Publication bibliography

- Adams, Katrina L.; Gallo, Vittorio (2018): The diversity and disparity of the glial scar. In *Nature neuroscience* 21 (1), pp. 9–15. DOI: 10.1038/s41593-017-0033-9.
- Andreu-Agulló, Celia; Morante-Redolat, José Manuel; Delgado, Ana C.; Fariñas, Isabel (2009): Vascular niche factor PEDF modulates Notch-dependent stemness in the adult subependymal zone. In *Nature neuroscience* 12 (12), pp. 1514–1523. DOI: 10.1038/nn.2437.
- Angelidis, Ilias; Simon, Lukas M.; Fernandez, Isis E.; Strunz, Maximilian; Mayr, Christoph H.; Greiffo, Flavia R. et al. (2019): An atlas of the aging lung mapped by single cell transcriptomics and deep tissue proteomics. In *Nature communications* 10 (1), p. 963. DOI: 10.1038/s41467-019-08831-9.
- Arvidsson, Andreas; Collin, Tove; Kirik, Deniz; Kokaia, Zaal; Lindvall, Olle (2002): Neuronal replacement from endogenous precursors in the adult brain after stroke. In *Nature medicine* 8 (9), pp. 963–970. DOI: 10.1038/nm747.
- Aviezer, David; Hecht, Dalit; Safran, Michal; Eisinger, Magdalena; David, Guido; Yaron, Avner (1994): Perlecan, basal lamina proteoglycan, promotes basic fibroblast growth factor-receptor binding, mitogenesis, and angiogenesis. In *Cell* 79 (6), pp. 1005–1013. DOI: 10.1016/0092-8674(94)90031-0.
- Barczyk, Malgorzata; Carracedo, Sergio; Gullberg, Donald (2010): Integrins. In *Cell and tissue research* 339 (1), pp. 269–280. DOI: 10.1007/s00441-009-0834-6.
- Barker, Roger A.; Götz, Magdalena; Parmar, Malin (2018): New approaches for brain repair—from rescue to reprogramming. In *Nature* 557 (7705), pp. 329–334. DOI: 10.1038/s41586-018-0087-1.
- Beckervordersandforth, Ruth; Tripathi, Pratibha; Ninkovic, Jovica; Bayam, Efil; Lepier, Alexandra; Stempfhuber, Barbara et al. (2010): In vivo fate mapping and expression analysis reveals molecular hallmarks of prospectively isolated adult neural stem cells. In *Cell stem cell* 7 (6), pp. 744–758. DOI: 10.1016/j.stem.2010.11.017.
- Bordiuk, Olivia L.; Smith, Karen; Morin, Peter J.; Semenov, Mikhail V. (2014): Cell proliferation and neurogenesis in adult mouse brain. In *PLoS one* 9 (11), e111453. DOI: 10.1371/journal.pone.0111453.
- Bornstein, Paul (2009): Matricellular proteins: an overview. In *Journal of cell communication and signaling* 3 (3-4), pp. 163–165. DOI: 10.1007/s12079-009-0069-z.
- Bornstein, Paul; Sage, E. Helene (2002): Matricellular proteins: extracellular modulators of cell function. In *Current Opinion in Cell Biology* 14 (5), pp. 608–616. DOI: 10.1016/S0955-0674(02)00361-7.
- Bovetti, Serena; Hsieh, Yi-Chun; Bovolin, Patrizia; Perroteau, Isabelle; Kazunori, Toida; Puche, Adam C. (2007): Blood vessels form a scaffold for neuroblast migration in the adult olfactory bulb. In *The Journal of neuroscience : the official journal of the Society for Neuroscience* 27 (22), pp. 5976–5980. DOI: 10.1523/JNEUROSCI.0678-07.2007.

- Brickman, Y. G.; Ford, M. D.; Small, D. H.; Bartlett, P. F.; Nurcombe, V. (1995): Heparan sulfates mediate the binding of basic fibroblast growth factor to a specific receptor on neural precursor cells. In *The Journal of biological chemistry* 270 (42), pp. 24941–24948. DOI: 10.1074/jbc.270.42.24941.
- Capizzi, Allison; Woo, Jean; Verduzco-Gutierrez, Monica (2020): Traumatic Brain Injury: An Overview of Epidemiology, Pathophysiology, and Medical Management. In *The Medical clinics of North America* 104 (2), pp. 213–238. DOI: 10.1016/j.mcna.2019.11.001.
- Cebrian-Silla, Arantxa; Nascimento, Marcos Assis; Redmond, Stephanie A.; Mansky, Benjamin; Wu, David; Obernier, Kirsten et al. (2021): Single-cell analysis of the ventricular-subventricular zone reveals signatures of dorsal and ventral adult neurogenesis. In *eLife* 10. DOI: 10.7554/eLife.67436.
- Chaudhuri, Ovijit; Cooper-White, Justin; Janmey, Paul A.; Mooney, David J.; Shenoy, Vivek B. (2020): Effects of extracellular matrix viscoelasticity on cellular behaviour. In *Nature* 584 (7822), pp. 535–546. DOI: 10.1038/s41586-020-2612-2.
- Clause, Kelly C.; Barker, Thomas H. (2013): Extracellular matrix signaling in morphogenesis and repair. In *Current opinion in biotechnology* 24 (5), pp. 830–833. DOI: 10.1016/j.cop-bio.2013.04.011.
- Codega, Paolo; Silva-Vargas, Violeta; Paul, Alex; Maldonado-Soto, Angel R.; Deleo, Annina M.; Pastrana, Erika; Doetsch, Fiona (2014): Prospective identification and purification of quiescent adult neural stem cells from their in vivo niche. In *Neuron* 82 (3), pp. 545–559. DOI: 10.1016/j.neuron.2014.02.039.
- Conover, Joanne C.; Todd, Krysti L. (2017): Development and aging of a brain neural stem cell niche. In *Experimental gerontology* 94, pp. 9–13. DOI: 10.1016/j.exger.2016.11.007.
- Cope, Elise C.; Gould, Elizabeth (2019): Adult Neurogenesis, Glia, and the Extracellular Matrix. In *Cell stem cell* 24 (5), pp. 690–705. DOI: 10.1016/j.stem.2019.03.023.
- Cox, Jürgen; Hein, Marco Y.; Lubner, Christian A.; Paron, Igor; Nagaraj, Nagarjuna; Mann, Matthias (2014): Accurate proteome-wide label-free quantification by delayed normalization and maximal peptide ratio extraction, termed MaxLFQ. In *Molecular & cellular proteomics : MCP* 13 (9), pp. 2513–2526. DOI: 10.1074/mcp.M113.031591.
- Crane, Genevieve M.; Jeffery, Elise; Morrison, Sean J. (2017): Adult haematopoietic stem cell niches. In *Nature reviews. Immunology* 17 (9), pp. 573–590. DOI: 10.1038/nri.2017.53.
- David, Linda Suzanne; Schachner, Melitta; Saghatelian, Armen (2013): The extracellular matrix glycoprotein tenascin-R affects adult but not developmental neurogenesis in the olfactory bulb. In *The Journal of neuroscience : the official journal of the Society for Neuroscience* 33 (25), pp. 10324–10339. DOI: 10.1523/JNEUROSCI.5728-12.2013.
- David-Bercholz, Jennifer; Kuo, Chay T.; Deneen, Benjamin (2021): Astrocyte and Oligodendrocyte Responses From the Subventricular Zone After Injury. In *Frontiers in cellular neuroscience* 15, p. 797553. DOI: 10.3389/fncel.2021.797553.
- Deepa, Sarama Sathyaseelan; Carulli, Daniela; Galtrey, Clare; Rhodes, Kate; Fukuda, Junko; Mikami, Tadahisa et al. (2006): Composition of perineuronal net extracellular matrix in rat brain:

a different disaccharide composition for the net-associated proteoglycans. In *The Journal of biological chemistry* 281 (26), pp. 17789–17800. DOI: 10.1074/jbc.M600544200.

Domogatskaya, Anna; Rodin, Sergey; Tryggvason, Karl (2012): Functional diversity of laminins. In *Annual review of cell and developmental biology* 28, pp. 523–553. DOI: 10.1146/annurev-cellbio-101011-155750.

Donnelly, Hannah; Salmeron-Sanchez, Manuel; Dalby, Matthew J. (2018): Designing stem cell niches for differentiation and self-renewal. In *Journal of the Royal Society, Interface* 15 (145). DOI: 10.1098/rsif.2018.0388.

Douet, V.; Kerever, A.; Arikawa-Hirasawa, E.; Mercier, F. (2013): Fractone-heparan sulphates mediate FGF-2 stimulation of cell proliferation in the adult subventricular zone. In *Cell proliferation* 46 (2), pp. 137–145. DOI: 10.1111/cpr.12023.

Douet, Vanessa; Arikawa-Hirasawa, Eri; Mercier, Frederic (2012): Fractone-heparan sulfates mediate BMP-7 inhibition of cell proliferation in the adult subventricular zone. In *Neuroscience letters* 528 (2), pp. 120–125. DOI: 10.1016/j.neulet.2012.08.077.

Erkkinen, Michael G.; Kim, Mee-Ohk; Geschwind, Michael D. (2018): Clinical Neurology and Epidemiology of the Major Neurodegenerative Diseases. In *Cold Spring Harbor perspectives in biology* 10 (4). DOI: 10.1101/cshperspect.a033118.

Faissner, Andreas; Roll, Lars; Theocharidis, Ursula (2017): Tenascin-C in the matrix of neural stem and progenitor cells. In *Molecular and cellular neurosciences* 81, pp. 22–31. DOI: 10.1016/j.mcn.2016.11.003.

Falcão, Ana Mendanha; Marques, Fernanda; Novais, Ashley; Sousa, Nuno; Palha, Joana A.; Sousa, João Carlos (2012): The path from the choroid plexus to the subventricular zone: go with the flow! In *Frontiers in cellular neuroscience* 6, p. 34. DOI: 10.3389/fncel.2012.00034.

Farrukh, Aleeza; Ortega, Felipe; Fan, Wenqiang; Marichal, Nicolás; Paez, Julieta I.; Berninger, Benedikt et al. (2017): Bifunctional Hydrogels Containing the Laminin Motif IKVAV Promote Neurogenesis. In *Stem cell reports* 9 (5), pp. 1432–1440. DOI: 10.1016/j.stemcr.2017.09.002.

Faulkner, Jill R.; Herrmann, Julia E.; Woo, Michael J.; Tansey, Keith E.; Doan, Ngan B.; Sofroniew, Michael V. (2004): Reactive astrocytes protect tissue and preserve function after spinal cord injury. In *J. Neurosci.* 24 (9), pp. 2143–2155. DOI: 10.1523/JNEUROSCI.3547-03.2004.

Fawcett, James W. (2015): The extracellular matrix in plasticity and regeneration after CNS injury and neurodegenerative disease. In *Progress in brain research* 218, pp. 213–226. DOI: 10.1016/bs.pbr.2015.02.001.

Friess, Christian; Götz, Magdalena; Kjell, Jacob (2021): Cryo-section Dissection of the Adult Subependymal Zone for Accurate and Deep Quantitative Proteome Analysis. In *Journal of visualized experiments : JoVE* (176). DOI: 10.3791/63047.

Frisén, Jonas (2016): Neurogenesis and Gliogenesis in Nervous System Plasticity and Repair. In *Annual review of cell and developmental biology* 32, pp. 127–141. DOI: 10.1146/annurev-cellbio-111315-124953.

Fujioka, Teppei; Kaneko, Naoko; Sawamoto, Kazunobu (2019): Blood vessels as a scaffold for neuronal migration. In *Neurochemistry international* 126, pp. 69–73. DOI: 10.1016/j.neu-int.2019.03.001.

Garcion, Emmanuel; Halilagic, Aida; Faissner, Andreas; French-Constant, Charles (2004): Generation of an environmental niche for neural stem cell development by the extracellular matrix molecule tenascin C. In *Development (Cambridge, England)* 131 (14), pp. 3423–3432. DOI: 10.1242/dev.01202.

Garg, Pallavi; Yang, Shiqi; Liu, Anguo; Pallero, Manuel A.; Buchsbaum, Donald J.; Mosher, Deane F. et al. (2011): Thrombospondin-1 opens the paracellular pathway in pulmonary microvascular endothelia through EGFR/ErbB2 activation. In *American journal of physiology. Lung cellular and molecular physiology* 301 (1), L79-90. DOI: 10.1152/ajplung.00287.2010.

Gioia, Roberta de; Biella, Fabio; Citterio, Gaia; Rizzo, Federica; Abati, Elena; Nizzardo, Monica et al. (2020): Neural Stem Cell Transplantation for Neurodegenerative Diseases. In *International journal of molecular sciences* 21 (9). DOI: 10.3390/ijms21093103.

Girard, F.; Eichenberger, S.; Celio, M. R. (2014): Thrombospondin 4 deficiency in mouse impairs neuronal migration in the early postnatal and adult brain. In *Molecular and cellular neurosciences* 61, pp. 176–186. DOI: 10.1016/j.mcn.2014.06.010.

Gómez-Gaviro, María Victoria; Scott, Charlotte E.; Sesay, Abdul K.; Matheu, Ander; Booth, Sarah; Galichet, Christophe; Lovell-Badge, Robin (2012): Betacellulin promotes cell proliferation in the neural stem cell niche and stimulates neurogenesis. In *Proceedings of the National Academy of Sciences of the United States of America* 109 (4), pp. 1317–1322. DOI: 10.1073/pnas.1016199109.

Götz, Magdalena; Nakafuku, Masato; Petrik, David (2016): Neurogenesis in the Developing and Adult Brain—Similarities and Key Differences. In *Cold Spring Harbor perspectives in biology* 8 (7). DOI: 10.1101/cshperspect.a018853.

Hack, Iris; Bancila, Mircea; Loulier, Karine; Carroll, Patrick; Cremer, Harold (2002): Reelin is a detachment signal in tangential chain-migration during postnatal neurogenesis. In *Nature neuroscience* 5 (10), pp. 939–945. DOI: 10.1038/nn923.

Hall, Peter E.; Lathia, Justin D.; Caldwell, Maeve A.; French-Constant, Charles (2008): Laminin enhances the growth of human neural stem cells in defined culture media. In *BMC neuroscience* 9, p. 71. DOI: 10.1186/1471-2202-9-71.

Herrera, D. G.; Garcia-Verdugo, J. M.; Alvarez-Buylla, A. (1999): Adult-derived neural precursors transplanted into multiple regions in the adult brain. In *Annals of neurology* 46 (6), pp. 867–877. DOI: 10.1002/1531-8249(199912)46:6<867::aid-ana9>3.0.co;2-z.

Hu, H. (1999): Chemorepulsion of neuronal migration by Slit2 in the developing mammalian forebrain. In *Neuron* 23 (4), pp. 703–711. DOI: 10.1016/s0896-6273(01)80029-5.

Huang, Lei; Zhang, Lubo (2019): Neural stem cell therapies and hypoxic-ischemic brain injury. In *Progress in neurobiology* 173, pp. 1–17. DOI: 10.1016/j.pneurobio.2018.05.004.

Iozzo, Renato V.; Schaefer, Liliana (2015): Proteoglycan form and function: A comprehensive nomenclature of proteoglycans. In *Matrix Biology* 42, pp. 11–55. DOI: 10.1016/j.matbio.2015.02.003.

Kalamakis, Georgios; Brüne, Daniel; Ravichandran, Srikanth; Bolz, Jan; Fan, Wenqiang; Ziebell, Frederik et al. (2019): Quiescence Modulates Stem Cell Maintenance and Regenerative Capacity in the Aging Brain. In *Cell* 176 (6), 1407-1419.e14. DOI: 10.1016/j.cell.2019.01.040.

- Kerever, Aurelien; Arikawa-Hirasawa, Eri (2021): Optimal Extracellular Matrix Niches for Neurogenesis: Identifying Glycosaminoglycan Chain Composition in the Subventricular Neurogenic Zone. In *Frontiers in neuroanatomy* 15, p. 764458. DOI: 10.3389/fnana.2021.764458.
- Kerever, Aurelien; Mercier, Frederic; Nonaka, Risa; Vega, Susana de; Oda, Yuka; Zalc, Bernard et al. (2014): Perlecan is required for FGF-2 signaling in the neural stem cell niche. In *Stem cell research* 12 (2), pp. 492–505. DOI: 10.1016/j.scr.2013.12.009.
- Kerever, Aurelien; Schnack, Jason; Vellinga, Dirk; Ichikawa, Naoki; Moon, Chris; Arikawa-Hirasawa, Eri et al. (2007): Novel extracellular matrix structures in the neural stem cell niche capture the neurogenic factor fibroblast growth factor 2 from the extracellular milieu. In *Stem cells (Dayton, Ohio)* 25 (9), pp. 2146–2157. DOI: 10.1634/stemcells.2007-0082.
- Khalilgharibi, Nargess; Mao, Yanlan (2021): To form and function: on the role of basement membrane mechanics in tissue development, homeostasis and disease. In *Open biology* 11 (2), p. 200360. DOI: 10.1098/rsob.200360.
- Kjell, Jacob; Fischer-Sternjak, Judith; Thompson, Amelia J.; Friess, Christian; Sticco, Matthew J.; Salinas, Favio et al. (2020): Defining the Adult Neural Stem Cell Niche Proteome Identifies Key Regulators of Adult Neurogenesis. In *Cell stem cell* 26 (2), 277-293.e8. DOI: 10.1016/j.stem.2020.01.002.
- Koh, Seong-Ho; Park, Hyun-Hee (2017): Neurogenesis in Stroke Recovery. In *Translational stroke research* 8 (1), pp. 3–13. DOI: 10.1007/s12975-016-0460-z.
- Kokovay, Erzsebet; Goderie, Susan; Wang, Yue; Lotz, Steve; Lin, Gang; Sun, Yu et al. (2010): Adult SVZ lineage cells home to and leave the vascular niche via differential responses to SDF1/CXCR4 signaling. In *Cell stem cell* 7 (2), pp. 163–173. DOI: 10.1016/j.stem.2010.05.019.
- Kreuzberg, Maria; Kanov, Evgeny; Timofeev, Oleg; Schwaninger, Markus; Monyer, Hannah; Khodosevich, Konstantin (2010): Increased subventricular zone-derived cortical neurogenesis after ischemic lesion. In *Experimental neurology* 226 (1), pp. 90–99. DOI: 10.1016/j.expneurol.2010.08.006.
- Kuhn, H. G.; Winkler, J.; Kempermann, G.; Thal, L. J.; Gage, F. H. (1997): Epidermal growth factor and fibroblast growth factor-2 have different effects on neural progenitors in the adult rat brain. In *The Journal of neuroscience : the official journal of the Society for Neuroscience* 17 (15), pp. 5820–5829.
- Kuhn, H. Georg; Toda, Tomohisa; Gage, Fred H. (2018): Adult Hippocampal Neurogenesis: A Coming-of-Age Story. In *J. Neurosci.* 38 (49), pp. 10401–10410. DOI: 10.1523/JNEUROSCI.2144-18.2018.
- Kulak, Nils A.; Geyer, Philipp E.; Mann, Matthias (2017): Loss-less Nano-fractionator for High Sensitivity, High Coverage Proteomics. In *Molecular & cellular proteomics : MCP* 16 (4), pp. 694–705. DOI: 10.1074/mcp.O116.065136.
- Lalo, Ulyana; Koh, Wuhyun; Lee, C. Justin; Pankratov, Yuriy (2021): The tripartite glutamatergic synapse. In *Neuropharmacology* 199, p. 108758. DOI: 10.1016/j.neuropharm.2021.108758.
- Lehtinen, Maria K.; Zappaterra, Mauro W.; Chen, Xi; Yang, Yawei J.; Hill, Anthony D.; Lun, Melody et al. (2011): The cerebrospinal fluid provides a proliferative niche for neural progenitor cells. In *Neuron* 69 (5), pp. 893–905. DOI: 10.1016/j.neuron.2011.01.023.

- Lepko, Tjasa; Pusch, Melanie; Müller, Tamara; Schulte, Dorothea; Ehses, Janina; Kiebler, Michael et al. (2019): Choroid plexus-derived miR-204 regulates the number of quiescent neural stem cells in the adult brain. In *The EMBO journal* 38 (17), e100481. DOI: 10.15252/embj.2018100481.
- Levental, Kandice R.; Yu, Hongmei; Kass, Laura; Lakins, Johnathon N.; Egeblad, Mikala; Eler, Janine T. et al. (2009): Matrix crosslinking forces tumor progression by enhancing integrin signaling. In *Cell* 139 (5), pp. 891–906. DOI: 10.1016/j.cell.2009.10.027.
- Lim, Daniel A.; Alvarez-Buylla, Arturo (2016): The Adult Ventricular-Subventricular Zone (V-SVZ) and Olfactory Bulb (OB) Neurogenesis. In *Cold Spring Harbor perspectives in biology* 8 (5). DOI: 10.1101/cshperspect.a018820.
- Lim, Daniel A.; Suárez-Fariñas, Mayte; Naef, Felix; Hacker, Coleen R.; Menn, Benedicte; Takebayashi, Hirohide et al. (2006): In vivo transcriptional profile analysis reveals RNA splicing and chromatin remodeling as prominent processes for adult neurogenesis. In *Molecular and cellular neurosciences* 31 (1), pp. 131–148. DOI: 10.1016/j.mcn.2005.10.005.
- Lindvall, Olle; Kokaia, Zaal (2015): Neurogenesis following Stroke Affecting the Adult Brain. In *Cold Spring Harbor perspectives in biology* 7 (11). DOI: 10.1101/cshperspect.a019034.
- LLorens-Bobadilla, Enric; Zhao, Sheng; Baser, Avni; Saiz-Castro, Gonzalo; Zwadlo, Klara; Martin-Villalba, Ana (2015): Single-Cell Transcriptomics Reveals a Population of Dormant Neural Stem Cells that Become Activated upon Brain Injury. In *Cell stem cell* 17 (3), pp. 329–340. DOI: 10.1016/j.stem.2015.07.002.
- Llorente, Vicente; Velarde, Pedro; Desco, Manuel; Gómez-Gaviro, María Victoria (2022): Current Understanding of the Neural Stem Cell Niches. In *Cells* 11 (19). DOI: 10.3390/cells11193002.
- Lois, C.; Alvarez-Buylla, A. (1994): Long-distance neuronal migration in the adult mammalian brain. In *Science (New York, N.Y.)* 264 (5162), pp. 1145–1148. DOI: 10.1126/science.8178174.
- Macas, Jadranka; Nern, Christian; Plate, Karl H.; Momma, Stefan (2006): Increased generation of neuronal progenitors after ischemic injury in the aged adult human forebrain. In *The Journal of neuroscience : the official journal of the Society for Neuroscience* 26 (50), pp. 13114–13119. DOI: 10.1523/JNEUROSCI.4667-06.2006.
- Marques, Fernanda; Sousa, João C.; Coppola, Giovanni; Gao, Fuying; Puga, Renato; Brentani, Helena et al. (2011): Transcriptome signature of the adult mouse choroid plexus. In *Fluids and barriers of the CNS* 8 (1), p. 10. DOI: 10.1186/2045-8118-8-10.
- Mercier, Frederic (2016): Fractones: extracellular matrix niche controlling stem cell fate and growth factor activity in the brain in health and disease. In *Cellular and molecular life sciences : CMLS* 73 (24), pp. 4661–4674. DOI: 10.1007/s00018-016-2314-y.
- Mercier, Frederic; Douet, Vanessa (2014): Bone morphogenetic protein-4 inhibits adult neurogenesis and is regulated by fractone-associated heparan sulfates in the subventricular zone. In *Journal of chemical neuroanatomy* 57-58, pp. 54–61. DOI: 10.1016/j.jchemneu.2014.03.005.
- Mercier, Frederic; Kitasako, John T.; Hatton, Glenn I. (2002): Anatomy of the brain neurogenic zones revisited: fractones and the fibroblast/macrophage network. In *The Journal of comparative neurology* 451 (2), pp. 170–188. DOI: 10.1002/cne.10342.

- Midwood, Kim S.; Chiquet, Matthias; Tucker, Richard P.; Orend, Gertraud (2016): Tenascin-C at a glance. In *Journal of cell science* 129 (23), pp. 4321–4327. DOI: 10.1242/jcs.190546.
- Mirzadeh, Zaman; Doetsch, Fiona; Sawamoto, Kazunobu; Wichterle, Hynek; Alvarez-Buylla, Arturo (2010): The subventricular zone en-face: wholemount staining and ependymal flow. In *Journal of visualized experiments : JoVE* (39). DOI: 10.3791/1938.
- Mizrak, Dogukan; Levitin, Hanna Mendes; Delgado, Ana C.; Crotet, Valerie; Yuan, Jinzhou; Chaker, Zayna et al. (2019): Single-Cell Analysis of Regional Differences in Adult V-SVZ Neural Stem Cell Lineages. In *Cell reports* 26 (2), 394–406.e5. DOI: 10.1016/j.celrep.2018.12.044.
- Nascimento, Marcos Assis; Sorokin, Lydia; Coelho-Sampaio, Tatiana (2018): Fractone Bulbs Derive from Ependymal Cells and Their Laminin Composition Influence the Stem Cell Niche in the Subventricular Zone. In *The Journal of neuroscience : the official journal of the Society for Neuroscience* 38 (16), pp. 3880–3889. DOI: 10.1523/JNEUROSCI.3064-17.2018.
- Nozaki, Miho; Sakurai, Eiji; Raisler, Brian J.; Baffi, Judit Z.; Witta, Jassir; Ogura, Yuichiro et al. (2006): Loss of SPARC-mediated VEGFR-1 suppression after injury reveals a novel antiangiogenic activity of VEGF-A. In *The Journal of clinical investigation* 116 (2), pp. 422–429. DOI: 10.1172/JCI26316.
- Obernier, Kirsten; Alvarez-Buylla, Arturo (2019): Neural stem cells: origin, heterogeneity and regulation in the adult mammalian brain. In *Development (Cambridge, England)* 146 (4). DOI: 10.1242/dev.156059.
- Ottone, Cristina; Krusche, Benjamin; Whitby, Ariadne; Clements, Melanie; Quadrato, Giorgia; Pitulescu, Mara E. et al. (2014): Direct cell-cell contact with the vascular niche maintains quiescent neural stem cells. In *Nature cell biology* 16 (11), pp. 1045–1056. DOI: 10.1038/ncb3045.
- Paterno, Rosalia; Folweiler, Kaitlin A.; Cohen, Akiva S. (2017): Pathophysiology and Treatment of Memory Dysfunction After Traumatic Brain Injury. In *Current neurology and neuroscience reports* 17 (7), p. 52. DOI: 10.1007/s11910-017-0762-x.
- Pekny, Milos; Pekna, Marcela (2014): Astrocyte reactivity and reactive astrogliosis: costs and benefits. In *Physiological reviews* 94 (4), pp. 1077–1098. DOI: 10.1152/physrev.00041.2013.
- Petridis, Athanasios K.; El Maarouf, Abderrahman (2011): Brain-derived neurotrophic factor levels influence the balance of migration and differentiation of subventricular zone cells, but not guidance to the olfactory bulb. In *Journal of clinical neuroscience : official journal of the Neurosurgical Society of Australasia* 18 (2), pp. 265–270. DOI: 10.1016/j.jocn.2010.06.021.
- Petrik, David; Myoga, Michael H.; Grade, Sofia; Gerkau, Niklas J.; Pusch, Melanie; Rose, Christine R. et al. (2018): Epithelial Sodium Channel Regulates Adult Neural Stem Cell Proliferation in a Flow-Dependent Manner. In *Cell stem cell* 22 (6), 865–878.e8. DOI: 10.1016/j.stem.2018.04.016.
- Petzold, Jonna; Gentleman, Eileen (2021): Intrinsic Mechanical Cues and Their Impact on Stem Cells and Embryogenesis. In *Frontiers in cell and developmental biology* 9, p. 761871. DOI: 10.3389/fcell.2021.761871.
- Ramírez-Castillejo, Carmen; Sánchez-Sánchez, Francisco; Andreu-Agulló, Celia; Ferrón, Sacri R.; Aroca-Aguilar, J. Daniel; Sánchez, Pilar et al. (2006): Pigment epithelium-derived factor is a

- niche signal for neural stem cell renewal. In *Nature neuroscience* 9 (3), pp. 331–339. DOI: 10.1038/nn1657.
- Rolfe, Andrew; Sun, Dong (2015): Brain Neurotrauma: Molecular, Neuropsychological, and Rehabilitation Aspects. *Stem Cell Therapy in Brain Trauma: Implications for Repair and Regeneration of Injured Brain in Experimental TBI Models*. Edited by Firas H. Kobeissy. Boca Raton (FL).
- Rosa, Alexandra I.; Grade, Sofia; Santos, Sofia D.; Bernardino, Liliana; Chen, Thomas C.; Relvas, João et al. (2016): Heterocellular Contacts with Mouse Brain Endothelial Cells Via Laminin and $\alpha 6 \beta 1$ Integrin Sustain Subventricular Zone (SVZ) Stem/Progenitor Cells Properties. In *Frontiers in cellular neuroscience* 10, p. 284. DOI: 10.3389/fncel.2016.00284.
- Saini, Vasu; Guada, Luis; Yavagal, Dileep R. (2021): Global Epidemiology of Stroke and Access to Acute Ischemic Stroke Interventions. In *Neurology* 97 (20 Suppl 2), S6-S16. DOI: 10.1212/WNL.00000000000012781.
- Sato, Kaoru (2015): Effects of Microglia on Neurogenesis. In *Glia* 63 (8), pp. 1394–1405. DOI: 10.1002/glia.22858.
- Sato, Yuya; Kiyozumi, Daiji; Futaki, Sugiko; Nakano, Itsuko; Shimono, Chisei; Kaneko, Naoko et al. (2019): Ventricular-subventricular zone fractones are speckled basement membranes that function as a neural stem cell niche. In *Molecular biology of the cell* 30 (1), pp. 56–68. DOI: 10.1091/mbc.E18-05-0286.
- Sawamoto, Kazunobu; Wichterle, Hynek; Gonzalez-Perez, Oscar; Cholfin, Jeremy A.; Yamada, Masayuki; Spassky, Nathalie et al. (2006): New neurons follow the flow of cerebrospinal fluid in the adult brain. In *Science (New York, N.Y.)* 311 (5761), pp. 629–632. DOI: 10.1126/science.1119133.
- Schaberg, Elena; Götz, Magdalena; Faissner, Andreas (2022): The extracellular matrix molecule tenascin-C modulates cell cycle progression and motility of adult neural stem/progenitor cells from the subependymal zone. In *Cell. Mol. Life Sci.* 79 (5), p. 897. DOI: 10.1007/s00018-022-04259-5.
- Schaefer, Liliana; Tredup, Claudia; Gubbiotti, Maria A.; Iozzo, Renato V. (2017): Proteoglycan neofunctions: regulation of inflammation and autophagy in cancer biology. In *The FEBS journal* 284 (1), pp. 10–26. DOI: 10.1111/febs.13963.
- Schiller, Herbert B.; Fernandez, Isis E.; Burgstaller, Gerald; Schaab, Christoph; Scheltema, Richard A.; Schwarzmayr, Thomas et al. (2015): Time- and compartment-resolved proteome profiling of the extracellular niche in lung injury and repair. In *Molecular systems biology* 11 (7), p. 819. DOI: 10.15252/msb.20156123.
- Schwartz, Nancy B.; Domowicz, Miriam S. (2018): Proteoglycans in brain development and pathogenesis. In *FEBS letters* 592 (23), pp. 3791–3805. DOI: 10.1002/1873-3468.13026.
- Seidenfaden, Ralph; Desoeuvre, Angélique; Bosio, Andreas; Virard, Isabelle; Cremer, Harold (2006): Glial conversion of SVZ-derived committed neuronal precursors after ectopic grafting into the adult brain. In *Molecular and cellular neurosciences* 32 (1-2), pp. 187–198. DOI: 10.1016/j.mcn.2006.04.003.

- Šekeljić, Vera; Andjus, Pavle R. (2012): Tenascin-C and its functions in neuronal plasticity. In *The international journal of biochemistry & cell biology* 44 (6), pp. 825–829. DOI: 10.1016/j.biocel.2012.02.014.
- Shah, Prajay T.; Stratton, Jo A.; Stykel, Morgan Gail; Abbasi, Sepideh; Sharma, Sandeep; Mayr, Kyle A. et al. (2018): Single-Cell Transcriptomics and Fate Mapping of Ependymal Cells Reveals an Absence of Neural Stem Cell Function. In *Cell* 173 (4), 1045–1057.e9. DOI: 10.1016/j.cell.2018.03.063.
- Sharma, Kartavya; Selzer, Michael E.; Li, Shuxin (2012): Scar-mediated inhibition and CSPG receptors in the CNS. In *Experimental neurology* 237 (2), pp. 370–378. DOI: 10.1016/j.expneurol.2012.07.009.
- Sharma, Kirti; Schmitt, Sebastian; Bergner, Caroline G.; Tyanova, Stefka; Kannaiyan, Nirmal; Manrique-Hoyos, Natalia et al. (2015): Cell type- and brain region-resolved mouse brain proteome. In *Nature neuroscience* 18 (12), pp. 1819–1831. DOI: 10.1038/nn.4160.
- Shen, Qin; Wang, Yue; Kokovay, Erzsebet; Lin, Gang; Chuang, Shu-Mien; Goderie, Susan K. et al. (2008): Adult SVZ stem cells lie in a vascular niche: a quantitative analysis of niche cell-cell interactions. In *Cell stem cell* 3 (3), pp. 289–300. DOI: 10.1016/j.stem.2008.07.026.
- Silva-Vargas, Violeta; Maldonado-Soto, Angel R.; Mizrak, Dogukan; Codega, Paolo; Doetsch, Fiona (2016): Age-Dependent Niche Signals from the Choroid Plexus Regulate Adult Neural Stem Cells. In *Cell stem cell* 19 (5), pp. 643–652. DOI: 10.1016/j.stem.2016.06.013.
- Snappyan, Marina; Lemasson, Morgane; Brill, Monika S.; Blais, Mathieu; Massouh, Mireille; Ninkovic, Jovica et al. (2009): Vasculature guides migrating neuronal precursors in the adult mammalian forebrain via brain-derived neurotrophic factor signaling. In *The Journal of neuroscience : the official journal of the Society for Neuroscience* 29 (13), pp. 4172–4188. DOI: 10.1523/JNEUROSCI.4956-08.2009.
- Sorushanova, Anna; Delgado, Luis M.; Wu, Zhuning; Shologu, Naledi; Kshirsagar, Aniket; Raghunath, Rufus et al. (2019): The Collagen Suprafamily: From Biosynthesis to Advanced Bio-material Development. In *Advanced materials (Deerfield Beach, Fla.)* 31 (1), e1801651. DOI: 10.1002/adma.201801651.
- Tang, Vivian W. (2020): Collagen, stiffness, and adhesion: the evolutionary basis of vertebrate mechanobiology. In *Molecular biology of the cell* 31 (17), pp. 1823–1834. DOI: 10.1091/mbc.E19-12-0709.
- Tavazoie, Masoud; van der Veken, Lieven; Silva-Vargas, Violeta; Louissaint, Marjorie; Colonna, Lucrezia; Zaidi, Bushra et al. (2008): A specialized vascular niche for adult neural stem cells. In *Cell stem cell* 3 (3), pp. 279–288. DOI: 10.1016/j.stem.2008.07.025.
- Theocharis, Achilleas D.; Skandalis, Spyridon S.; Tzanakakis, George N.; Karamanos, Nikos K. (2010): Proteoglycans in health and disease: novel roles for proteoglycans in malignancy and their pharmacological targeting. In *The FEBS journal* 277 (19), pp. 3904–3923. DOI: 10.1111/j.1742-4658.2010.07800.x.
- Theocharis, Achilleas D.; Skandalis, Spyros S.; Gialeli, Chrysostomi; Karamanos, Nikos K. (2016): Extracellular matrix structure. In *Advanced drug delivery reviews* 97, pp. 4–27. DOI: 10.1016/j.addr.2015.11.001.

- Tucić, Milena; Stamenković, Vera; Andjus, Pavle (2021): The Extracellular Matrix Glycoprotein Tenascin C and Adult Neurogenesis. In *Frontiers in cell and developmental biology* 9, p. 674199. DOI: 10.3389/fcell.2021.674199.
- Vining, Kyle H.; Mooney, David J. (2017): Mechanical forces direct stem cell behaviour in development and regeneration. In *Nature reviews. Molecular cell biology* 18 (12), pp. 728–742. DOI: 10.1038/nrm.2017.108.
- Vos, Theo; Lim, Stephen S.; Abbafati, Cristiana; Abbas, Kaja M.; Abbasi, Mohammad; Abbasifard, Mitra et al. (2020): Global burden of 369 diseases and injuries in 204 countries and territories, 1990–2019: a systematic analysis for the Global Burden of Disease Study 2019. In *The Lancet* 396 (10258), pp. 1204–1222. DOI: 10.1016/S0140-6736(20)30925-9.
- Walker, Cameron; Mojares, Elijah; Del Río Hernández, Armando (2018): Role of Extracellular Matrix in Development and Cancer Progression. In *International journal of molecular sciences* 19 (10). DOI: 10.3390/ijms19103028.
- Winkler, C.; Fricker, R. A.; Gates, M. A.; Olsson, M.; Hammang, J. P.; Carpenter, M. K.; Björklund, A. (1998): Incorporation and glial differentiation of mouse EGF-responsive neural progenitor cells after transplantation into the embryonic rat brain. In *Molecular and cellular neurosciences* 11 (3), pp. 99–116. DOI: 10.1006/mcne.1998.0674.
- Xu, Dan; Li, Fengyang; Xue, Gou; Hou, Kai; Fang, Weirong; Li, Yunman (2020): Effect of Wnt signaling pathway on neurogenesis after cerebral ischemia and its therapeutic potential. In *Brain research bulletin* 164, pp. 1–13. DOI: 10.1016/j.brainresbull.2020.07.005.
- Zhu, Chang; Mahesula, Swetha; Temple, Sally; Kokovay, Erzsebet (2019): Heterogeneous Expression of SDF1 Retains Actively Proliferating Neural Progenitors in the Capillary Compartment of the Niche. In *Stem cell reports* 12 (1), pp. 6–13. DOI: 10.1016/j.stemcr.2018.11.022.
- Ziegler, Amber N.; Feng, Qiang; Chidambaram, Shravanthi; Testai, Jaimie M.; Kumari, Ekta; Rothbard, Deborah E. et al. (2019): Insulin-like Growth Factor II: An Essential Adult Stem Cell Niche Constituent in Brain and Intestine. In *Stem cell reports* 12 (4), pp. 816–830. DOI: 10.1016/j.stemcr.2019.02.011.

List of Publications

1. Friess, C., Götz, M., Kjell, J. Cryo-section Dissection of the Adult Subependymal Zone for Accurate and Deep Quantitative Proteome Analysis. *J. Vis. Exp.* (176), e63047, doi:10.3791/63047 (2021).
2. Kjell J, Fischer-Sternjak J, Thompson AJ, Friess C, Sticco MJ, Salinas F, Cox J, Martinelli DC, Ninkovic J, Franze K, Schiller HB, Götz M. Defining the Adult Neural Stem Cell Niche Proteome Identifies Key Regulators of Adult Neurogenesis. *Cell Stem Cell.* 2020 Feb 6;26(2):277-293.e8. doi: 10.1016/j.stem.2020.01.002 .

Declaration of author contribution

1. Friess, C., Götz, M., Kjell, J. Cryo-section Dissection of the Adult Subependymal Zone for Accurate and Deep Quantitative Proteome Analysis. *J. Vis. Exp.* (176), e63047, doi:10.3791/63047 (2021).

J.K. and M.G. conceived the project. C.F. and J.K. conceptualized and planned the project. C.F. and J.K. designed experiments. C.F. performed the experiments and analysed the results except the wholemount standard dissection, which was done by T.S.-E., and the proteolytic tissue sample preparation for mass spectrometry, which was done by J.K.; C.F. and J.K. wrote the paper and the video script with feedback from M.G.

2. Kjell J, Fischer-Sternjak J, Thompson AJ, Friess C, Sticco MJ, Salinas F, Cox J, Martinelli DC, Ninkovic J, Franze K, Schiller HB, Götz M. Defining the Adult Neural Stem Cell Niche Proteome Identifies Key Regulators of Adult Neurogenesis. *Cell Stem Cell.* 2020 Feb 6;26(2):277-293.e8. doi: 10.1016/j.stem.2020.01.002 .

M.G. conceived the project. J.K., H.B.S., M.G., and K.F. conceptualized and planned the project. J.K., J.F.-S., H.B.S., K.F., A.J.T., and M.G. designed experiments. J.K. performed all experiments and analysed all results other than the following: J.F.-S. performed Tgm2 experiments including FACS sorting, whole-mount stainings, qPCR, and sample collection for the microarrays; J.N. performed osmotic minipump implantation and microarray analysis; A.J.T. performed AFM and its analysis and conceptualized these experiments with K.F.; C.F. performed SEZ cryo-dissections and SEZ stainings; M.J.S. and D.C.M. provided C1q13-mVenus reporter mice. J.K. and M.G. wrote the paper with feedback from the co-authors.

Affidavit



Eidesstattliche Versicherung

Frieß, Christian Johannes

Name, Vorname

Ich erkläre hiermit an Eides statt, dass ich die vorliegende Dissertation mit dem Titel:

“Dissection and Proteome Analysis to Characterize the Adult Neural Stem Cell Niche”

selbständig verfasst, mich außer der angegebenen keiner weiteren Hilfsmittel bedient und alle Erkenntnisse, die aus dem Schrifttum ganz oder annähernd übernommen sind, als solche kenntlich gemacht und nach ihrer Herkunft unter Bezeichnung der Fundstelle einzeln nachgewiesen habe.

Ich erkläre des Weiteren, dass die hier vorgelegte Dissertation nicht in gleicher oder in ähnlicher Form bei einer anderen Stelle zur Erlangung eines akademischen Grades eingereicht wurde.

I hereby confirm that the dissertation **“Dissection and Proteome Analysis to Characterize the Adult Neural Stem Cell Niche”** is the result of my own work and that I have only used sources or materials listed and specified in the dissertation.

München, 07. November 2022

Christian Johannes Frieß

Acknowledgements

I want to thank Magdalena for giving me the opportunity to do my MD thesis in her lab. The environment you generate supports young researchers in their learning process, fosters work enthusiasm and facilitates the implementation of scientific ideas and projects. The atmosphere is more than cooperative, researchers in your group support and encourage each other in good faith. I was intrigued by the flat hierarchy as well as by your personal support and instructive input on problems and questions arising during my project. Your high standards for likewise scientific excellence and science ethic made a permanent impression on me and will hopefully guide me in future research projects. I am truly grateful for the rewarding and informative time I was allowed to spend in your lab.

Thank you very much, Jacob, for your continuous support, feedback, and teaching during my research. I enjoy reminiscing about our countless discussions about the project, but also science in general. Despite being a young student with no prior experience in life science at all, you managed to guide me to finishing and publishing my first own little research project. Not only did you teach me the principles of science, but also of project management and self-directed work. I cannot imagine a better direct supervisor and project partner a young scientist could wish for.

I would like to acknowledge the help of Fabian Coscia with the performance of the laser capture microdissections and the opportunity to run the mass spectrometry experiments in the lab of Matthias Mann at the Max Planck Institute of Biochemistry in Munich.

Special thanks to the secretaries for the throughout friendly and immediate help with all organizational problems. Also, of course a big thank you to all lab members and technicians helping me with the project and overall, essentially keeping the lab running.

Finally, I want to thank my girlfriend and my family for their constant and reliable support during this time, their encouragement, and their affection, which crucially helped me accomplish this project.